SUPERCRITICAL CO_2 FOAMED BIODEGRADABLE POLYMER BLENDS OF POLYCAPROLACTONE AND MATER-BI

Emmanuel Olusegun Ogunsona, B.S.

Thesis Prepared for the Degree of

MASTER OF SCIENCE

UNIVERSITY OF NORTH TEXAS

December 2007

APPROVED:

Nandika A. D'Souza, Major Professor
Thomas Scharf, Committee Member
Amit Dharia, Committee Member
Richard F. Reidy, Committee Memberand Chair of the Department of Materials Science and Engineering
Sandra L. Terrell, Dean of the Robert B. Toulouse School of Graduate Studies

Ogunsona, Emmanuel Olusegun, Supercritical CO_2 foamed biodegradable polymer blends of polycaprolactone and Mater-Bi. Master of Science (Material Science and Engineering), December 2007, 117 pp., 19 tables, 63 illustrations, references, 70 titles.

Supercritical CO_2 foam processing of biopolymers represents a green processing route to environmentally friendly media and packaging foams. Mater-Bi, a multiconstituent biopolymer of polyester, starch and vegetable oils has shown much promise for biodegradation. The polymer, however, is not foamable with CO_2 so blended with another polymer which is. Polycaprolactone is a biopolymer with potential of 4000% change in volume with CO_2. Thus we investigate blends of Mater-Bi (MB) and polycaprolactone (PCL) foamed in supercritical CO_2 using the batch process. Characterization of the foamed and unfoamed samples were done using X-ray diffraction (XRD), differential scanning calorimetry (DSC) and scanning electron microscopy (SEM). Micrographs of the samples from the SEM revealed that the cell size of the foams reduced and increased with increase in MB concentration and increase in the foaming temperature respectively. Mechanical tests; tensile, compression, shear and impact were performed on the foamed samples. It was noted that between the 20-25% wt. MB, there was an improvement in the mechanical properties. This suggests that at these compositions, there is a high interaction between PCL and MB at the molecular level compared to other compositions. The results indicate that green processing of polymer blends is viable.

ACKNOWLEDGEMENTS

I would like to deeply express my gratitude to my adviser, Dr. Nandika Anne D'Souza, who has equipped me with the knowledge to undertake and write this thesis. Her guidance, support (scholarships, funding and tuition waivers) and encouragement contributed immensely throughout my research work. Most importantly, she has always driven and motivated me to turn out my possible best and never to relent not only in academics but also in life.

I would also like to thank David Garrett and John Sawyer for their training and technical assistance with instrumentations, Wendy Agnes, Joan Jolly and Olga Reyes for their assistance in making my research work and stay in the Material Science and Engineering Department a smooth sail.

Lots of thanks to my friends and colleagues, especially Koffi Dagnon, Ali Shaito, Divya Kosuri, Sunny Ogbomo, Anjana Rajendra and all others in the Materials Science and Engineering Department for encouraging and assisting me during my research work.

Finally, I would like to thank my family, for their continuous support in every way. I would like to thank my parents; my mentors for their encouragement, advise and financial support not only throughout the research and writing of this thesis but throughout my education, words cannot express how grateful I am. To my brother, who has always encouraged and advised me. To my sister, for her assistance and advice at all times.

TABLE OF CONTENTS

Page

LIST OF TABLES

Page

LIST OF FIGURES

Page

CHAPTER 1

INTRODUCTION

1.1. Cellular Polymers

Cellular polymers (foams) are materials containing voids surrounded by a denser matrix, which is usually a solid. Foams have been mainly known to be made of thermoplastic polymers but they have in the recent years also been made of different materials like epoxies, ceramics and metals and their alloys. Foams have been widely used in a variety of applications: e.g. filtration in water purification plants, acoustical and thermal insulation in studios and power plants, cushions, absorbents and weight-bearing structures in the building industry. Polymeric foams had a market value in the US of about $2 billion as of 2000.[4] The value of just polystyrene foam products manufactured in the United States in 1997 was approximately 5 billion dollars according to the US 1997 economic census (US 1997 Economic census). The use of polymer foams has become wide spread. It is almost impossible to point a finger at any industry where polymeric foams are not used or do not have a role to play. They are found in industries and their applications like sports products, military applications, automobiles, all aircraft, and home furnishing. Consumer applications have grown. Everyday, people encounter polymer foams in one form or another, whether it be in refrigerators insulations, in packaging, in their cars, or in some other common application.

Foams can be categorized using several criteria. They can be categorized through their structural morphology. They can be divided into either open cell or closed cell foams. Open cell foams are those that contain interconnected voids within strut like

structures while closed cell foams do not have interconnected voids; the voids or bubbles are discrete.[5] They are encapsulated by a thin wall of plastic membrane. Foams can also be categorized by the diameter of the voids. The voids can range in diameter from nanometers to millimeters. Voids, cells or bubbles that have diameters in the nanometers, micrometers and millimeters are called nanocellular, microcellular and macrocellular foams respectively.

Open cell foams are ideal for various porous applications especially with those that involve absorption; applications such as filters and sponges. Closed cell foams are ideal for applications where maximum mechanical properties are needed. Some of the areas of application are in heavy equipment packaging, weight bearing structures and impact absorption. The foam discussed in this thesis is closed cell flexible foam properties. Another way cellular polymers are categorized is through their stiffness or rigidity. Foams can be divided into flexible and rigid. Some researchers further divide them into flexible, semi-flexible and rigid. This division is primarily a function of the plasticity of the polymer foam precursor[5]. Placing flexible and semi-flexible foams under the same category can be concluded because they both have polymers with a glass transition (T_g) below their service temperature which is usually at room temperature while rigid foams have polymers with glass transitions above their service temperature.

Foam manufacturing processes can be categorized into physical, chemical and mechanical (frothing). Foams, especially closed cell foams most often consist of a gas phase which is dispersed in a solid phase (polymer) except when there is a total diffusion of the gas out of the foam. Open cell foams consist of a gas phase which is inevitably air. This gas is replaced with water vapor, carbon dioxide and air from the atmosphere. The

gas in the void is referred to as the blowing agent. Blowing agents can be categorized as physical blowing agent (PBA) and chemical blowing agent (CBA).

PBAs are used primarily in the foaming of thermoplastics because they are mostly nontoxic and have a low boiling point which provides the most vapor pressure for foam expansion at their processing conditions.[5] In several conditions, blowing agents are introduced into the polymer in a densified phase such as liquids or supersaturated fluids (SCF) and then change to a gaseous phase to create the voids within the polymer. For a long time, chlorofluorocarbons (CFCs), an efficient low cost blowing agent with low boiling temperature, toxicity, flammability and non-reactive properties have been used. They have been known to be amongst the top five ozone depleting substances: CFC-11, CFC-12, CFC-114, HCFC-22, HCFC-141b, and HCFC-142b. In 1987, the Montreal Protocol took action to reduce their use and eventually stopped the use of any type of CFCs in 2002.[5] It was reported by the Montreal Protocol that CFCs were still being used and traces had been found in the atmosphere. In order to replace these ozone depleting substances (ODS), substitute physical blowing agents (PBAs) have been researched. Some of these PBAs are inert gases such as nitrogen, carbon dioxide, hydrocarbons (pentane and cyclopentane), organic liquids like citrus juices. The most widely used of these are nitrogen and carbon dioxide. In this study, carbon dioxide has been used because of inertness and process being considered environmentally friendly (green).

CBAs are steady materials (usually solids) at normal storage temperatures but react to give off gas at a reaction temperature which is usually their thermal decomposition temperature.[6] Thermal decomposition of these materials can either be endothermic (heat absorption) or exothermic (heat generation). Endothermic chemical

foaming agents mostly produce carbon dioxide while exothermic chemical foaming agents produce nitrogen. Very popular CBAs are in the class of organic nitrogen compounds such as azodicarbonamide. They produce mostly nitrogen gas and very small portions of other gases. Water, another chemical blowing agent is still used in the production of polyurethane foams. Most chemical foaming agents produce nitrogen gas. They are exothermic and the gas bubbles produced are not stable and therefore not favorable for the growth of foam structures. The gas produced is usually immiscible and non-homogenous solution by itself.[7] Chemical foaming is a process where chemical blowing agents are used. The gas producing material is mixed and thermally decomposed. Examples are the production of PVC using an organic nitrogen compound that gives off gas[6], polycaprolactone (PCL) using an inert citrus based compound that gives off carbon dioxide gas upon thermal decomposition. This temperature is right at about the melting temperature of PCL which makes it a very compatible blowing agent.

Physical foaming (also called solid state foaming) are environmentally friendly techniques that have been developed.[8] There are two methods in this category of foaming; the first is the saturation of the polymer with CO_2 often at high pressures for a certain soaking period. This is then followed by the expansion of the foam by an increase in the temperature above the glass transition temperature (also called processing temperature) of the saturated polymer. The second is also the saturation of the polymer usually at high pressures and temperatures (processing and supercritical conditions). This is followed by a rapid change in the pressure (depressurization). The change in thermodynamic state in the supersaturated polymer/gas solution induces nucleation and growth of microvoids in the polymer matrix.[4] Mechanical foaming (frothing), which

means dispersing of bubbles is usually used in fast curing and high temperature polymeric materials. This process utilizes the bubbling of gases into polymer based melts, suspensions or solution. The bubbles are entrapped in the matrix as the polymer hardens or cures, producing a cellular structure.[6]

During the physical foaming process with a physical blowing agent, a depression in the glass transition is seen. Plasticization affects the melt viscosity, gas diffusivity in the melt, and the gas-melt interfacial tension. Chen et al.[9], studied the plasticization effects during foaming and also proposed a model for plasticization during bubble growth and estimated its effects under typical foaming conditions. Zhang et al.[10] studied the relationship of blowing agent content with foam grade and cell size. They found that an increase in the blowing agent content in the polymer increased the cell size of the foam. E. Reverchon et al.[11] studied the relationship of temperature, pressure and contact time of the foaming agent during foaming process on the microcellular structure of the foam. They found that an increase in the temperature or pressure produced larger cells. They found that the longer contact time of the blowing agent assured homogeneous diffusion inside the sample and a symmetric microcellular structure.

Naturally occurring polymer foams or biofoams have been known to exist for a very long time. Examples of these are sponges and corks. Synthetic polymer foams have only been around and in production for approximately fifty years. The research and development of new polymers especially biodegradable polymers have always been followed by the production of their expanded state (foam). Biodegradable foams have received a lot of attention and focus in the recent years. Industries are focusing on making every product environmentally safe and friendly. Examples of some biodegradable

polymers are polylactic acid (PLA), Polyhydroxyalkanoates (PHA). Biodegradable foams have become a focus especially since they are used in medical applications like tissue scaffolding, drug administration, in decomposable packaging areas where recycling processing poses a difficulty and food industries.

1.2. Biodegradable Polyblends

Whenever the phrase biodegradability of a material or biodegradable materials is mentioned, it basically means the rate, ability and amount of a material that undergoes degradation under exposure to certain conditions like light, air, organic chemicals and bacteria. The most common biodegradation test is soil degradation. Materials or blends that undergo degradation when exposed to light and air are called oxy-degradable and UV-degradable. Polymer blends are a mixture of two or more polymers in order to achieve a material that has certain properties of each of the composition of the blend. Blending two or more polymers together can be done through two methods, melt blending and solution blending. In these blending methods, the mixtures could either be miscible (homogeneous mixture) or immiscible (non-homogeneous mixture). A miscible blend is one that exhibits a single phase while an immiscible blend is one that exhibits separation of phases with multiple phases are present.

Solution blending is done by dissolving the polymers in a solvent and allowing the solvent to evaporate with time. What is left after evaporation has taken place is the blend of the polymers assuming that the polymers are miscible. This is an expensive, time consuming and not an environmentally friendly method. Evaporating the solvent could take a lot of time, is expensive and toxic to the environment when the evaporated solvent is not recaptured for reuse or disposal. Most blends used or studied for medical

applications are made by this method; examples are blends of poly (L-lactide) with lecithin studied by Zhu et al.[12] for biomedical tissue sutures and PLA with PCL for tissue scaffolding studied by Chen et al.[13]

Melt blending is achieved by heating the polymers together in a mixing machine, like an extruder, until the glass transition of all polymers has been exceeded. The blend should be left to cool and a new polymer blend is made assuming the polymers are miscible. Polymer blends usually have properties that lie between those of the individual polymers. The properties can be altered by changing the compositions of the blend. Properties like the glass transition, tensile and compressive strength, melting temperature and foamability could increase or decrease depending on the composition and sought after properties.

1.3. Biodegradable Polymer Foams

Biodegradable polymer foams are a new development in the area of polymeric foamed materials. They have wide applicability especially within the medical field. The main utility of these foams lies in their exceptional combination of thermal and chemical stability, compatibility, biodegradability and even high strength to weight ratio. Since their properties favor a lot of applications in the medical field and food industry, a lot of research is being conducted for its use in packaging applications.

A lot of biodegradable foams are processed using inert physical blowing agents like CO_2 and N_2 gas at their supercritical (SC) state because of their ability to foam solid polymers without completely melting or sometimes not melting them at all. Supercritical CO_2 ($scCO_2$) which has a lower supercritical temperature of the above mentioned agents is usually preferred since it takes less time and expenses to achieve such a temperature.

When polymer blends are not mixed well, there is no homogeneity; agglomerations can be seen in the blend. Foamed polymer blends with agglomerations cause the nucleation of cells to start at the particles or agglomerations. These particles clog the pores and give the foam an irregular and unstable structure.

1.4. Scope

The biodegradable foam presented in this thesis is a copolymer of MB and polycaprolactone prepared by thermal blending. Since MB (starch) is not easily foamed, Polycaprolactone which is easy to foam, 100 percent biodegradable and inert was chosen to enhance MB's foamability. Secondly, its flexible nature is ideal for degradable foam packaging and its blend compatibility with other polymers.[14]

The basic foaming process for this study is the physical foaming or solid state foaming with a constant pressure and variable temperature that was derived from previous works by Miller et. al.[15] In the former works, polyetherimide (PEI) was foamed at different processing temperatures and pressures above the glass transition temperature of PEI. This was done to determine how these conditions affect the density of the foams. In this study, microcellular foams were formed at high pressures (1100 psi) and temperatures ranging from 31°C-35°C. These parameters were investigated along with MB presence on foam nucleation, growth and microstructure were investigated. Analysis techniques used for this investigation include differential scanning calorimetry (DSC), scanning electron microscopy (ESEM) and X-ray Diffraction (XRD). A hydraulic MTS machine was used to run tensile, shear and compression tests on the samples while an impact tester was used to test the impact properties.

CHAPTER 2

LITERATURE REVIEW

2.1. Biodegradable Polyblends

Biodegradable polymers (BDPs) make up a loosely defined family of polymers that are designed to be degraded by living organisms. They offer a possible alternative to conventional non-biodegradable polymers (NBDPs) when recycling is unfeasible or uneconomical. Technologies, such as composting used for the disposal of food and yard waste, account for 25-40% of the total municipal solid waste, and are the most suitable for the disposal of biodegradable materials.

International organizations, such as the European Standardization Committee (CEN), the International Standardization Organisation (ISO), the German Institute for Standardization (DIN), the Italian Standarization Agency (UNI), the American Society for Testing and Materials (ASTM), in connection with the institute for Standards Research (ISR), the Organic Reclamation and Composting Association (ORCA), are all dynamically involved in developing definitions and tests methods for biodegradability in different environments and compostibility.

Although a standard world-wide definition for biodegradable plastics has not been established, the definitions already in place (ASTM, CEN, ISO) associate the biodegradability of a material to a specific disposal environment and to a specific standard test method which stimulates this environment in a time period which determines its classification.

CEN, ORCA, UNI and DIN have defined the basic requirements for a product to be declared compostable according to this approach based on:

- Complete biodegradability of the product, measured through respirometric tests like ASTM D5338-92, ISO/CD14855 and the modified Strum test ASTM D5209, in a time period compatible with the composting technology
- Disintegration of the material during the fermentation phase
- No negative effects on the compost quality and in particular no toxic effects of the compost and leachates on terrestrial and aquatic organisms
- Control of laboratory-scale results on pilot/full scale composting plants

These requirements set a common foundation for a universal marking system to readily identify products to be composted.

Polymer blends have long been used in the industry for various applications. Industrial applications of polymer blends can be found in coatings, adhesives and rubber making. Blending of two or more polymers was introduced into the plastic industry about 50 years ago and ever since then, it has quickly become a major area of study and market in the industry. The total amount of plastics in the market is approximately 20% - 40% of blended polymers. In recent years, biodegradable polymers have been an area of focus. Now, different applications and areas of biodegradable polymers are been exploited, especially their blends.

Polymer blends, both miscible and immiscible have been found to be useful in various applications. Miscibility of a blend is the capability of a mixture to form a single phase over certain ranges of temperature, pressure and composition; miscible blends can be thermodynamically stable or metastable[16] while immiscible blends do not show a single but multiple phases. They are non homogeneous upon observation. An example of an immiscible polymer blend is high impact polystyrene (HIPS). HIPS is a blend of

polystyrene (PS) and polybutadiene (PB); PB does not mix with PS, there agglomerations within the phase of the PS which gives HIPS its impact strength. We call this an immiscible but compatible blend. In a study made, a copolymer was used to bind two immiscible polymers.[17] Poly (vinyl alcohol) (PVA) and lignin were blended and studied. The result of the study was that the two polymers are immiscible but there is some attraction between lignin and PVA in the PVA rich phase. It was found that the crystallinity of PVA was reduced with increasing lignin content.[18] Generally, immiscible or partially miscible blends typically do not show a depression in the T_m while a depression is a characteristic of a miscible blend in the melting state. Poly (tetrahydrofurfuryl methacrylate) (PTHFMA) and poly (hydroxyl ether of bisphenol A) (phenoxy) were found to be miscible through the identification of the existence of a single glass transition temperature in each of the blend compositions.[19] From the thermodynamic point of view, the strength of the specific interaction energy density parameter *B*, which can be obtained from the depression in the equilibrium melt point (T_m)[20]; this is based on the Nishi-Wang equation for an amorphous and semicrystalline blend.[21]

$$T_m^0 - T_{m2}^0 = -T_m^0 \frac{BV_{2u}}{\Delta H_{2u}} \phi_1^2 \tag{1}$$

where $\Delta H_{2u}/V_{2u}$ is the latent heat of fusion of the 100% crystalline component per unit volume, *B* represents the interaction energy density between blend components, Φ_2 is the volume fraction of the amorphous component and T_{m2}^0 is the equilibrium temperature of the blends.

There are various factors that can determine if a blend is miscible or immiscible. Miscibility and immiscibility could result from the polarity of the blends. Polymers that have very similar structures are more likely to attract each other to form miscible blends. Polymer blends with differing polarities usually produce immiscibility. Miscibility is very likely to occur in polymer blends when the individual polymers are drawn to each other either by acid base, charge transfer, ion dipole, hydrogen bonds or transition metals complexes. This is very uncommon but when attractions like these occur, there is a high probability that the properties will exceed those of the individual polymers. An example is the glass transition temperature (T_g) of the blends; it is likely that the T_g will exceed that of both the individual polymers.

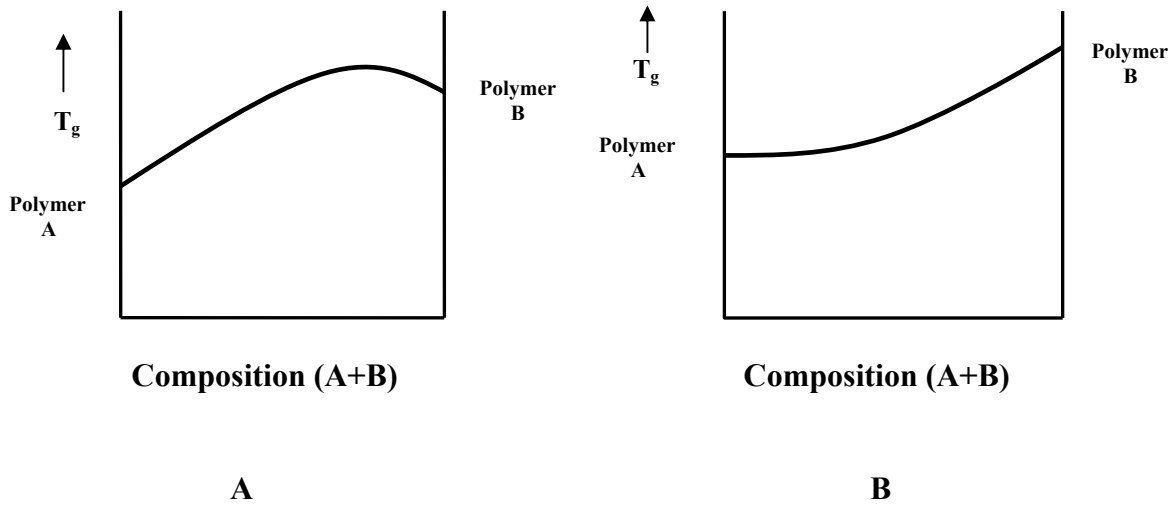

Figure 1 Plot showing the change in T_g in miscible blends with (a) high attractions and (b) normal.

Figure1(a) shows the T_g increasing from polymer A to polymer B when there is an attraction in the blends with varying compositions while Figure 1(b) shows the increase in T_g of a normal blend with varying compositions from polymer A to polymer B.

In an immiscible blend, the extent to which the individual polymers separate and to which each phase is actually not pure polymer A and pure polymer B, but rather a solution of B in A and A in B can be explained using the phase rule.[22] Typically, the main phase will create the continuous matrix and control most of the properties of the blend while the minor phase will create dispersed microdomains which contribute certain properties to the blend. Rheology is another factor that affects the miscibility of blends. The viscosities of the individual polymers determine which one forms the continuous matrix and dispersed domain regardless of the amount of constituent polymers present. The less viscous phase tends to form the continuous matrix while the more viscous phase tends to form the dispersed domains. The morphology of the dispersed domains usually appears to be spherical in shape because it tries to minimize the surface energy. Usually, as the size of the dispersed domains reduces, it increases the compatibility of the blend as the attraction between the phases increase. In a study by Jang et al., the melting temperature and thermal stability of enhanced nylon 6 (PA6) with acrylonitrile-butadiene-styrene (ABS) did not significantly change but the mechanical properties of the blends were found to be enhanced. This was explained by the formation of a micro-domain structure in the blends. The high viscosity and entanglements of large polymer molecules slow the phase separation kinetics and morphology formation. The shape and size of the dispersed domains might initially be changed by the temperature and mechanical shear but the system eventually tends reverts back to thermodynamic equilibrium over a period of time.

2.2. Poly (ε – caprolactone) (PCL)

Synthetic polymers are extensively used in the manufacturing of products because of their physical and chemical properties and low cost of production, however, these polymers are by and large resistant to biological degradation when discarded in the environment. In the last 50 years, significant efforts have been dedicated to the development of low cost polymers that can be degraded by microorganisms, bacteria, enzymes and fungi in the environment. The use of biodegradable polymers provides an alternative to the use of non-biodegradable polymers and a solution to the problem of the buildup of waste plastic in the environment. In recent years, PCL has become one of the most sought after flexible (semi rigid) and easy to process polymers among synthetic biodegradable polymers.[23] It degrades by hydrolytic or enzymatic pathways and in several biotic environments, including river and lake waters, sewage sludge, farm paddy soil, compost and various sediments[14], thereby making it suitable for packaging and medical uses. It is a high molecular weight aliphatic polyester thermoplastic that is synthesized from crude oil. PCL is a semi crystalline polymer that is miscible with several polymers including poly(benzylmethacrylate) (PBMA)[24], novolac[25] because the carbonyl groups of PCL can form intermolecular hydrogen bonds with the hydroxyl groups of the second polymer.[26-28]

PCL is polymerized from the monomer ε-caprolactone; Figure 2 and table 1 show the polymerization process from ε-caprolactone to polycaprolactone and material properties.

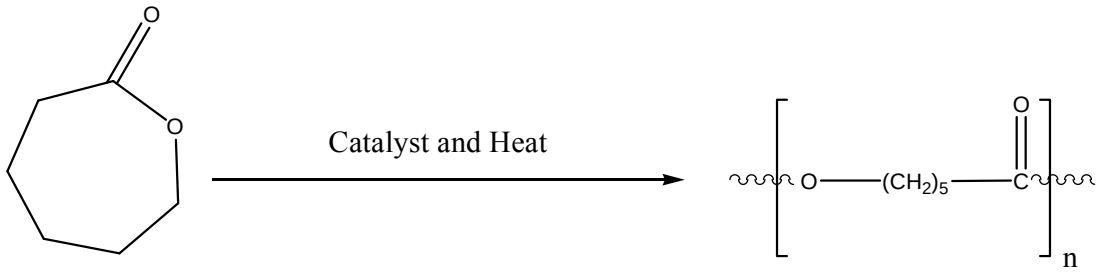

ε – Caprolactone Polycaprolactone

Figure 2: Ring opening polymerization of ε-caprolactone into polycaprolactone using heat and catalyst.

Table 1 Material properties of PCL.

Density, (g/cm^3)	**Average Molecular Weight, (g/mol)**	**Glass Transition Temperature, (°C)**	**Melting Temperature, (°C)**	**Melt Index, (g/min)**
1.145	100,000	-60	67	0.1

2.3. Starch-Based Material

Starch-based materials are now being used in industrial products and are leading the way in the fast growing market of biodegradable products. The market prospects for biodegradable products in the next 5 years can be estimated at approximately 150000-200000 ton/year in Europe. American and Japanese markets are of great potential and are beginning to employ these materials. MB, a family of thermoplastic materials derived from renewable resources which cover a variety of applications in the fields of packaging, agriculture and food catering. MB is a blended biodegradable thermoplastic composed of corn starch, vegetable oil derivatives and of biodegradable synthetic polyester. It is produced and marketed by Novamont. MB – starch based materials are currently used in specific industrial applications where biodegradability is required such as the composting bags and sacks, packaging, hygiene, food service ware. Not much is known about this thermoplastic since the manufacturer has held back on the

specifications; polyester and derivative from vegetable oil used. Table 2 below shows some of its properties.

Table 2 Material properties of MB.

Density, (g/cm^3)	Water Vapor Permeability (gx30μm/m_x24h)	Melting Temperature, (°C)	Melt Index, (g/min)
1.29	850	110	3

Starch comprises of two main components namely amylose and amylopectin. Amylose, which is generally an alpha-D-(1-4)-glucan and amylopectin, an alpha-D-(1-4) glucan having alpha-D-(1-6) linkages at the branch point. The molecular weight of linear amylase molecules of starch is 0.2-2000000 and that of branched amylopectin molecules is 100-400000000.[29, 30] Naturally, starch can be found as crystalline beads of approximately 15-100μm in diameter in tubers, cereal and various beans which are all characterized by left handed, six-fold double helices.

Extrusion cooking is a comparable process used in the making of thermoplastics from starch. Extrusion cooking and foaming process constitutes the application of sufficient work and heat being applied to a cereal-based product to cook or gelatinize completely all the ingredients. The heating and continual compression of the materials during processing is done by equipment used for high pressure extrusion.

By altering the temperature and the pressure in the extruder and the moisture content of the raw product, thermoplastic starch products with different viscosity, water solubility and water absorption could be made. A thermoplastic can be solubilized without the formation of maltodextrins and the extent of solubilization depends on the extrusion temperature, the moisture content of the starch before extrusion and the amylase/amylopectin ratio.[31-33] Thermoplastic starch only can be processed as a

conventional plastic. Its sensitivity to humidity, however, makes it unsuitable for most applications. Soluble compostable foams, such as loose-fillers, expanded trays, shape molded parts; expanded layers are some of the major employment of thermoplastic starch.

Starch can be destructurized in combination with different synthetic polymers to satisfy a broad spectrum of market needs.[34-39] Thermoplastic starch composites can reach starch contents higher than 50%; the combination of thermoplastic starch with synthetic polymers can give rise to three distinct groups of materials. These distinct groups could arise from the combination of thermoplastic starch complexed with synthetic copolymers containing hydrophilic and hydrophobic units; examples are polyester-urethane and copolymers of vinyl-alcohol, thermoplastic starch blended with imcompatible synthetic polymers like aliphatic polyesters and cellulose derivatives, partially complexed and/or compatibilized thermoplastic starch blended with incompatible or slightly compatible synthetic polymers. The biodegradation behavior of the different products is mainly influenced by the biodegradability of the synthetic component, although the presence of starch can significantly influence the biodegradation rate of intrinsically biodegradable synthetic components.

Starch can also be destructurized in the presence of more hydrophobic polymers such as aliphatic polyesters; it has been found that the blending of starch with aliphatic polyesters improves their processibilty and degradation behavior. Specifically, polyesters that are suitable is polycaprolactone and its copolymers or polymers at higher melting point formed by the reaction of glycols as 1,4 butandiol with sucinic acid or with sebacic acid, adipic acid, azelaic acid, decanioc acid or brassilic acid. The presence of

compatibilizers between starch and aliphatic polyesters, such as amylase complexed with aliphatic polyesters or with polymers partially or completely compatible with polyesters, starch grafted polyesters, chain extenders like diisocyanates, epoxides, etc., can improve the properties of starch composites. These materials are characterized by excellent compostability, good mechanical properties and reduced sensitivity to water.

Some of the classes of MB produced by novamont are reported in Table 3 below; all of which are based on starch and different synthetic components.

Table 3 MB: classes and grades. [40]

Z class	• **Biodegradable and compostable mainly for films and sheets.** • **Biodegradation time of 20-45 days in composting conditions.** • **Made of thermoplastic starch and polycaprolactone.**	
Grade	**Technology**	**Use**
ZF03U/A	Film blowing	**Bags, nets, paper lamination, mulch films, twines, wrapping film…**
ZFO2U/A	Film blowing	**Diaper backsheets, paper lamination…**
ZI01U	Film blowing/extrusion/casting injection molding	**General purpose, wrapping film…**
ZI01U/T	Extrusion/calandering/injection molding	**Thermoformed and injected items…**
Y class	• **Biodegradable and compostable for rigid and dimensionally stable injection molded items.** • **Biodegradation time of about 4 months in composting conditions and 30 days in anaerobic conditions (1mm in thickness)** • **Made of thermoplastic starch and cellulose derivative.**	
Grade	**Technology**	**Use**
YI01U	Injection molding	**Cutlery, boxes, flower pots, seedling planter trays, golf tees. Vending cups, pens…**
V class	• **Biodegradable, compostable and soluble for rigid and expanded items.** • **Biodegradation time even shorter than Z grades.** • **Content of thermoplastic starch more than 85%**	
Grade	**Technology**	**Use**
PE02U	Foaming	**Loose filters and packaging foams as a replacement of polystyrene…**
PE03U	Injection molding	**Soluble cotton swabs, soluble items…**
A class	• **Biodegradable, not compostable, mainly for molded items** • **Biodegradable time of about 2 years in an environment simulating a sewage sludge treatment plant.** • **Made of starch and ethylene vinyl-alcohol copolymer, used in applications where compostability is not required**	
N/A class	**Technology** **N/A**	
Grade	**N/A**	**Use**
NF01U		**N/A**

2.4. Supercritical Fluid (CO_2)

The supercritical phase of a compound is a phase in which the compound is above the critical points (critical pressure P_c, and critical temperature T_c). In this phase, a compound bears both the properties of a gas and a liquid. Every substance has a critical temperature (T_c) and pressure (P_c). At T_c and P_c, no increase in pressure can force the substance into its liquid phase[1]. A substance is said to be in a supercritical state or a supercritical fluid (SCF) when the temperature and pressure of the substance are either equal or higher than the T_c and P_c for that substance. The most important property of all is its tunability (ability of the fluid to change in its density and other variables) within the temperature range since a small change in temperature will cause changes in the pressure, accompanied by changes in other physical variables related to pressure and temperature.

The main variables that are affected by such changes and that play important roles in supercritical applications are the density (d) and the dielectric constant (ε). The density is a variable known to be directly proportional to the solvency power, and this is the basis for supercritical fluid extraction processes. The tunability of the dielectric constant also gives power to tune the solvency power since it relates to the solvent polarity and other important solvent effects. Supercritical fluids have many important properties that increase their attractiveness for use. Their high diffusivity, low viscosity and high density make them suitable for continuous-flow processes. Since they have tunable solvating power, different conditions may be set for a wide range of applications concerning different compounds. Supercritical fluids can be easily removed after usage, avoiding any solvent wastes and costly separations. Even though the costs of the equipment needed to

run a supercritical process are high, they are generally outweighed by the economic benefits brought by SCF applied processes.

The high potential for some supercritical fluids to replace toxic industrial solvents and the possibility of producing new materials at inexpensive and environmentally friendly conditions have led to the consideration of and scientific research of supercritical fluids. Supercritical fluid was first discovered by French scientist Baron Charles Cagniard de la Tour, in 1821. Ever since, rigorous research has been going on and significant discoveries have come from the last few decades. SCFs were originally employed in the extraction separation and chromatographic separation processes. A very common and important utilization of SCF today is in the extraction process which is used in caffeine removal from coffee. Recently, the process has been expanded to various extraction applications with products such as tea and spices.[2] Many fields are now using $scCO_2$ in various processes; polymer recycling, waste destruction, geology and mineralogy and in particle dispersion and substrate formation.

Figure 3 illustrates a general pressure-temperature phase diagram for a pure compound. The supercritical phase and the pressure-temperature range defining this phase are shown on the Figure. A little change in the pressure and/or temperature at or near the critical point of a supercritical fluid can significantly change the density and therefore increase the solubility. The physico-chemical properties of the SCF can be made diverse without changing the molecular structure of the substance. This makes it an excellent solvent since it can act and replace other series of solvents.

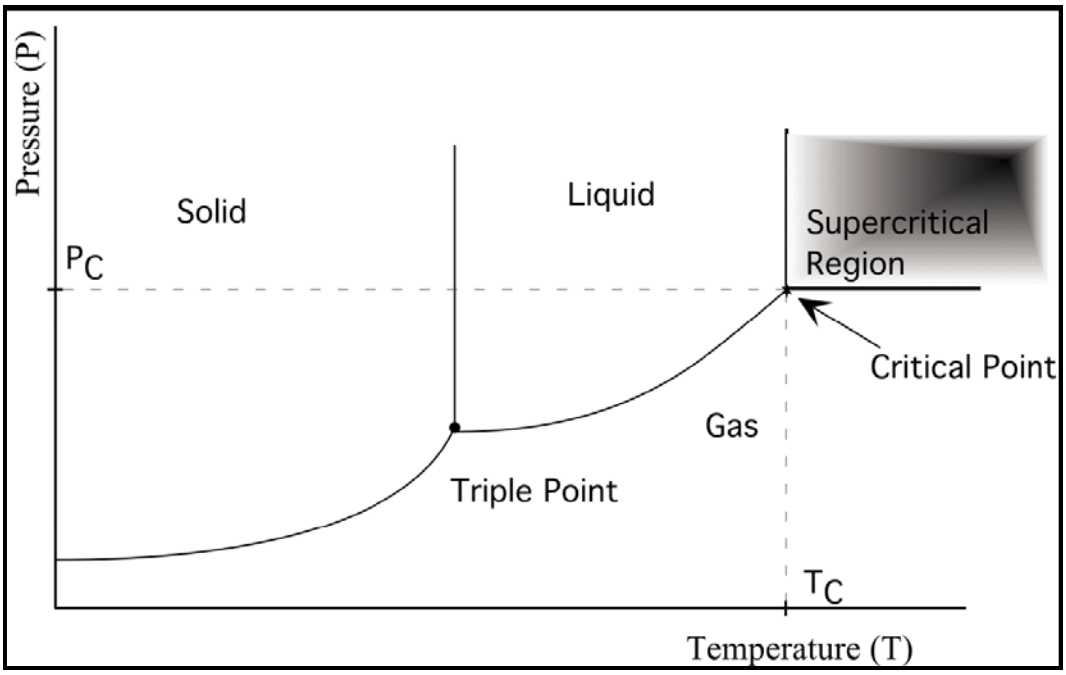

Figure 3 Pressure-temperature diagram for a pure substance.[1]

The condition at which the densities of the coexisting equilibrium phases of liquid and gas intersect is called the critical point. Compressed CO_2 exists in equilibrium as a binary phase system of liquid and gas at ambient temperature. The vapor pressure of the compressed gas phase at the temperature of 24.85ºC is constant at a pressure and density of 6.41MPa and 0.24g/ml respectively. The net pressure of a system containing CO_2 will not be changed when CO_2 is removed or added as long as there are both liquid and gas phases present in the system. If more CO_2 is added to the system, it takes the form of a liquid. According to the ideal gas law, the density and pressure of the gas phase of the isochoric (constant volume) system increases as the temperature increases while the density of the liquid phase decreases due to the thermal expansion that takes place between the molecules of the liquid phase. If the temperature continues to increase, the difference between the densities of the two phases become undistinguishable at a unique

point; that point which is called the critical point is reached at a temperature and pressure of 31ºC and 7.38 MPa (1074 psi) for CO_2 at a density of 0.468 g/ml. the physico-chemical properties of $scCO_2$ is shown in table 4 below.

Table 4 Thermophysical properties of fluids.

Phase	**Density, (g/cm^3)**	**Diffusion Coefficient, (cm^3/s)**	**Viscosity, (poice) (g/cm.s)**	**Surface Tension, (dynes/cm)**
Liquid	0.929	10^{-6}	10^{-2}	45-60
Supercritical Fluid	0.2-0.8	10^{-3}	10^{-3}	0
Gas	0.001	10^{-1}	10^{-4}	N/A

Some important summaries of supercritical properties are that a SCF is a substance under pressure above its critical temperature, the division between gas and liquid does not apply under this condition, SCFs have physical intermediate properties to those of gases and liquids and these properties are controlled by the pressure, SCFs do not condense or evaporate to form a liquid or a gas, as the density increases, the solubility increases and that the fluids are completely miscible with permanent gases (N_2 or H_2) and this leads to much higher concentrations of dissolved gases than can be achieved in conventional solvents.

2.5. Solubility of Supercritical Carbon Dioxide ($scCO_2$) in Polymers

Due to its non-toxic, non-flammable, chemically inert, inexpensive, the supercritical conditions can be easily reached (T_c = 304K, P_c = 7.38Mpa) and can easily be removed and captured by simply depressurization, supercritical carbon dioxide has become one of the most widely used substances in the area of green processing. While it is abundant in the atmosphere and a by product of the human respiratory process, it is

also a by product from hydrogen and ethanol production. ScCO2 is a good solvent for many non polar and some polar low molecular weight compounds.[41]

The solubility efficiency is closely related to the transport properties of a solvent. These properties are defined by the diffusion coefficient and the viscosity. When compared with those of liquid solvents, the diffusion coefficient (diffusivity) and viscosity of SCFs are several magnitudes higher and lower, respectively. Then the rate of diffusion of the species in a SCF will be faster than in a liquid solvent; this faster rate will directly contribute to a more efficient solubility in a SCF, just as the density is affected by pressure changes, the diffusion coefficient also varies with changes in the pressure and temperature, and at the same time is affected by the changes in the density and the viscosity.

A lot of time and attention have been put into systems where $scCO_2$ is dissolved in polymers. Tomasko et al.[42] gave a broad range of information on the different applications of supercritical CO_2 in regards to polymer synthesis and processing. Polymerization, polycondensation reactions and hydrothermal waste treatment in supercritical CO_2 were reviewed by Cansell et al.[2] in the last decade. From the thermodynamic point of view, the criteria for the solubility of a melt in a solvent are defined by the equations below.

$$\Delta G_m = \Delta H_m - T\Delta S_m < 0 \text{ and } (\partial^2 \Delta G_m / \partial \varphi^2)_{T,P} > 0 \qquad (2)$$

where ΔG_m, ΔH_m, ΔS_m and φ are the free energy, the enthalpy, the entropy of mixing and the volume fraction of the polymer, respectively. In the study of miscibility of binary systems (two systems), their miscibility could either be immiscible, partially miscible or completely miscible. This corresponds to the three forms of Gibbs free energy function

for binary systems. Figure 4 shows a schematic of the Gibbs free energy of mixture with respect to the polymer concentration.

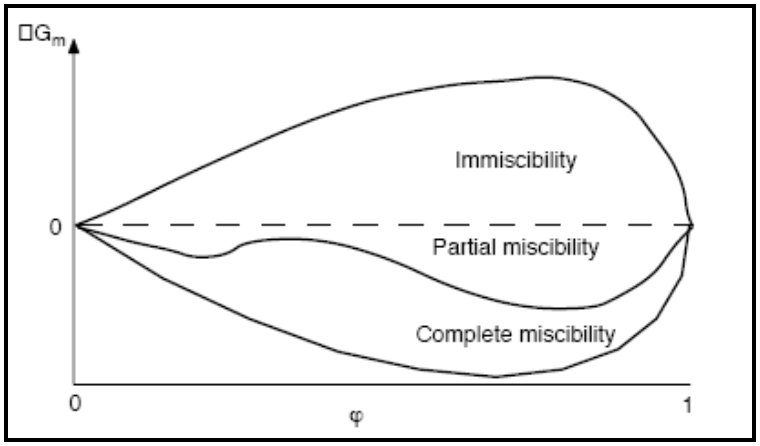

Figure 4 Gibbs free energy of a mixture as a function of polymer concentration.[2]

The behavior of a polymer in different solvents or in a particular solvent but at different temperatures and pressures is described by the three forms of Gibbs free energy.

Polymers usually dissolve in solvents having similar in properties to theirs, the rule of "like dissolves like." This rule can likewise be applied to the solubility of polymers in SCF. Polar and hydrocarbons polymers are soluble in polar and hydrocarbon SCFs.[2] The Hildebrand solubility parameter was derived from this idea and it states that: "A polymer should have a good solubility in a solvent if its solubility parameters are closely matched." The Hildebrand solubility for supercritical fluids can be calculated from the equation below.

$$\delta = \left((u^{ig} - u)/v\right)^{0.5} = \left((h^{ig} - RT - h + Pv)/v\right)^{0.5} \quad (3)$$

Where u is the internal energy per mole, h is the enthalpy per mole, v is the molar volume and the ideal gas value is the exponent ig.

2.5.1. Effects of Pressure on Solubility

Increasing the pressure of a supercritical system at constant temperature causes the polymer to be more soluble in the supercritical fluid which densifies simultaneously. In this state, crystalline and amorphous polymers exhibit fluid-fluid equilibria. Many polymers become highly swollen and plasticized in the presence of $scCO_2$.[43] This is caused by the depression in the melting temperature of the polymer. Plasticization is caused by the change in melt properties due to small molecule solvents in the polymer[9]. In cellular polymer production (Figure 5), plasticization takes place when the blowing agent dissolves into the melt under pressure. Plasticization affects three major areas are vital to cellular polymer production.

- Viscosity μ: a polymer melt usually experiences a drop in the viscosity with increase in the gas concentration
- Gas diffusivity *D*: the ability of the gas to diffuse into the polymer depends on the gas-melt interactions
- Crystallinity of the polymer
- Gas-polymer interfacial tension σ: this is dependent on the interfacial tension of the gas-melt, gas, and melt

$ScCO_2$ has no interfacial tension which makes it very suitable in solubility applications. Its solubility depends also on temperature and pressure.[43, 44]

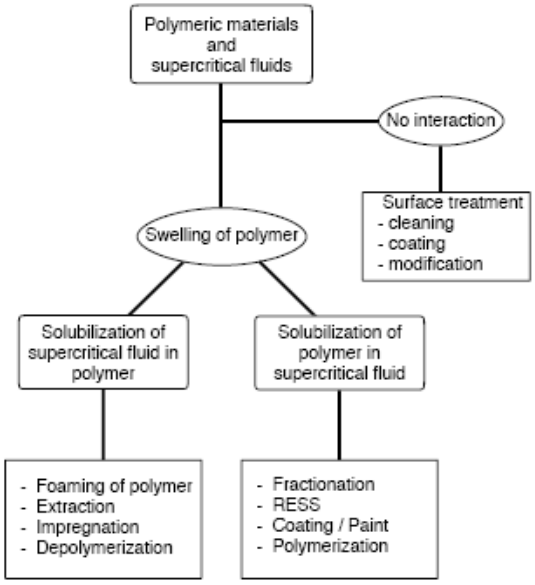

Figure 5 SCF (CO_2) interactions and potential applications with polymers.[2]

The temperature of $scCO_2$ being below 35°C enables work at moderate temperatures; thus, $scCO_2$ is more convenient for processes carried out with thermally unstable materials. In addition, removal of the supercritical solvent by simply releasing the pressure eliminates the costly solvent separations and provides solvent free high purity products. $ScCO_2$ processes are also very important environmentally.

2.5.2. Effects of Temperature on Solubility

When the temperature is increased within a polymer-fluid system, there is relaxation or increase in the flow of the polymer. This can cause full miscibility between the polymer and the supercritical fluid. A critical concentration is a distinctive point where it is a function of the molar weight and distribution of the polymer.[45] Figure 6 shows the Lower and Upper Critical Solution Temperature (L-U-CST) at constant pressure. As the temperature increases in a binary system, a two phase system moves into

a single phase and as the temperature is further increased, the single phase goes back into a two phase system.

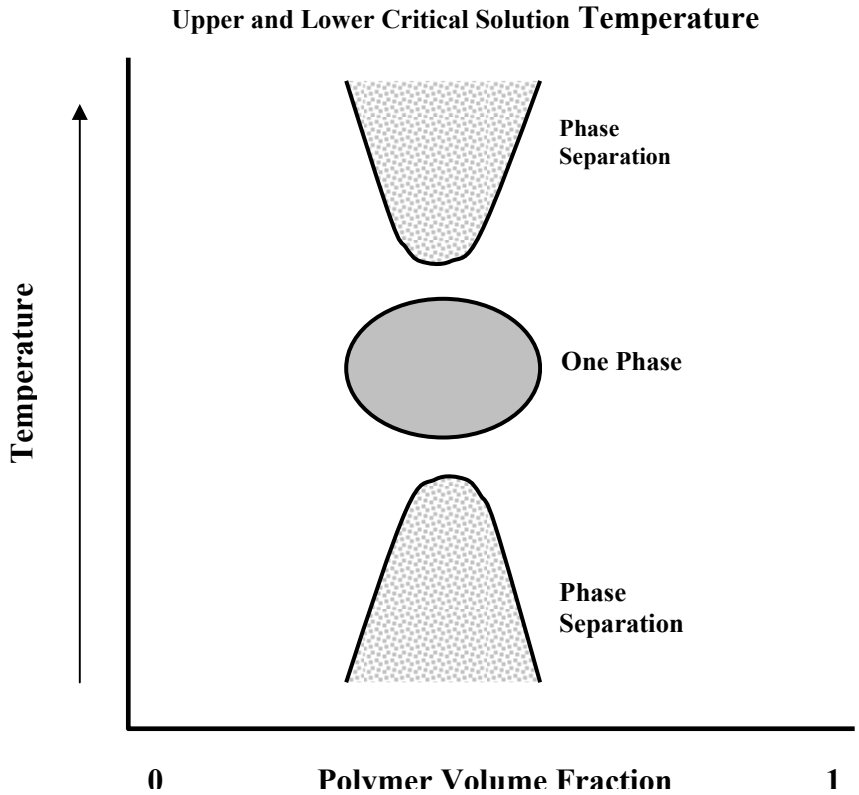

Figure 6 Lower and upper critical solution temperature at constant pressure with increasing temperature.

Due to the liquid like density of $scCO_2$, many compounds dissolve at degrees higher than the ones predicted by the ideal gas formulations. Since the solvating power of a SCF is directly proportional to its density, varying the temperature and pressure will make it possible to tune the density and thus control the solubility and separation of a specific material as stated previously. Below are the critical temperatures and pressures

of commonly used supercritical fluids and important properties of $scCO_2$ and (Table 5 and 6)

Table 5 $ScCO_2$ fluids.

Fluid	T_c **(°C)**	P_c **(MPa)**	ρ_c**(kg.m^{-3})**
Carbon dioxide	31	7.38	468
Nitrogen dioxide	36.4	7.24	457
Ammonia	132.4	11.299	235
Water	374.1	22.1	317
Ethylene	9.5	5.06	220
Ethane	32.5	4.91	212
Propane	96.8	4.26	225
n-Pentane	196.6	3.37	232
Cyclohexane	279.9	4.03	270
Benzene	289.5	4.92	304
Toluene	320.8	4.05	290
Methanol	240.0	7.95	275
Ethanol	243.1	6.39	280
Isopropanol	235.6	5.37	274
Acetone	235.0	4.76	273
Trifluoromethane	26.2	4.86	N/A
Chlorotrifluoromethane	28.9	3.87	N/A
Propylene	91.8	4.60	N/A
Trichlorofluoromethane	198.1	4.41	N/A

Table 6 Benefits of $scCO_2$ as industrial solvents.

Environmental Benefits	**Health and Safety Benefits**	**Chemical Benefits**	**Process Benefits**
Does not contribute to smog	Non-carcinogenic	High miscibility with gases	No solvent residues
Does not damage ozone layer	Non-toxic	Altered cage strength	Facile separation of products
No acute ecotoxicity	Non-flammable	High compressibility	Low viscosity
No liquid waste		Local density augmentation	Adjustable solvent power
		High diffusion rate	Adjustable density
			Inexpensive

2.5.3. Solubility Experiments

In the past years, not much attention on the measurement of solubility of CO_2 in molten polymers at high pressures due to the lack of understanding of supercritical CO_2 in the role polymer processing. Approximately five decades ago, solubility measurements were done and data was obtained at average pressures in polystyrene and polypropylene melts.[46-48] The measurement was performed by placing a molded sample of the polymer in a hollow cylindrical tube and pressurized with gas. The change in the pressure (pressure drop) as a function of time was used to determine diffusion coefficient. The solubility was determined from the system volume, temperature, same weight and the pressure drop.

In recent years, the development of various experimental techniques for measuring the solubility has been created. These techniques can be divided into two categories: static and dynamic.[5] Static methods are the most widely used of the two categories because they are simple and allow the measurement of a broad range of properties compared to the dynamic methods; this attractive to investigators and researchers studying the broad field of solvent-solute interactions. The most frequently used static methods are phase separation[49], volumetric[50] and in-situ and ex-situ gravimetric[51] methods. More complex and elaborate equipments and more sample material are required when using the dynamic methods. It is used in measuring solubility in semi-continuous and continuous processes such as extrusion and extraction. Dynamic methods used are view cell and various gas flow methods.

The main idea or principle behind the use of the gravimetric method is the weight difference between an unsaturated polymer and gas saturated polymer. A magnetic suspension balance (MSB) has been developed[52] to measure the solubility of CO_2 in

polymers (Figure 7). One of the merits of the MSB is that it can be used to measure solubility at high temperatures and pressures without having direct contact between the balance and sample.

The amount of CO_2 absorbed by the polymer sample can be determined from the relationship below

$$W_{CO_2} = \Delta W + \rho_{CO_2}\left(V_P(P,T,S) + V_B\right) \quad (4)$$

where ΔW is the weight difference between a polymer sample in the absence of CO_2 at time $t = 0$ and the same sample equilibrated with CO_2 at a desired temperature T and pressure P until a constant weight id reached. The second term in Eqn. (4) is a buoyancy correction term which is required since polymers swell significantly in the presence of dissolved CO_2. ρ_{CO2}, V_P (P, T, S), and V_B are the density of CO_2, the volume of the swollen polymer after contacting CO_2 with a solubility (S), and the volume of the basket, respectively.

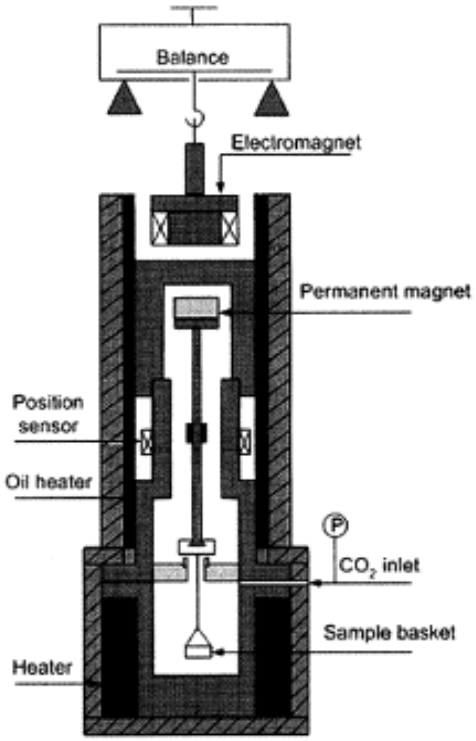

Figure 7 The MSB apparatus used for the solubility measurements.[3]

2.5.3.1. Phase Separation Method

In using this method, the polymer samples are exposed to the desired gas pressure ($scCO_2$) in an autoclave. After a desired exposure time, samples are taken from the polymer rich phase and CO_2 rich phase of the system. The amount of CO_2 in the polymer rich phase determines the solubility of the CO_2 in the polymer. This method of testing the solubility is primarily used for polymers with low viscosity. Polymers with high viscosity are not suitable because the mixing of CO_2 with the melt would be low therefore hindering solubility.

2.5.3.2. Pressure Decay (Volumetric) Method

The sorption of a gas into a polymer reduces the pressure in a closed system as a function of time until equilibrium is reached. The pressure, temperature, empty volume of

the system and the volume occupied by the sample are all used in the calculation of the amount of CO_2 initially present in the system. Even with a very small reduction in the pressure, it will be noticed and marked by using the system volume. Since swelling inevitably occurs in a pressurized system the theoretical Sanchez Lacombe Equations of State (S-L EOS) is used to estimate the swelling of polymers due to the dissolved CO_2. The temperature, pressure and swelling of the polymer are all used to calculate amount of free CO_2 present. This is then used to calculate the amount of CO_2 dissolved by subtracting it from the initial amounts of CO_2. According to the S-L EOS theory, the molecules of the polymer are ordered in regards to a lattice structure. Due to the presence of "holes" in the lattice, the theory accounts for the change in volume and does not require a separate parameter to account for the flexibility of the molecule. The S-L EOS is given by

$$\tilde{\rho}^2 + \tilde{P} + \tilde{T}\left[\ln\left(1-\tilde{\rho}\right) + \left(1-\frac{1}{r}\right)\tilde{\rho}\right] = 0 \tag{5}$$

$$\tilde{\upsilon} = \frac{1}{\tilde{\rho}} \tag{6}$$

where $\tilde{\rho}$, $\tilde{\upsilon}$, $\tilde{P}$, $\tilde{T}$ and r are the reduced density, specific volume, pressure, temperature and the number of the lattice positions occupied by the molecules respectively.

2.5.3.3. Gravimetric Method

This method of solubility measurement is one of the most common amongst scientists and researchers. Gravimetric measurement technique can be divided into two types: in-situ gravimetric and ex-situ gravimetric.

In-situ gravimetric measurements of polymer-gas solubility have been used and made popular by works of investigators such as Bonner and Prausnitz, Wissinger and Paulaitis and Sato et al. and the inexpensive and simplicity of the system. The measurements are conducted by placing dry samples of polymer material in a pan suspended from a calibrated spring within a high pressure vessel. The polymer begins to swell as SCF is introduced under pressure due to the absorption of CO_2 by the polymer. A cathetometer records the weight of the polymer sample extension. Usually the polymer is denser that the surrounding SCF and as the SCF is absorbed into the free volume of the polymer, it becomes even denser. The new weight of the sample is used to calculate the amount of gas absorbed by the polymer. The equation for calculating the solubility which is based on the spring extension as presented by Zhang:

$$\Delta m = k(x - x_0) + \rho_g (V_P + V_t) \tag{7}$$

where Δm is the mass of CO_2 absorbed, k is the spring constant, and ρ_g is the density of the SCF. The term (x-x_0) is the spring extension from initial conditions, and the term (V_p+V_t) is the total volume of swollen polymer plus pan and spring volumes.

The ex-situ gravimetric measurement technique was developed by Berens et al. in 1988[53] and is conceivably the most easy to use technique when looking from an instrumentation point of view. The technique process first involves the saturation of a polymer in SCF in a high pressure vessel for a desired time to achieve equilibrium conditions which is then followed by quickly removing the sample from the pressure vessel and measuring the weight loss over a time period in ambient air.[53] The solubility is obtained by plotting the desorption data and using a fit curve to extrapolate backwards

from the time of the first recorded measurement to the time pressure was initially released.

2.5.3.4. Dynamic Method

In dynamic solubility experiments where semi-continuous and continuous processes are used to accomplish it, two of the most commonly used techniques for polymer-gas solubility studies are the dynamic view cell and the flow methods. In the dynamic view cell method, the polymer sample is continuously compressed through an extruder in the presence of gas (SCF) while in the flow method, gas (SCF) is continuously passed through the system in the presence of palletized polymer sample. Solubility of $scCO_2$ in extruded polystyrene (PS) has been explored by Zhang, Xanthos and Dey.[54, 55] In the dynamic system, pressure is produced by an extruder upstream of a sight glass and is controlled through a metering valve downstream of the sight glass. Solubility is calculated by metering CO_2 and the polymer introduced to the extruder. This process is less precise and unfavorable for small scale experiments since it requires a large amount of extrudable samples and it is limited to conditions above the glass transition of the polymer-SCF system since it has to be extruded.

2.5.4. Difficulties and Drawbacks of $ScCO_2$

$ScCO_2$ has a low dielectric constant and a very low polarizability in the compressed phase which diminishes the ability to form sufficient strong van der Waals interactions between the solvent and the solute. This makes $scCO_2$ a poor solvent for most non-polar compounds and for most of the polar non-volatile compounds. Most polymers having high molecular mass are not soluble in $scCO_2$.

2.5.5. Glass Transition (T_g) Depression

The glass transition is a property of a polymeric material. It is the temperature at which a polymer transits from a hard or stiff, glass like state to a soft or flexible, rubber like state. There are three basic methods used in the measurement of the glass transition temperature: physical, thermal and mechanical. Gravimetric and dilatory methods are types of physical methods used in the measurement of T_g. They are usually used in conjunction with sorption experiments because they use very similar instrumentation. The T_g is detected by a change in the rate of polymer weight gain during solvent sorption and changes in the rate of polymer swelling in the gravimetric and dilatory methods respectively. Neither of the methods is used in extensive and comprehensive studies of the glass transition because of the imprecise result which is caused by the understated discontinuities of the slope relied upon.

The use of the thermal measurement technique for the T_g is usually centered on the use of a differential scanning calorimetry (DSC). The idea behind the use of this technique is the difference in the amount of heat required to raise the temperature of a sample and reference are measured as a function of temperature. As the sample is heated to the glass transition temperature within the calorimeter, the T_g is recognized by a sudden change in the heat capacity of the sample as compared to that of a reference.

The mechanical approach uses changes in creep compliance and density measurement via ultrasonic waves. The simple and easy approach to achieve precise measurements makes the creep compliance method a very commonly used method. A piece of sample material is suspended vertically at one end in a pressure vessel with a weight attached to the other end. Pressure is introduced to the chamber and the creep

compliance rate is measured visually using a cathetometer as a function of pressure. The immediate incraese in the creep compliance is used to identify the T_g.

The change in the speed of high frequency sound correlates to the the change in the Young's modulus of a material; this is used in the ultrasonic method technique[21]. Sudden changes in the Young's modulus identifies the T_g when pulse-echo ultrasound measurements of a polymer-SCF system inside a pressure vessel are taken and overlayed with reference spectra.

CHAPTER 3

EXPERIMENTAL

CHARACTERIZATION OF UNFOAMED AND FOAMED PCL-MB BLENDS

3.1. Materials

The poly (ε-Caprolactone) PCL (CAPA FB100) PCL resin used in this work with a molecular weight of 100D (M_w = 100,000) was supplied by Solvay Caprolactones (Cheshire, UK). The MB NFO1U ™ resin, a biodegradable material comprising starch, synthetic polyester, and plasticizers was supplied by Novamont S.p.a (Italy). Pure components and blends containing 10, 20, 25 and 33% by weight of MB were investigated. Table 7 shows the sample and their designation.

Table 7 Sample designation.

	PCL	**MB10**	**MB20**	**MB25**	**MB33**	**MB**
MB (%)	0	10	20	25	33	100
PCL (%)	100	90	80	75	67	0

3.2. Experimental

3.2.1. Preparation of Blends

Both materials were blended using a co-rotating twin screw batch-type mini-extruder Brabender, USA mixing system equipped with stainless steel screws at 80rpm and a temperature of 80°C and 175°C for PCL and its blends respectively for 2 to 3 minutes. The blends were pelletized using a Fritsch pelletizer, Germany and dried in an oven at 50°C for 24hrs and then compression molded into (40 x 40) mm square sheets with thickness of 2.45mm using a Carver hydraulic hot press at 200 F for (10 to 15) minutes using 6 tons of pressure. Carbon dioxide (99.9%) was used as physical foaming agent (PFA) which gets to its supercritical point at a temperature and pressure of 31^{o}C

and 1071 psi[5]. In this study, the blends were foamed from compression molded sheets at a constant pressure of 1100 psi and at temperatures of 31°C, 33°C and 35°C and a constant temperature of 31°C and at pressures of 1100 psi, 1300 psi and 1500 psi in order to compare and evaluate the best foaming conditions that maximizes their physical, structural and mechanical properties. All the tests performed on the foams were processed at the foaming conditions.

3.2.2. CO_2 Sorption Rate

The pressure, temperature and time all play a role in the gas uptake. In this experiment, the temperature is kept constant while the pressure is changed for a soaking period. Kumar and Weller[57] studied the CO_2 uptake in polycarbonate at constant temperature and pressure. They found that at around the 75th hour with an uptake of about 90 mg/g, the equilibrium state or saturation was reached. This is caused by the different states of pressure within the system. The system is trying to achieve equilibrium; therefore there is a diffusion of CO_2 into the sample until pressure concentrations are equal.

The PCL blends are compression molded into (20 x 10) mm sheets with a thickness of 2 mm. the samples were placed in a pressure vessel and pressurized with CO_2 at 200 psi, 400 psi and 600 psi. The gas sorption was carried out at room temperature. The pressure inside the vessel was monitored and regulated by a valve whenever the pressure was dropping. The amounts of gas absorbed by the samples were monitored by periodically weighing them at intervals of 30 minutes using a precision balance with an accuracy of 10 micrograms because the amounts of CO_2 absorbed were on the order of milligrams. This method of measurement is a rough but not precise

estimate the gas sorption by the blends. Whenever the samples are removed from the pressurized chamber, desorption starts to take place. Between the time of depressurization and measurement of the samples, there could be a significant rate of desorption taking place. The glass transition of the polymer also has a role to play with this; the closer and farther away the glass transition of the polymer is above and below the temperature of where the measurement takes place, the greater the chances for desorption rates to increase. The better way of accurately measuring the sorption rate is to use an in-situ gravimetric balance technique. This is placed inside the pressure chamber with the samples on it. Measurements can be read of a gage outside the chamber while the samples are kept pressurized. In this case, measurement errors due to desorption are eliminated. In the study of the sorption of CO_2 in polymethyl methacrylate-clay nanocomposites investigated by Naquib et al., the measurement of CO_2 was done by the use of an in-situ gravimetric technique.[62]

3.2.3. Preparation of Cellular Foams

The foaming of the samples was performed by the second method of sudden depressurization. The pressure vessel was cooled down to -100°C using liquid nitrogen. The compression molded samples were then saturated in the pressure vessel with CO_2 gas to their processing temperatures, constant pressure and vice versa as stated previously which is at or above the supercritical temperature and pressure of CO_2. At the processing temperature and pressure, the vessel was depressurized. The sudden change in pressure caused the nucleation of microvoids in the polymer matrix. This also results from the change in the thermodynamic state. Figure 8 shows the schematic of the process. The CO_2 tank (A) supplies CO_2 into the chamber (C) which contains the sample through a gas

line (B). The heat supply (D) raises the temperature and pressure to the required processing temperature where it is then depressurized through the pressure release valve (E).

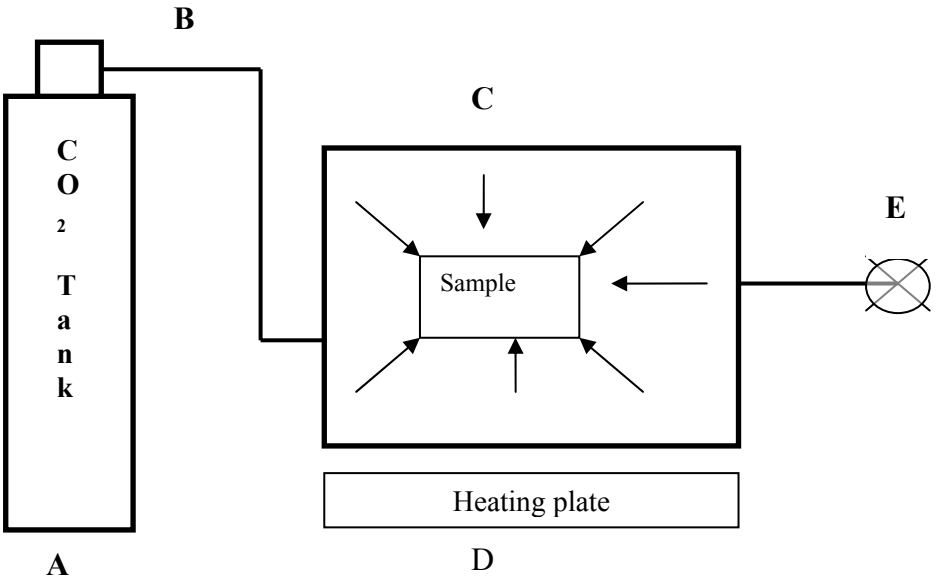

Figure 8 Schematic of the foaming process showing the CO2 tank, pressure vessel, heating plate and depressurization valve.

3.2.4. Foam Density Characterization, Calculations and Analysis

The polymer and foam density ρ_f and ρ_m were measured as per ASTM (D1505-98) and (D1622-98) standard testing method[56, 61] which is based Archimedes principle (water displacement); by measuring the volume of water displace by the sample when it is fully immersed and dividing it into the mass of the sample mass. Due to the thin layer of skin around the foam sample, there is no or insignificant absorption of water by the foam during this process.[11] The relative foam density ρ_r was determined using the method suggested by Kumar and Weller.[57] The relative foam density ρ_r is the ratio of the foam density ρ_f and the unfoamed polymer density ρ_m.[4, 57] The cell morphologies of the foamed

samples were characterized by scanning electron microscopy (SEM). The samples were cryo-fractured in liquid nitrogen. The fractured surfaces were coated with a thin layer of gold using a sputter coater to prevent sample charging. The surfaces were examined using a Quanta 200 environmental scanning microscopy. The micrographs obtained were analyzed to estimate the average cell diameters D, cell density N_o, and void fraction V_f using methods suggested again by Kumar and Weller.[57]

The cell morphologies of the foamed samples were characterized by a environmental scanning electron microscopy (SEM), Quanta 200 after being cryofractured in liquid nitrogen. The decision to cryo-fracture the sample was based on the fact that when a fracture meets a void or a cell, it will propagate along its weakest axis which is the diameter[4]. This provides the user with the maximum projected surface area of the cells unlike slicing the sample with a blade which will not run through the diameter of all cells within its range. To obtain the cell density N_f, V_f and N_o were calculated using a method suggested by Kumar and Weller.[57] An SEM micrograph containing 100-200 cells were obtained and the number of cells, n, in the micrograph is determined. If A represents the area of the micrograph in cm^2 and M is the magnification then the linear density or number of cells per cm of the foam is the square root of $(n/A/M^2)$. Therefore, the volume density or the number of cells per cm^3 of the foam will be the cube.

$$N_f = \left(\frac{nM^2}{A}\right)^{3/2} \tag{8}$$

At the same location of the micrograph, a high magnification image is obtained. The averaged diameter of the cells D is determined by measuring the major and minor diameters of approximately 25 cells was suggested by Kumar and Weller.[57] The volume occupied by the voids in one cm^3 of foam V_f can then be determined by

$$V_{\mathrm{f}} = \frac{\pi}{6} D^3 \times N_{\mathrm{f}}, \tag{9}$$

The volume occupied by the polymer in one cm^3 of foam is approximated by (1 - V_f). We can now estimate the number of cells nucleated per cm^3 of the initial unfoamed polymer N_o from Eqn. (10)

$$N_0 = \frac{N_{\mathrm{f}}}{1 - V_{\mathrm{f}}}, \tag{10}$$

3.2.5. Mechanical Properties

Cellular foams are one of the packaging industry's most commonly used materials. During the transportation of products or fragile items, these items are usually exposed to different kinds of forces like tensile, compressive, shear and impact forces. Due to the application of these blends, the tests that were carried out were compression test, tension test, quasi-static shear test, instrumented impact test.

3.2.5.1. Tensile Test

The foamed samples were prepared according to the Type C specimen of ASTM standard D1623[63]. The foamed samples were cut into rectangular shapes with a cross-sectional area of 645.14mm^2 and a thickness of 10mm. The bonding surfaces of the

fixtures were made of hardwood and mechanically fastened to the machine's test fixture made of aluminum. Due to the rougher and more porous surface of the hardwood, it has greater bond strength than aluminum or other kinds of metals with the samples when bonded by an epoxy. The epoxy used was a two part epoxy, epoxy and hardener. The epoxy contained polyamide, amorphous silica, amine curing agents and epoxy. The tests were conducted on a hydraulic MTS machine under room temperature at 22°C at a crosshead speed of 0.05in/min. The unfoamed samples were prepared according to Type IV specimen of ASTM standard D638.[64] The samples were compression molded with a width, thickness, narrow section length and overall length of 25.44mm, 3.3mm, 142.24mm and 67.45mm respectively. The tests were conducted on a hydraulic MTS machine under room temperature at 22°C and atmospheric pressure at a crosshead speed of 0.2in/min.

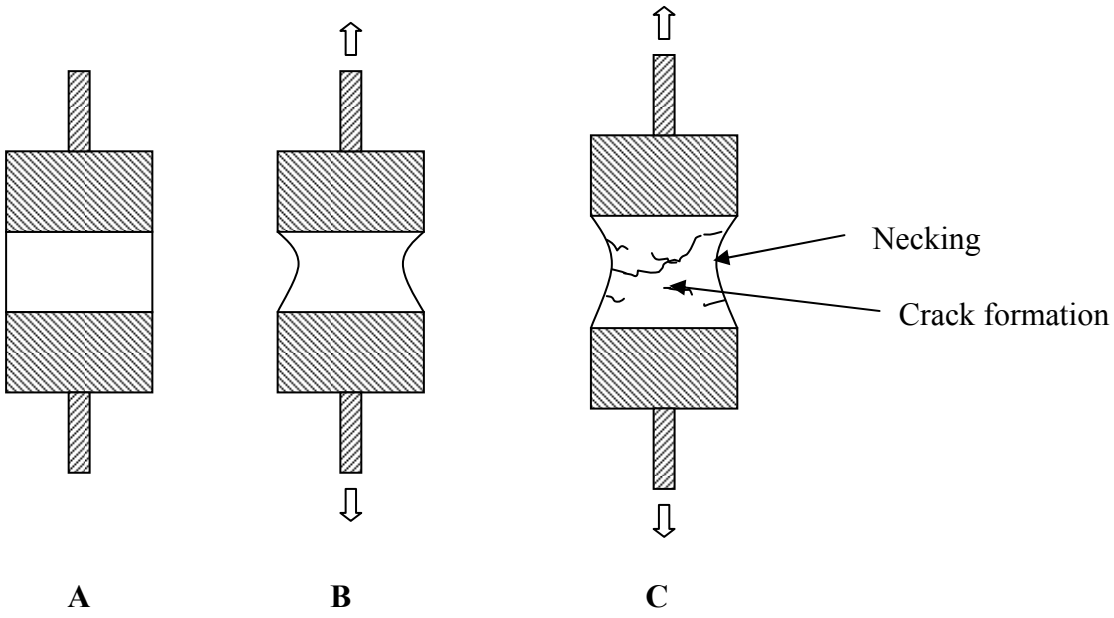

Figure 9 Deformation of the samples during testing; (A) Sample mounted to the fixture before loading. (B) Sample undergoing loading; necking of the sample. (C) Necking and crack formation of the sample.

Figure 9B shows necking occurring in the sample during the test; this is caused by work hardening (resistance to the applied force). Figure 9C shows further necking and crack formation due to the breaking of large, weak cell walls and struts. This crack formation eventually results in the line of fracture of the samples.

3.2.5.2. Quasi-static Shear Test

In many applications where microcellular sandwich or plastic structures are employed, these structures are subjected to transverse loading a lot of the time. In the process of this loading, the surface membranes of the sandwich usually experience tension/compression type of stress while the core usually experience pure shear. “Core shear failure”, is a common type of failure in sandwich structures. It occurs when the core

of the sandwich fails due to the shear stress reaching its critical value[66]. In a study conducted by Krishnan Kanny et. al.[67], PVC foams, HD130 and H130, linear and crosslinked respectively were tested and was found that both foams deformed without volume change and the foams failed by shearing in area of the centerline along the longitudinal axis.

The shear test was performed according to ASTM C273-61 standard test method[68]. Five samples each of PCL/MB blends were cut with dimensions of 60mm x 50mm x 5mm. The samples were bonded between two parallel loading hardwood plates which have been mechanically fastened to steel plates as shown in the Figure 10. The hardwood plates were used to improve adhesion between the samples and the fixtures. The plates were precisely parallel to each other because a small deviation in their parallelism can cause errors in the calculation of the shear strength and shear modulus. The epoxy used was a two part epoxy, epoxy and hardener. The epoxy contained polyamide, amorphous silica, amine curing agents and epoxy. The epoxy which has a curing time of 60 minutes was allowed to cure for 1440 minutes before testing took place. The parallel plate fixture was installed on a MTS machine. The tests were performed at room temperature with a displacement control at a crosshead speed of 0.0167mm/sec and a tensile mode of testing. Sample MB 33 was not tested due to low foamability which resulted in inadequate material for testing.

The shear stress τ is given by

$$\tau = P/Lb \tag{12}$$

where P is the load applied on the sample, L is the length of the sample and b is the width of the sample. The shear strain γ is given by

$$\gamma = \frac{r}{t} \tag{13}$$

where r is the displacement of one loading plate with respect to the other and t is the thickness of the sample core. The shear modulus G is given by

$$G = \frac{St}{Lb} \tag{14}$$

where S is the slope of the initial portion of load-deflection curve ($\Delta P/\Delta r$).

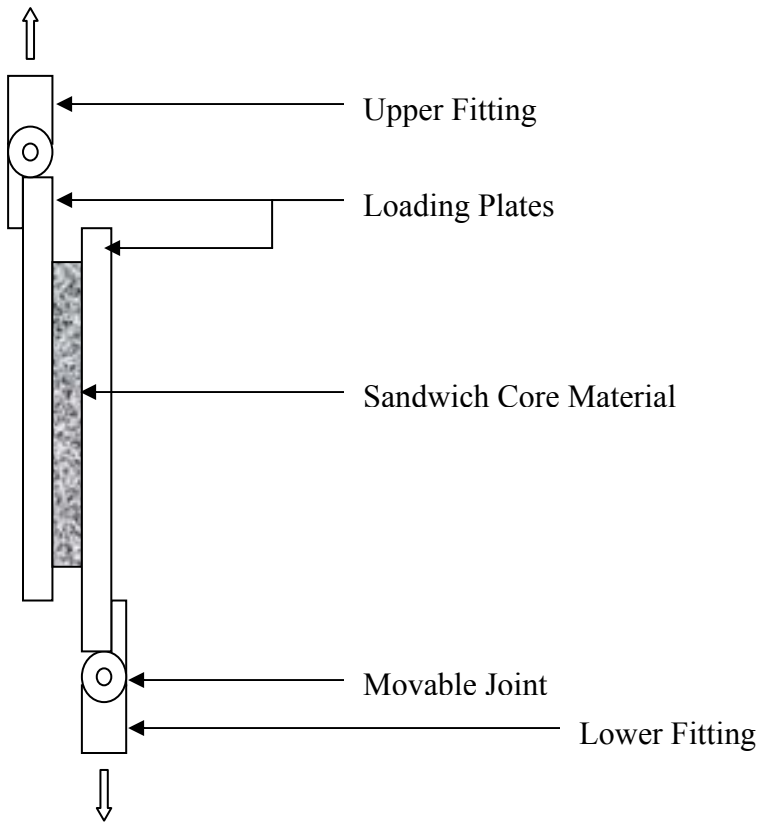

Figure 10 Schematic of shear test fixture.

3.2.5.3. Compression Test

The samples were cut into circular shapes with a cross-sectional area of 25.8cm^2 and a thickness of 2.54cm according to D1621 ASTM standard.[70] The tests were conducted on a hydraulic MTS machine under room temperature at 22°C at a crosshead speed of 0.01in/min. The samples were loaded and then unloaded; both loading and unloading curves were plotted from the incremental values obtained from the tests and used to determine the compressive strength and modulus. Sample MB33 was not tested due to the inadequate material for testing which is due to its low foamability.

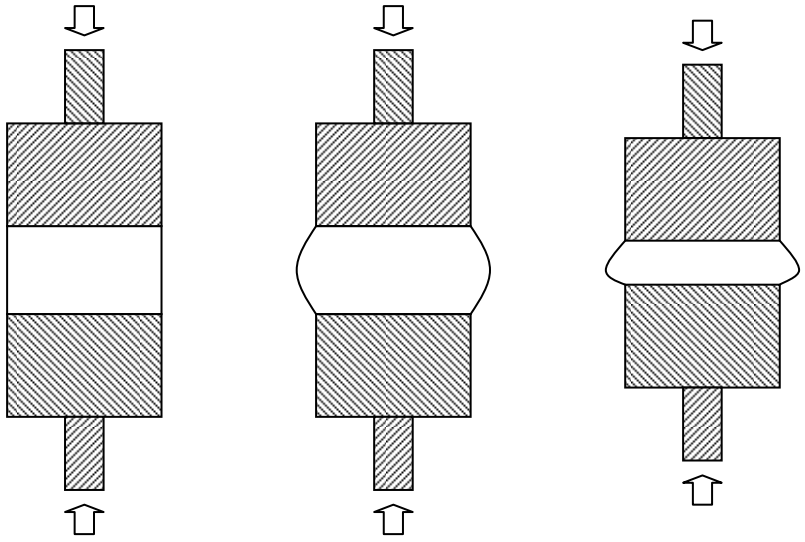

A **B** **C**

Figure 11 Deformation of the samples. (A) Sample mounted to the fixture just before loading. (B) Sample undergoing loading; there is a bulging of the sample. (C) More bulging of the sample.

Upon compressive force, the samples begin to bulge thereby increasing the cross sectional area of the sample. Figure 11 shows a deforming sample undergoing compressive load. This is preferable to a fractured sample because this foam is to be used for package. The increasing area helps cushion the package item even more.

The apparent modulus, E_C is given by

$$E_C = \frac{WH}{AD} \tag{15}$$

where W is the load applied on the sample at a point on the straight portion of the load-deflection curve, H is the initial height or thickness of the sample, A is the initial horizontal cross-sectional area and D is the deformation of the sample. The compressive strength C_s is given by

$$C_S = \frac{W}{A} \tag{16}$$

where W is the load applied on the sample at a point on the straight portion of the load-deflection curve.

3.2.6. X-Ray Diffraction (XRD)

XRD is used to analyze the degree of crystallinity in a substance. Approximately 90-95% of all solid materials can be depicted as crystalline materials. When X-rays interact with a crystalline material, the resulting diffracted ray exhibits a diffraction pattern. This pattern is like a materials signature. In 1919, A.W. Hull pointed out in report that "every crystalline substance gives a pattern; the same substance always gives the same pattern; and in a mixture of substances each produces its pattern independently of the others. " XRD is used to characterize and identify crystalline phases within a material. Today about 50,000 inorganic and 25,000 organic single components, crystalline phases, and diffraction patterns have been collected and stored on magnetic or optical media as standards[58]. XRD was used to check the crystallinity of PCL, MB and their blends before and after foaming. The existence of crystallinity in MB, PCL 100D and their blends was observed using XRD (Rigaku model D/Max – Ultima III, Japan). An angular range of 0° to 50° with a Cu-K wavelength of 1.542 A°, generated at 44mA and 40kV was used.

3.2.7. Thermal Analysis

3.2.7.1. Differential Scanning Calorimetry (DSC)

A Perkin Elmer DSC-6 differential scanning calorimeter was used to identify the endothermic peaks of the raw materials. Differential scanning calorimeter measures the

amount of energy absorbed or released by a sample as it is heated and cooled, providing quantitative and qualitative data on endothermic (heat absorption) and exothermic (heat evolution) processes. The samples were cut into small flat pieces weighing a total between 5 to 10mg which was then spread evenly to cover the base of a non volatile aluminum pan. The pan was sealed by crimping. The samples were held at 5°C for 5 minutes and then heated to 200°C at a constant scanning rate of 10°C per minute. The samples were held at 200°C for 5 minutes and then cooled down to 5°C at a rate of 10°C per minute. These heating and cooling cycles are called the first heating and cooling cycles. The sample was again held at 5°C for 5 minutes and then heated up to 200°C at a rate of 10°C per minute. The samples were held at 200°C for 5 minutes and then cooled down to 5°C at a rate of 10°C per minute where they are held. Calibration of the temperature and enthalpy scales was undertaken using a known weight of an empty scrimped aluminum pan before the test. The results give the endothermic heat flow (mW) as a function of temperature (°C). Thermal analysis was performed on the samples to investigate any effects of % wt. MB and CO_2 concentration on the melting temperatures (T_m) of the blends. The results of the investigation was used to establish the melting temperatures for the CO_2 unsaturated blends and saturated blends which were also used to establish the foam processing conditions and limits.

All the temperatures used to set the foaming conditions were taken from the DSC scans of the second heating cycles with the exception of those saturated with CO_2 which were taken from the first heating cycle. The results from the second heating cycles for the unsaturated samples were used alone because the first heating cycle usually contains residual stresses and sometimes impurities which alter the data obtained. After the first

heating cycle, the previous thermal history would have been erased from the samples; all residual stresses and possible impurities would have been erased. In the second heating cycle, the true thermal properties of the samples would be reflected in the captured data.

3.2.7.2. Dynamic Mechanical Analysis (DMA)

Dynamic mechanical analysis can be used to measure more accurately, the glass transition of a polymer compared to the DSC technique because it is more sensitive. The glass transition is derived by getting the ratio between the storage and loss modulus which are measured during the test. The alpha relaxation (α-relaxation) depicts the glass transition of the polymer.

The glass transition was measured using a dynamic mechanical analyzer (DMA), Rheometric Scientific Analyzer 3 (RSA3) operating in the compression mode. Deformation was applied in the 3 point bending mode. Samples were cut into 25mm X 7.9mm X 2.4mm and scanned at a heating rate of 2°C/min, and a frequency of 1Hz. The samples were scanned from -135°C to 150°C and at a strain and force of 0.2% and 50g which was determined from a sweep test run for each sample which were used for the dynamic temperature ramp test.

CHAPTER 4

RESULTS AND DISCUSSION

4.1. CO2 Sorption

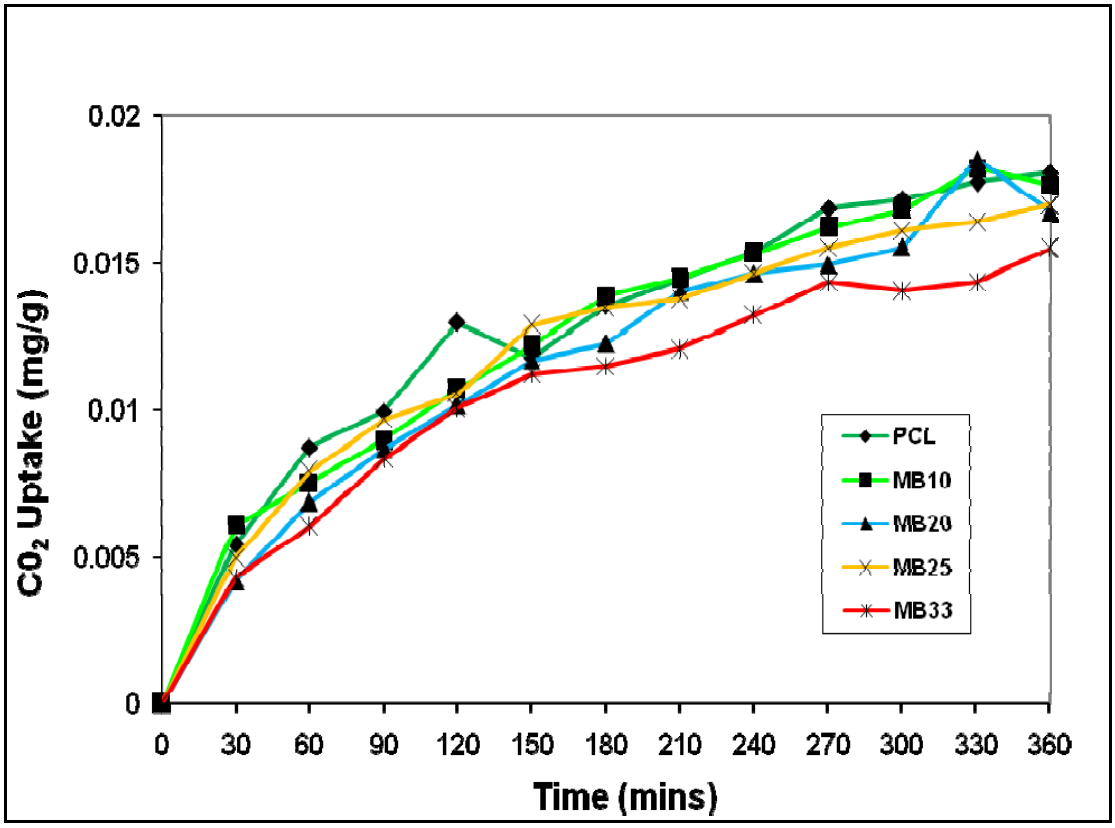

Figure 12 Plot of carbon dioxide uptake at 200 psi and room temperature in polycaprolactone-MB blends as a function of time.

In Figure 12, there is an initial steep incline and then a gradual decrease in the steepness which means a rapid and then slow uptake of CO_2 by the blends. From Figure 12, we can say that the blends are beginning to approach the point of saturation. It can also be noted that the sample with 33% wt. MB shows the lowest sorption rate. Overall, the rate of sorption within the time frame tested could be said to be fairly steady with the exception of some unstable regions.

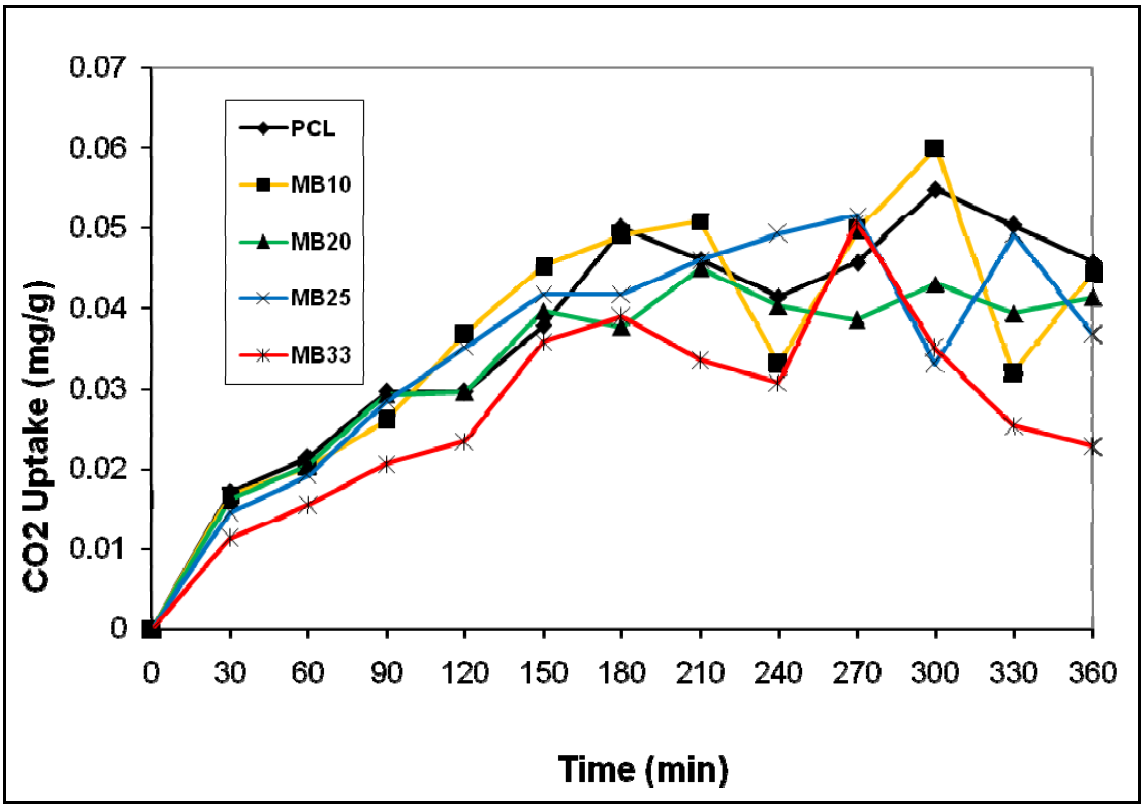

Figure 13 Plot of carbon dioxide uptake at 400 psi and room temperature in polycaprolactone-MB blends as a function of time.

Figure 13 shows initially a region between the 0th and the 150th minute where the sorption rate is steady and then another region between the 150th and 360th minute where the sorption rate is unsteady. This could be a result of the over saturation and then desorption during the measurement of the samples. Once again, it can be seen that the sample with the lowest sorption rate is the 33% wt. MB.

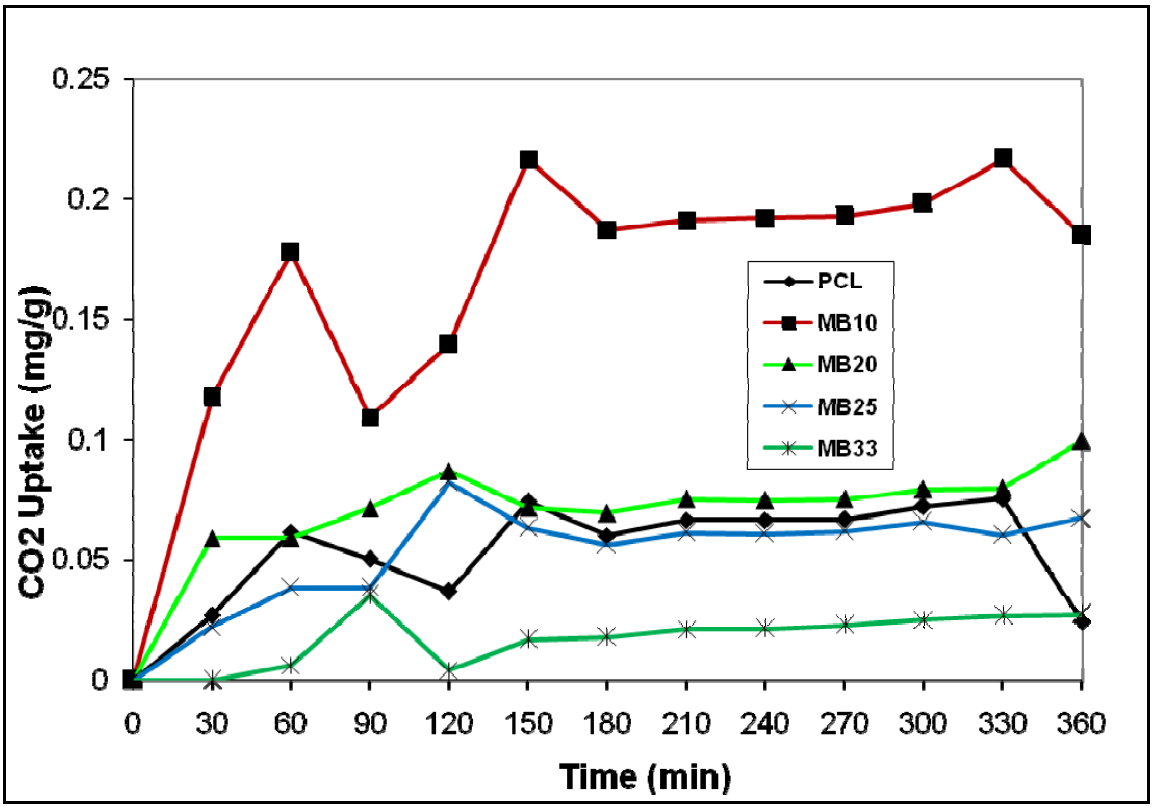

Figure 14 Plot of carbon dioxide uptake at 600 psi and room temperature in polycaprolactone-MB blends as a function of time.

In Figure 14, we can see that there are three major regions, the first between the 0th and 210th minute, the second between the 210th and 300th minute and the third which can be seen to start at around the 300th minute. The first region shows an unsteady rate of CO_2 sorption and then a steady linear rate of CO_2 sorption at the second region. The third region again begins to show instability in the sorption rate. We can also see the distinct difference in the rate of CO_2 intake of the 10% and 33% wt. MB compared to the other concentrations. The 10% and 33% wt. MB exhibit highest and the lowest rate of sorption compared to the rest of the compositions. It should be noted that the blend with the lowest sorption rate is again the 33% wt. MB. We can therefore conclude that the blend with the lowest sorption rate within the tested compositions and conditions is the 33% wt.

MB and that the rate of CO_2 sorption increases with the increase in the surrounding pressure. This reinforces the low foaming ability of that composition within the foaming process conditions.

4.2. Foam Density Characterization, Calculations and Analysis

Due to the plasticization (lowering of the glass transition T_g and melting temperature T_m of the sample caused by high concentration of co_2) that occurs and the temperature required to be reached for $scCO_2$, we are limited to a range of foam processing temperatures (31°C to 35°C). Figure 21 shows the micrographs structure of the foamed polymers under a constant gas saturation pressure of 1100 psi and at temperatures of 31°C and 33°C. Due to the depression in the glass transition, partial or sometimes complete melting of the sample takes place resulting in partially foamed samples. Therefore, the processing temperatures were performed at 31°C and 33°C.

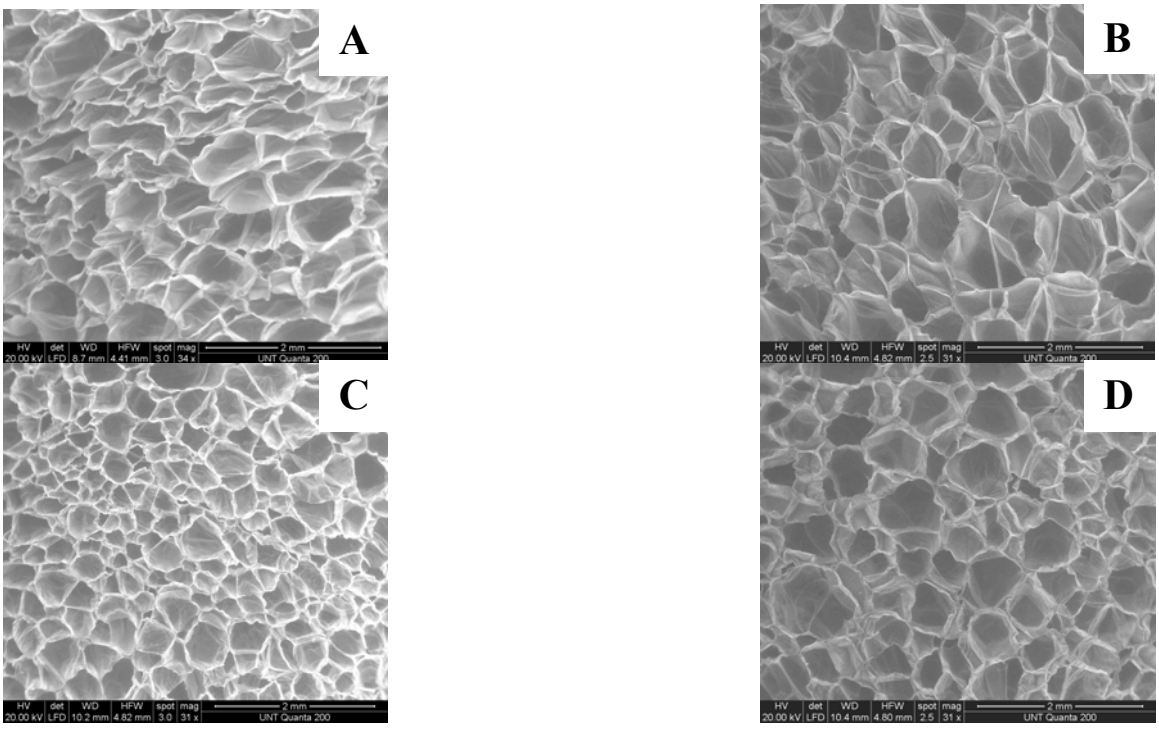

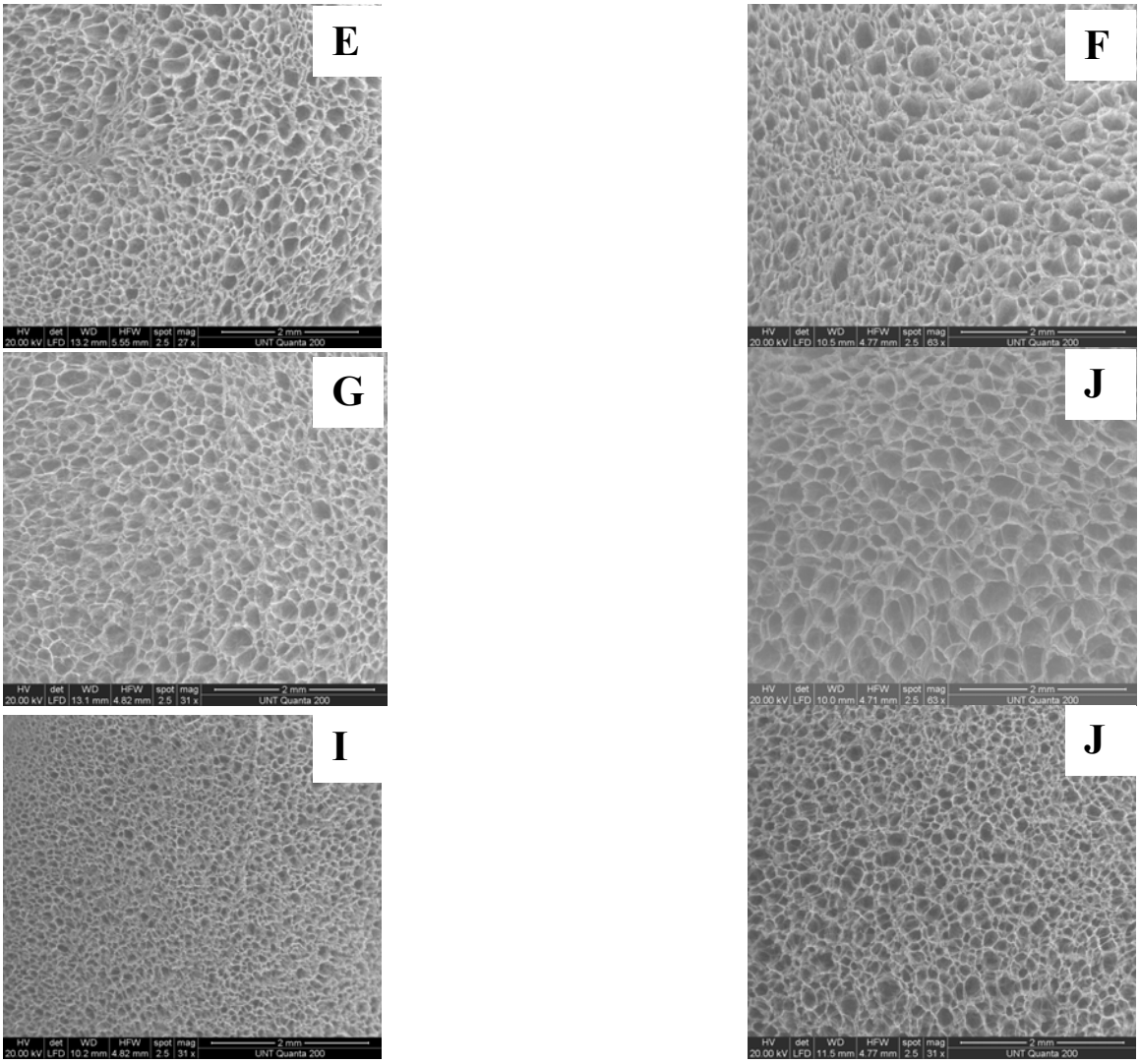

Figure 15 SEM micrograph of PCL 100D + % wt MB. (A) PCL 100D + 0% wt MB at 31°C. (B) PCL 100D + 0% wt MB at 33°C. (C) PCL 100D + 10% wt MB at 31°C (D) PCL 100D + 10% wt MB at 33°C. (E) PCL 100D + 20% wt MB at 31°C. (F) PCL 100D + 20% wt MB at 33°C (G) PCL 100D + 25% wt MB at 31°C. (H) PCL 100D + 25% wt MB at 33°C. (I) PCL 100D + 33% wt MB at 31°C. (J) PCL 100D + 33% wt MB at 33°C all processed at 1100 psi.

Table 8 Summary of experimental conditions and results at 31°C foaming temperature with foaming pressure and time held constant at 1100 psi and 10 sec, respectively.

Parameters	% wt MB				
	0	10	20	25	33
Polymer Density, (ρ_f) (g/cm^3)	1.133	1.06	1.181	1.360	1.167
Foam Density, (ρ_m) (g/cm^3)	0.0443	0.0389	0.0756	0.0680	0.0900
Relative Foam Density, (ρr)	0.0391	0.0367	0.064	0.0500	0.0771
Average Cell Diameter, (D) (mm)	0.00500	0.00317	0.00140	0.00158	0.00098
Cell Density, (N_o) (cells/cm^3)	76761	304397	3483261	10041360	2328348
Void Fraction, (V_f) (%)	96.09	96.57	95.56	95	92.29

Table 9 Summary of experimental conditions and results at 33°C foaming temperature with foaming pressure and time held constant at 1100 psi and 10 sec, respectively.

Parameters	% wt MB				
	0	10	20	25	33
Polymer Density, (ρ_f) (g/cm^3)	1.1330	1.06	1.181	1.360	1.167
Foam Density, (ρ_m) (g/cm^3)	0.0425	0.0567	0.0850	0.0756	0.0750
Relative Foam Density, (ρr)	0.03751	0.0535	0.072	0.0556	0.0750
Average Cell Diameter, (D) (mm)	0.00591	0.00567	0.00213	0.00291	0.00142
Cell Density, (N_o) (cells/cm^3)	46537	52175	979325	381706	3250262
Void Fraction, (V_f) (%)	96.25	95.00	95.00	94.44	92.50

Tables 8 and 9 above give the foam properties that have been determined from the various suggested measures by the ASTM standards[56, 61] and Kumar and Weller.[57] Upon further observation of the micrographs and tables above (Figure 15, Table 8 and 9), it can be seen that the cell sizes decrease and increase with an increase in the MB concentration and processing temperature, respectively. For example, when 10% MB is introduced into PCL, the effect of changing temperature is to increase the size by **%. In while in the pure PCL the increase is **%. The physical appearances of the samples also change with % wt MB concentration from bright white to cream white.

Overall, the physical, structural properties do not have significant changes from the processing temperatures between 31°C and 33°C. Therefore, we can say that the processing temperature and the MB concentration are directly and inversely proportional

to the cell size. Eqn. (11) and Figure 16 is the mathematical and graphical representation of the relationship between processing temperature and MB concentration in the PCL-MB blends respectively.

$$\boldsymbol{D}_{\text{(PCL-MB)}} = k\frac{T}{C} \qquad \textbf{(11)}$$

where D is the cell size of the blends, T is the processing temperature, k is a constant and C is the MB concentration.

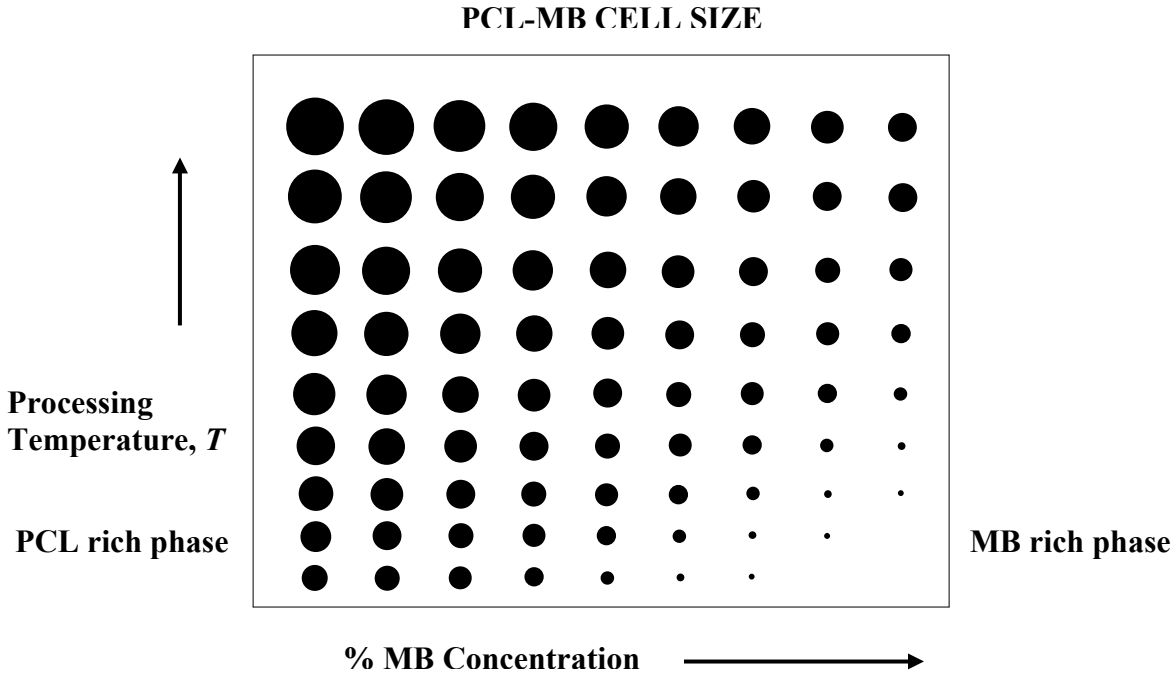

Figure 16 Graphical representation of cell size as a function of processing temperature and % MB concentration.

Upon closer observation of the PCL + 0 wt % MB at 31°C and 33°C (Figure 17), there have been found to be cell bubbles with distinct wall thickness; one which is common throughout the structure (Figure 17B) and another which can be seen in select

places within the structure (Figure 17A). For reference purposes, the common cell wall will be called the major wall while the uncommon cell wall will be called the minor wall.

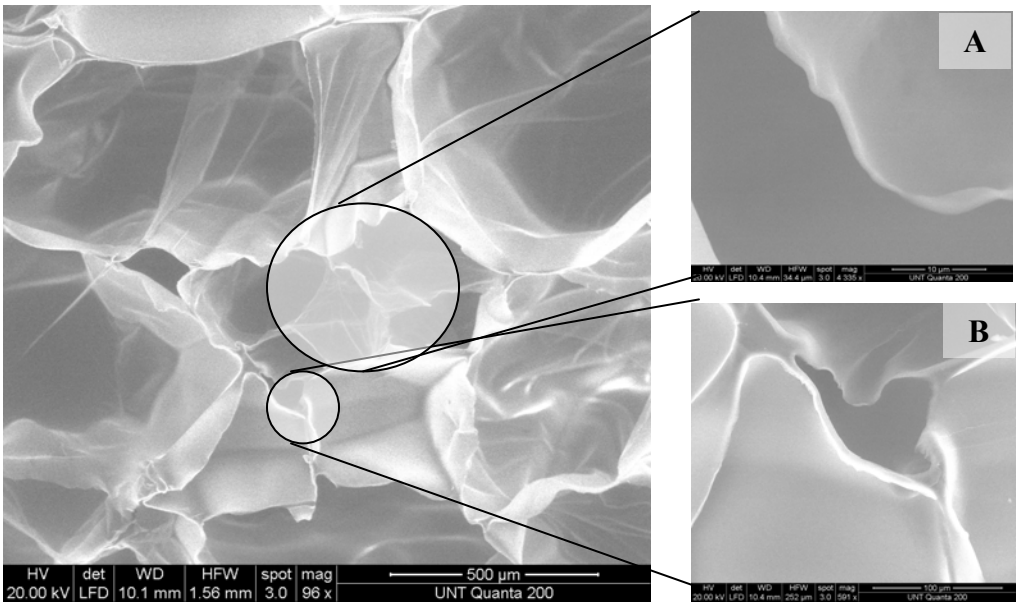

Figure 17 SEM micrograph of microcellular polycaprolactone foam with major and minor walls. (A) and (B) Shows a magnified graph of minor and major wall respectively.

The minor walls which are transparent seem to form within the major walls (common cell bubble) and have an average thickness of one tenth that of the major cell walls. The characteristics of the walls are shown in table 10 below.

Table 10 Characteristics and thickness of walls found in polycaprolactone SEM micrographs.

Walls	Thickness at 31°C (µm)	Thickness at 33°C (µm)	Thickness at 35°C (µm)	Transparency
Major	8.33	5.3000	N/A	Opaque
Minor	1.07	0.5858	N/A	Transparent

A potential explanation for the formation of such thin cell bubbles within thicker and bigger cell bubbles is that secondary nucleation takes place during the final seconds of the nucleation of the cells. This secondary nucleation grows from the original cell

bubble walls which still contain densified supercritical CO_2 ($scCO_2$) and form cell bubbles within them. PCL is a very elastic and ductile polymer. It can be stretched from sheets (not transparent) into thin films (transparent). This is one property that makes PCL applicable in the packaging industry as grocery biodegradable plastic bags. The only way to validate this hypothesis is to view the nucleation of cell bubbles in-situ. This is a technique that has not yet been done on the microscale and nanoscale level before.

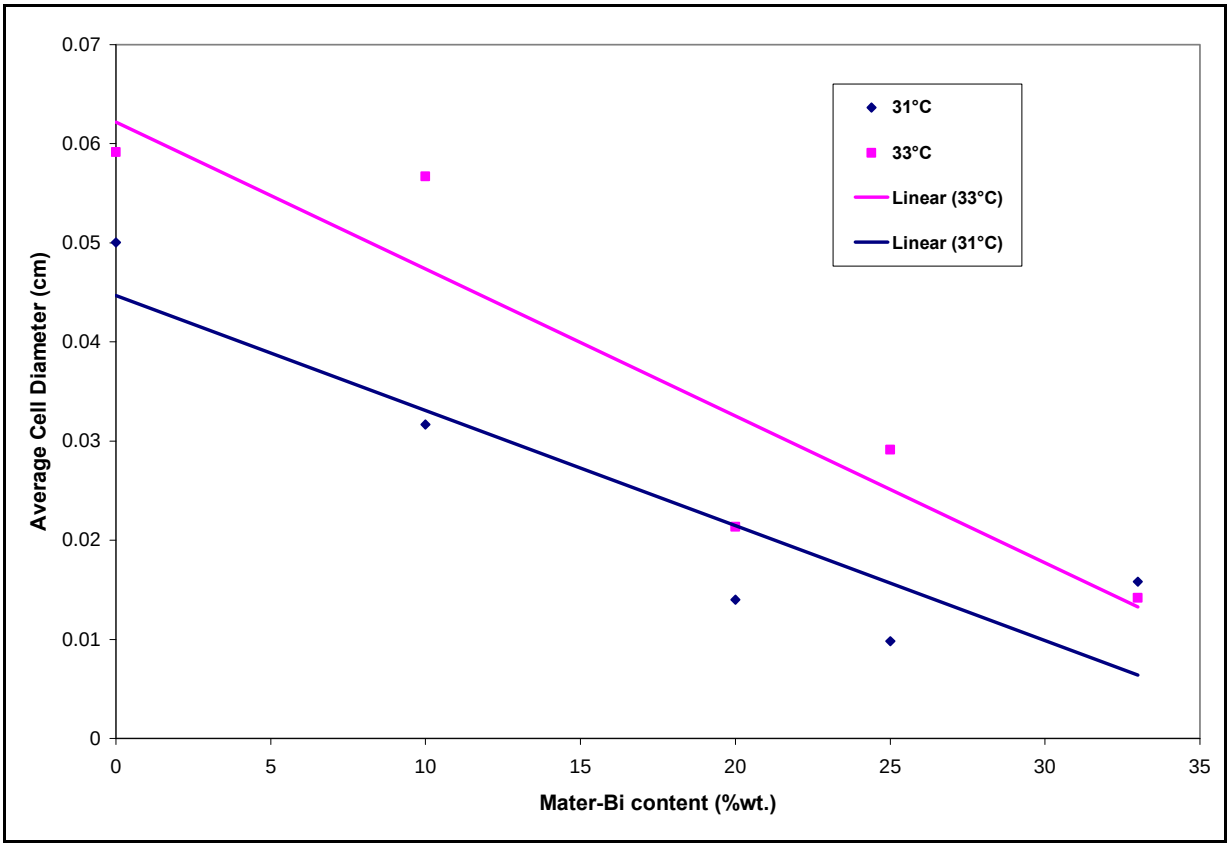

Figure 18 Plot of average cell diameter as a function of MB concentration (Samples were foamed at 31°C and 33°C at constant pressure of 110 psi).

The average cell diameter has been plotted in Figure 18 as a function of MB concentration. For the range of concentration explored in this experiment, we can say that the cell diameter decreases linearly with the increase in MB concentration. At the

foaming temperature of 31°C and 33°C, the difference in the cell diameter is at about 0.15cm and continues to plummet to about 0.075cm.

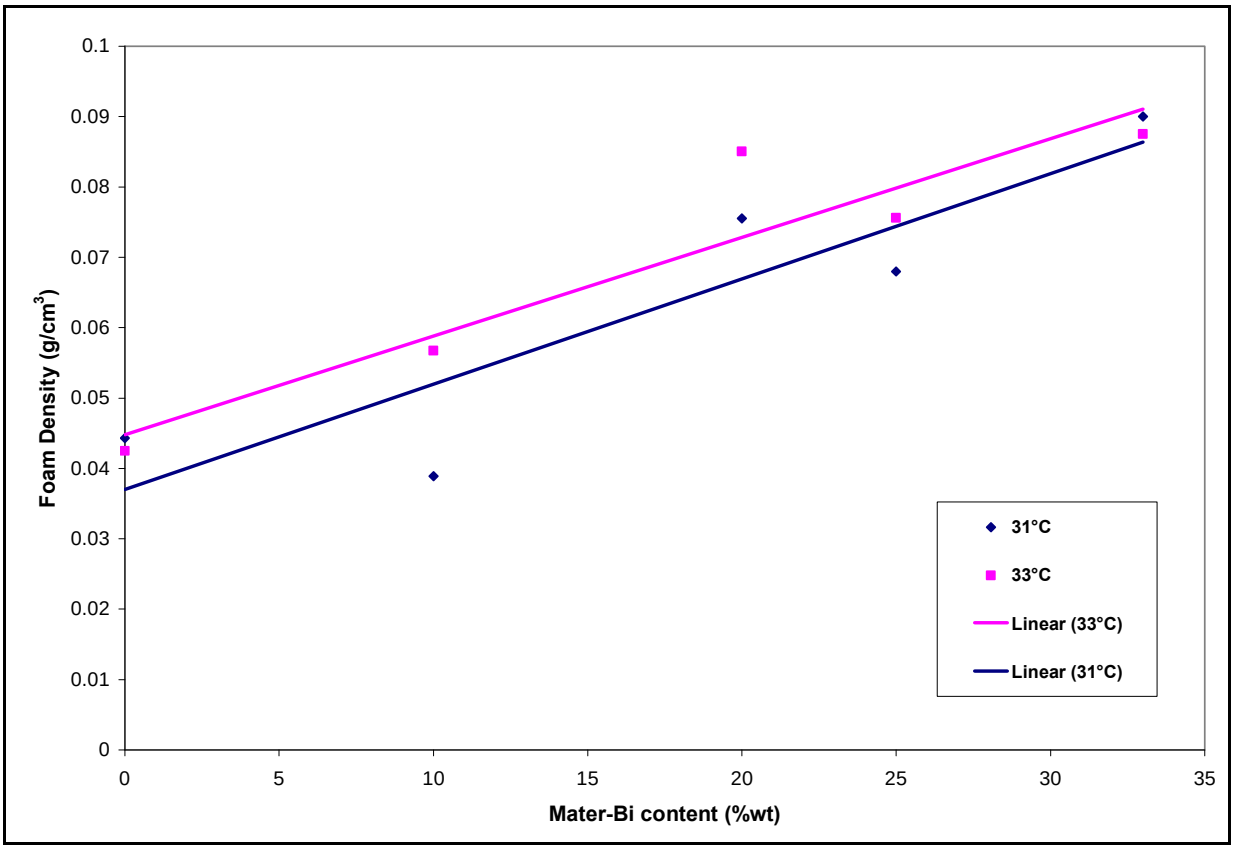

Figure 19 Plot of foam density as a function of MB concentration (Samples were foamed at 31°C and 33°C at constant pressure of 110 psi).

Figure 19 is a plot of the foam density as a function of MB concentration. From the plot, we can also say that the density decreases linearly with the increase in MB concentration. At both foaming temperatures 31°C and 33°C, the foam densities differ by approximately 0.01g/cm^3 and continue to reduce linearly. At this point, we can say that the density difference in the foamed samples at the different temperature is not of significance. From Figure 18 and 19, we can say that the nucleation growth rate decreases with the increase of MB concentration

4.3. Mechanical Properties

4.3.1. Tensile Test

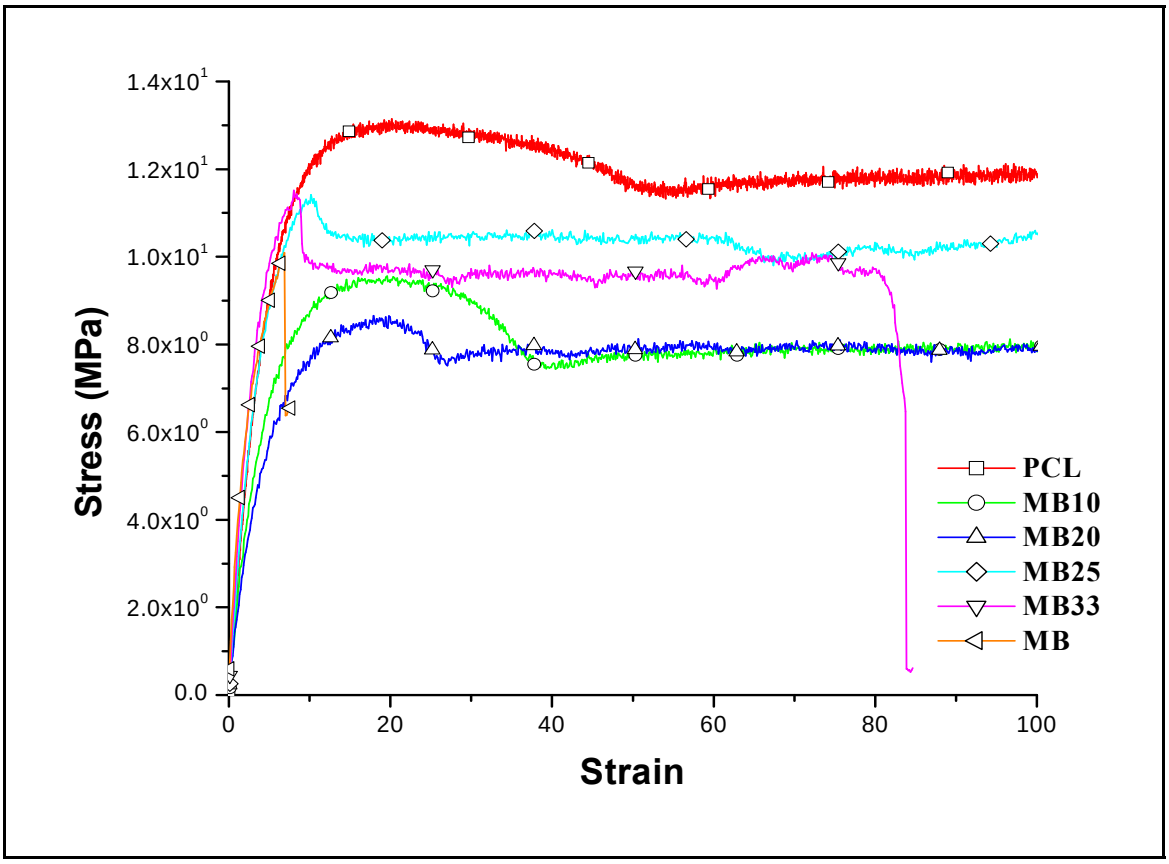

Figure 20 Plot of stress-strain curve of the unfoamed PCL/MB of blends.

In Figure 20, we can see that the ultimate tensile strength decreases until concentration of 20% wt. MB and then increases thereafter with an increase in MB concentration. It can also be noted that work hardening begins to occur in the samples at different strains which reduces as the MB concentration is increased.

The ultimate tensile strength of concentrations 0% wt. MB, 10% wt. MB and 20% wt. MB is reached at strains which are approximately at 20.05% and that of the 25% wt.

MB is reached at approximately 10.16% which is approximately one half of the strain of the other concentrations. The curve of the pure MB shows a brittle fracture around the yield point. It can be seen that the addition of PCL 100D increases the ductility of MB and at the 75% wt. PCL concentration, the tensile properties of MB is improved. Also, it can be observed that the pure MB exhibits a brittle fracture with insignificant yield. The 33% wt. MB also shows improvement in mechanical properties and a strain to failure. This is so because of the increased content of MB in the composition.

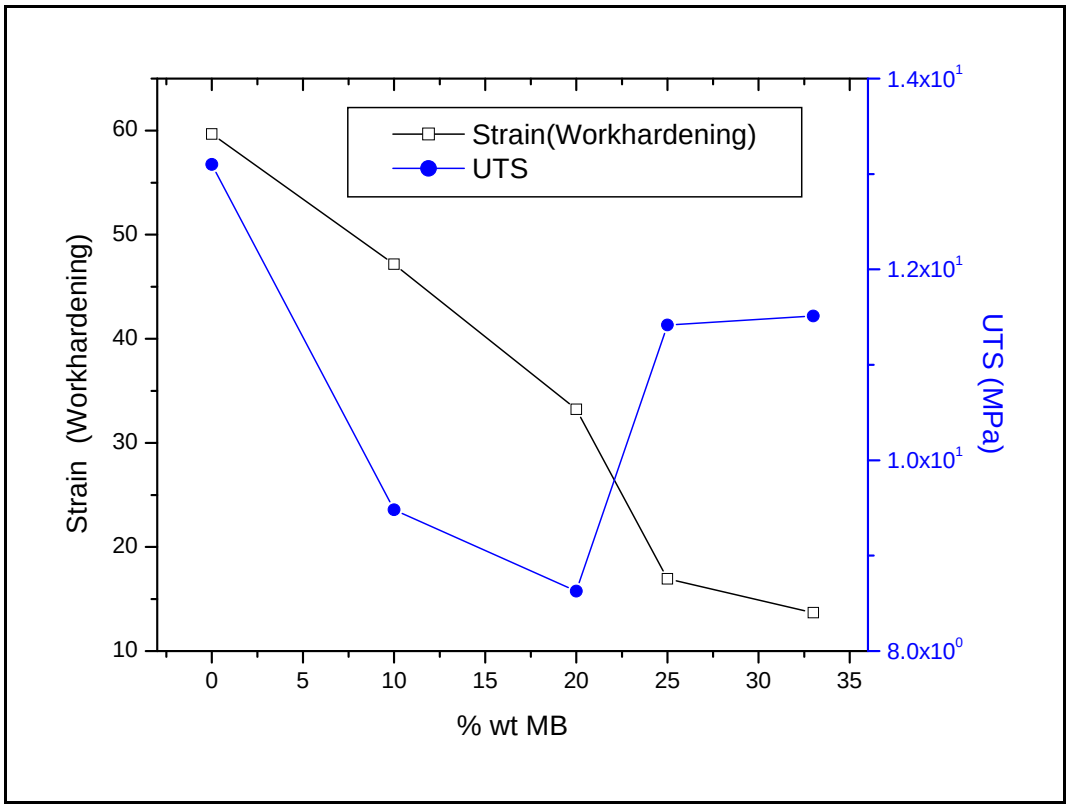

Figure 21 UTS and strain as a function of work hardening-MB concentration curve.

Figure 21 shows the plots of ultimate tensile strength and strain as a function of work hardening versus MB concentration. It can be seen that the strain as a function of work hardening exhibits a linear relationship. The 25% wt. MB concentration shows a steep drop (reduction) in the strain. This suggests that it exhibits more ductility compared

to the other samples. We can therefore say that the strain as a function of work hardening decreases linearly as a function of MB concentration.

Table 11 summarizes the experimental data obtained from the tensile test of the unfoamed samples. The percentage elongation at break could not be calculated because the fracture point was not reached for any of the samples which were due to the limitation of the testing equipment used. Figure 20 shows that 100% strain was reached for all the samples.

Table 11 Experimental data obtained after tensile test of the unfoamed samples.

Experimental Data	**% wt MB**					
	0	**10**	**20**	**25**	**33**	**100**
Ultimate Tensile Strength σ_{UTS} (MPa)	133.1±2.8	9.48±1.6	8.63±0.6	11.42±0.3	11.4±0.2	N/A
Tensile Stress σ (MPa)	11.02±0.4	8.02±0.1	5.91±0.2	10.2±0.5	11.1±0.4	2.04±0.05
Tensile Modulus E (MPa)	324.91±3.6	114.48±0.4	103.02±1.4	198.76±0.8	185.27±1.3	449.76±1.1
Percentage Elongation at Yield (%)	7.67±0.05	7.67±0.04	5.37±0.83	7.02±0.26	7.7±0.07	N/A
Percentage Elongation at Break (%)	N/A	N/A	N/A	N/A	83.73±1.3	6.9±0.4
Tensile Strength σ (MPa)	11.74±0.3	8.05±0.05	7.84±0.2	10.52±0.5	9.57±0.2	10.09±0.1

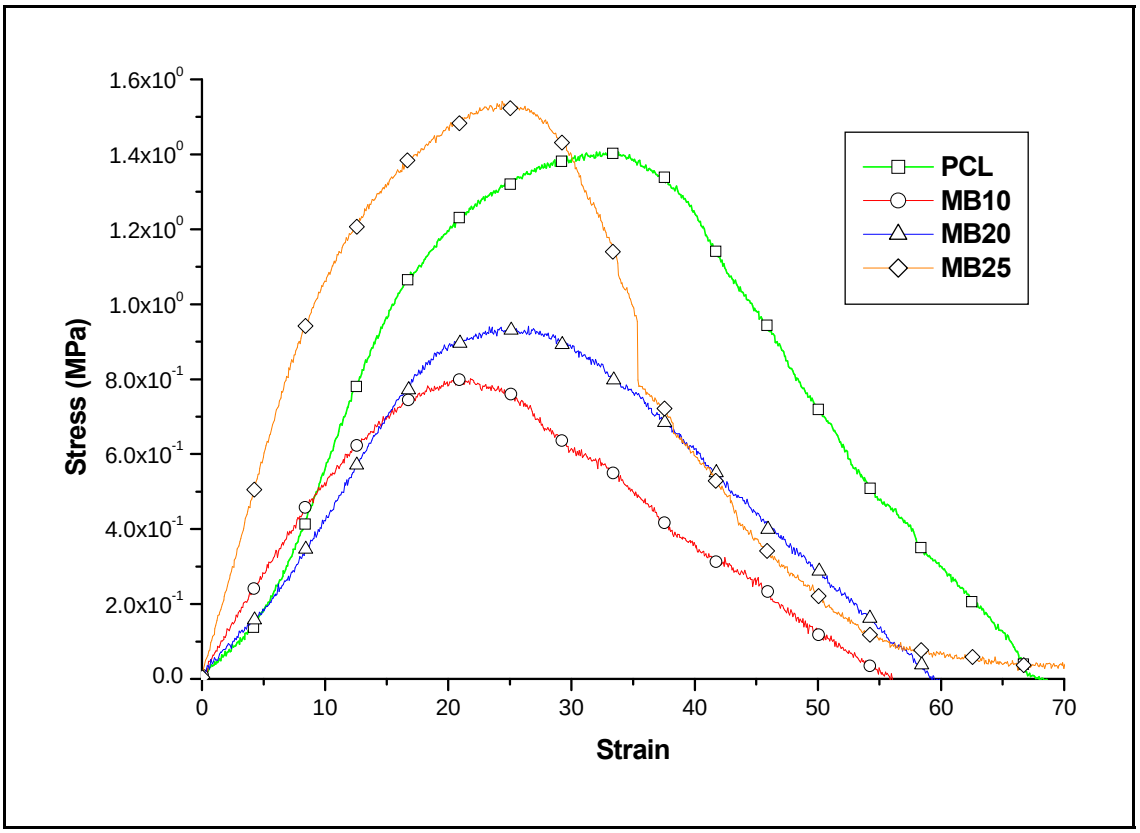

Figure 22 Plot of stress-strain curve of the foamed PCL/MB blends.

To analyze the data from Table 11, 12, and Figure 20 and 22, plots have been made of the Modulus-% wt. MB curve, ultimate tensile strength-% wt. MB and yield stress-% wt. MB curves of both foamed and unfoamed samples. These plots are shown in Figure 23, 24 and 25 respectively. It can be seen from the stress-strain curve in Figure 22 that the blend with 25% wt. MB concentration exhibits the highest modulus and tensile stress and the blend with 0% wt. MB concentration exhibits the largest strain at failure which is almost 68 %. Tensile test was not performed on sample MB33 due to its low foamability which results in inadequate testing material.

In Figure 23, it can be seen that the tensile modulus of both the foamed and unfoamed samples decrease as the MB concentration increases. There is a continuous decline until approximately the 18% and 14% MB concentration where it begins to

increase steeply for the foamed and unfoamed samples respectively. At about 22% MB concentration of the foamed sample, we begin to see improved modulus better than the 0% MB concentration. Of all compositions tested, we see that the 25% and 0% MB concentration shows the highest modulus for the foamed and unfoamed samples respectively.

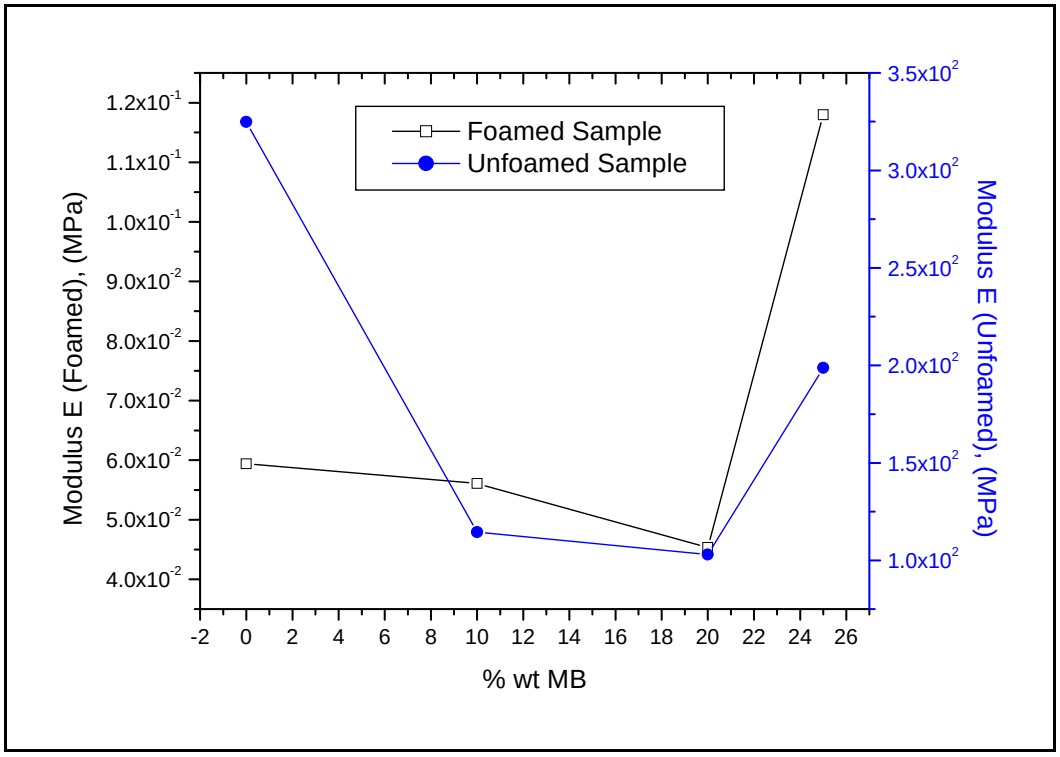

Figure 23 Plot of modulus-% wt. MB curve of the foamed samples of PCL/MB blends.

We can therefore say that the increase in MB concentration results in an increase the tensile modulus of the foamed sample. We can see that as at the 14% up to the 25% MB concentration of the unfoamed sample, the tensile modulus also increases. A similar result following the same trend can also be found in a study made by Dagnon et. al.[65]; they also found that the modulus eventually increased with increased MB concentration.

Upon observance of Figure 23, it can be seen that the modulus of both foamed and unfoamed blends follow the same trend. This further helps us understand that the property behavior of the samples is not due to the density but rather due to either the composition, individual material or both.

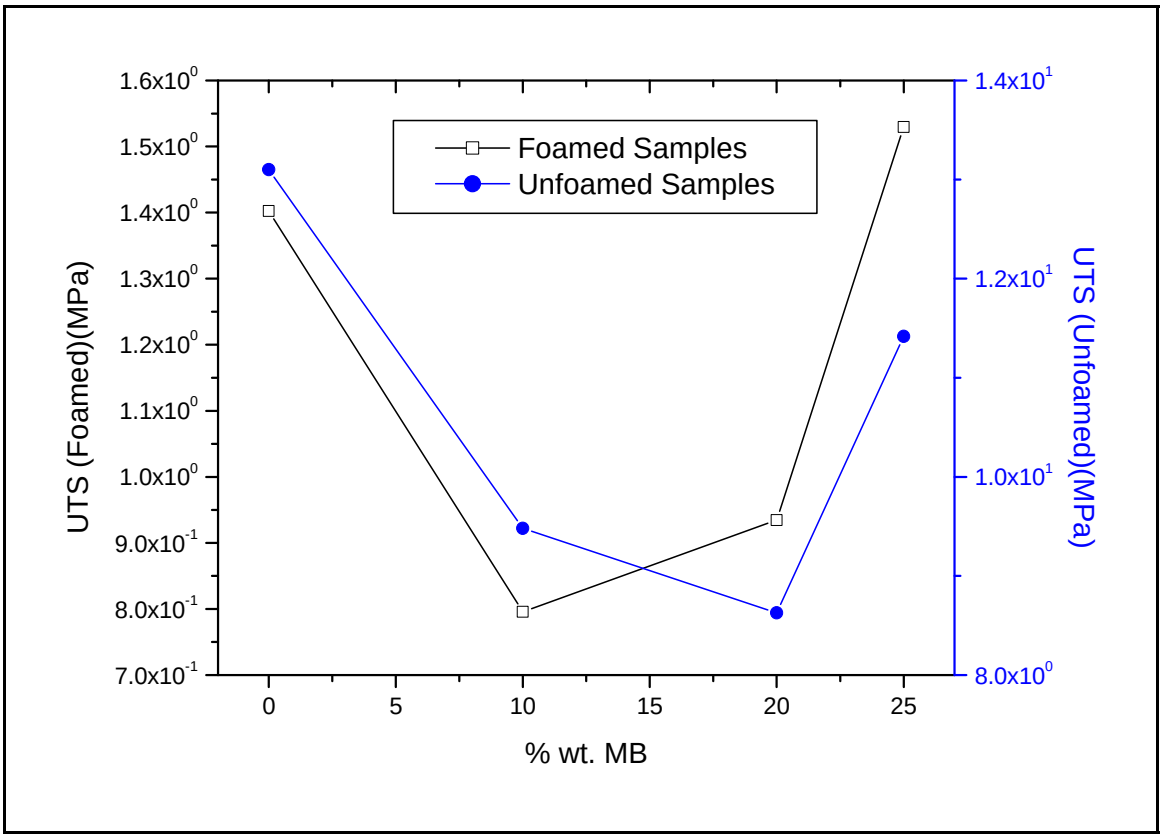

Figure 24 Plot of UTS-% wt. MB curve of the foamed samples of PCL/MB blends.

In Figure 24, we see that there is a linear decline in the UTS until approximately the 6.75% wt. MB concentration for both the foamed and unfoamed samples. The UTS of both foamed and unfoamed samples are at their lowest at MB concentrations of approximately (11.5%-14%) and (16.75%-19.5%) respectively and then begin to increase gradually and then steeply at a MB concentration of 20%. It can be noted from the

foamed sample that at the MB concentration of approximately 25%, there is an improvement in the UTS beyond that of the 0% wt. MB concentration. We can see that the UTS of both the foamed and unfoamed samples follow a very similar trend.

In Figure 25, we can see that the yield stress of both foamed and unfoamed samples decrease and then increase with an increase in the MB concentration. There is an initial linear decrease in the yield stress of both foamed and unfoamed samples at approximately 7% and 8.5% respectively.

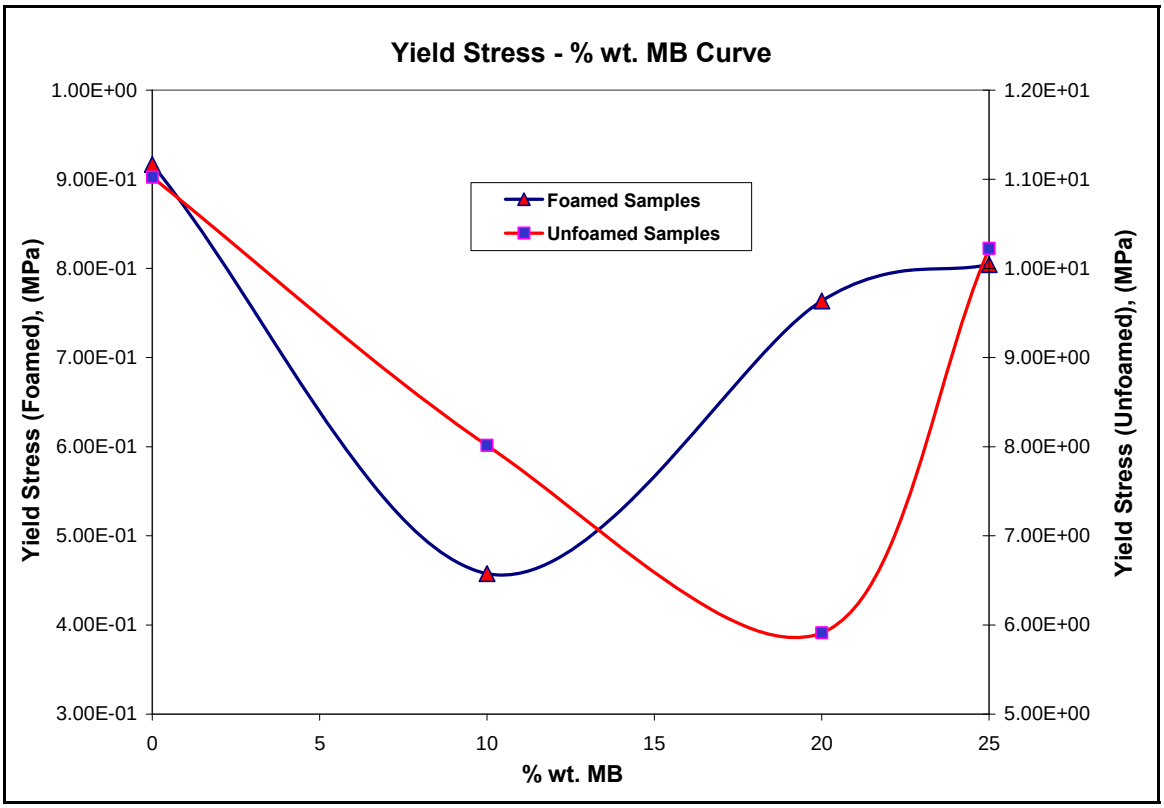

Figure 25 Plot of yield stress-% wt. MB curve of the foamed samples of PCL/MB blends.

The yield stress begins to increase steeply for the unfoamed samples and gradually for the foamed samples at MB concentrations of 10% and 20% respectively. At the MB concentrations of approximately 22.1%-25% of the foamed samples, there is the

exhibition of constant yield stress. Observing the data in Figure, we can see that the foamed and unfoamed samples follow a similar trend relating to the MB concentrations.

After analyzing the data obtained from the tensile test, we can choose a PCL-MB composition that will optimize all the properties depending on the use and application of the foams. Figure 22 shows the stress-strain curve from the tension test carried out on the foamed samples and Table 12 summarizes these experimental data.

Table 12 Experimental data obtained after tensile test of the foamed samples.

Experimental Data	**% wt MB**				
	0	**10**	**20**	**25**	**33**
Ultimate Tensile Strength (MPa)	1.40±0.02	0.8±0.03	0.93±0.04	1.53±0.02	N/A
Yield Stress (MPa)	0.92±0.02	0.46±0.03	0.76±0.04	0.80±0.03	N/A
Tensile Modulus (MPa)	0.06±0.002	0.056±0.003	0.045±0.003	0.11±0.02	N/A

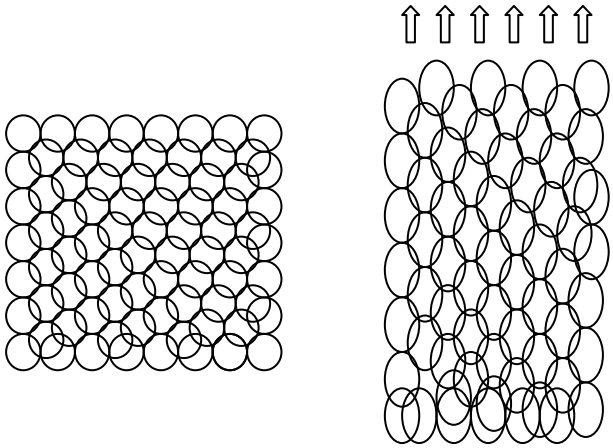

Figure 26 Cell expansion and realignment in the direction of applied force.

Figure 26 shows how the cells expanding and realigning themselves in the direction of the applied load. This can be seen visibly during the test.

4.3.2. Quasi-Static Shear Test

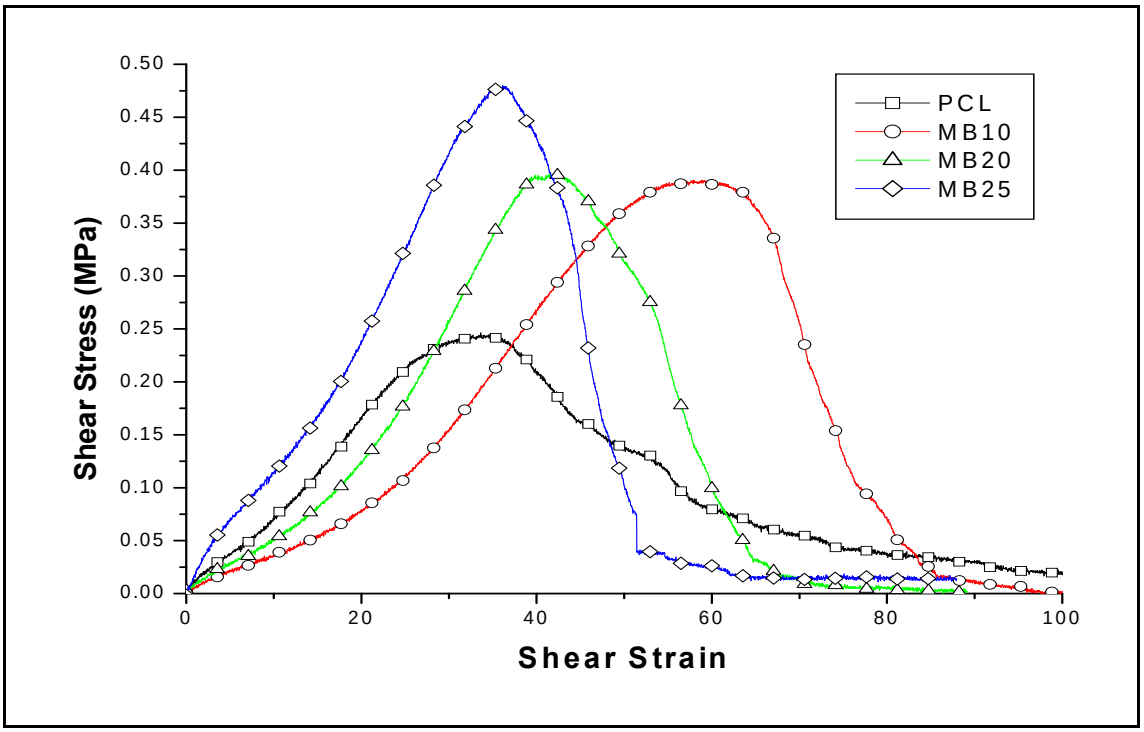

Figure 27 Plot of stress-strain curve of the foamed PCL/MB blends.

As noted during the test, the damage formation process in all the samples was similar. There is initially drawing of the thickness along the width and then deformation of the thickness along the length of the samples. The deformation along the length increased and became the line of fracture. The line of deformation was approximately 15° and propagated towards the moving plate. The fracture can be described more as tearing due to the plasticity; there are no visible pores or cracks that occur during the test. Tearing of the sample can be seen length wise along the deformation line.

Table 13 Experimental data obtained after shear test of the foamed samples.

Experimental Data	% wt MB				
	0	10	20	25	33
Ultimate Shear Strength τ_{USS} (MPa)	0.24±0.02	0.39±0.03	0.4±0.03	0.48±0.02	N/A
Shear Yield Stress τ_Y (MPa)	0.21±0.03	0.31±0.03	0.37±0.03	0.43±0.02	N/A
Shear Modulus G (Pa)	87.07±0.5	92.84±0.2	129.72±0.2	150.16±0.3	N/A

4.3.3. Instrumented Impact Test

The unfoamed samples were compression molded into a (40 x 40) mm sheet with a thickness of 2.45mm while the foamed samples were cut into a (40 x 40) mm sheet with a thickness of 5mm. The instrumented impact test was conducted on an Instron Instrument tester 9250 Piezotup unit with measurement capability of 10000lbs of load. An impact weight of 8.5 kg was used at a drop height of 0.666m as per ASTM standard D5628[69].

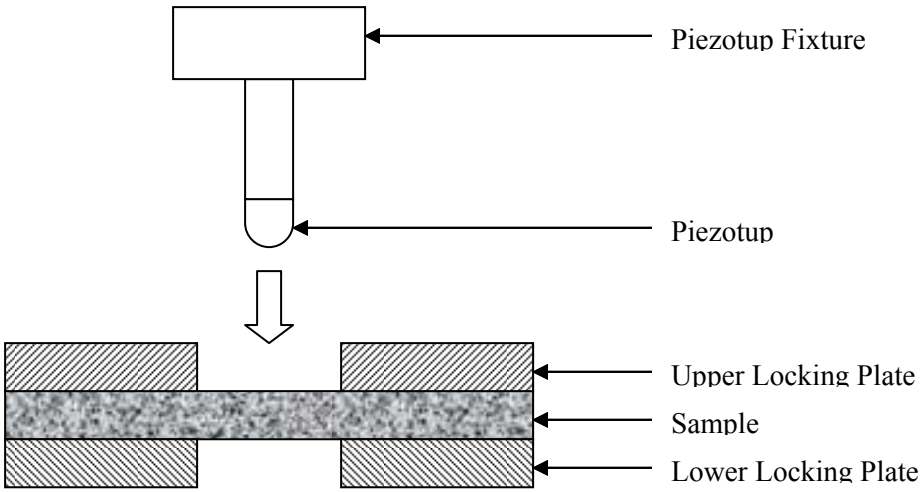

Figure 28 Schematic of instrumented impact testing with the piezotup and sample locked in between to plates.

The velocity at impact was 3.611m/s and all tests were performed under ambient temperature (22°C) to prevent any kind of deformation of the foamed sample during testing as shown in Figure 28.

Table 14 Values obtained after impact test of unfoamed samples.

% wt MB	Maximum load-1 (kN)	Time to max load-1 (ms)	Impact velocity-1 (m/s)	Total energy-1 (J)	Total time-1 (ms)
0	1.0679±0.0004	1.5594±0.0003	3.5942±0.006	15.7792±0.13	6.8878±0.002
10	0.8879±0.0003	1.3763±0.0004	3.6023±0.0007	11.1344±0.009	5.7892±0.004
20	0.9328±0.0003	1.651±0.0005	3.5976±0.0006	10.9249±0.0005	5.545±0.002
25	1.003±0.003	1.709±0.003	3.6006±0.001	7.9237±0.08	3.894±0.006
33	0.8418±0.0002	0.705±0.003	3.594±0.002	2.1868±0.002	1.181±0.007

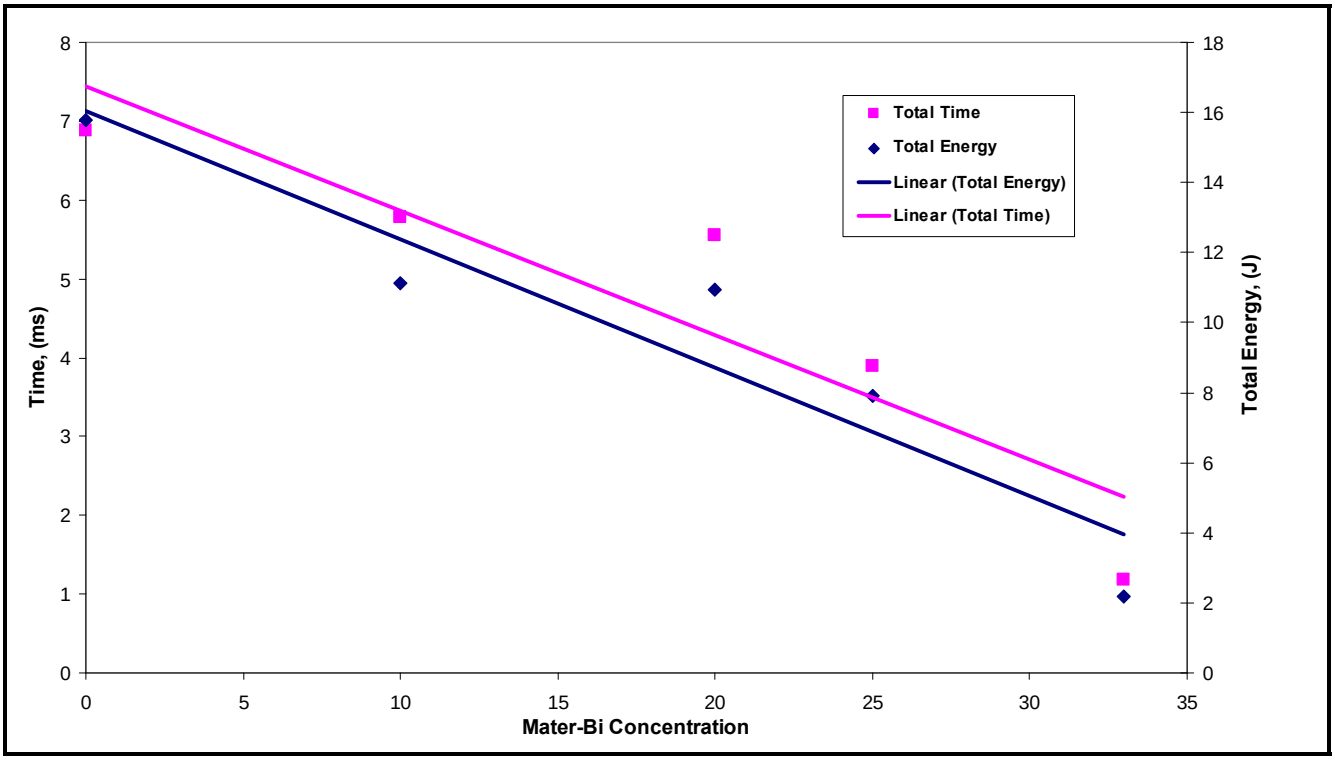

Figure 29 Plot of total time and energy required to cause fracture in the unfoamed samples as a function of MB concentration.

From Table 14 and Figure 29, it can be seen that the total time and energy required to fracture the unfoamed samples decreased with an increase in the MB concentration. We can say that the total time and energy required to fracture the samples is highly dependent on MB concentration.

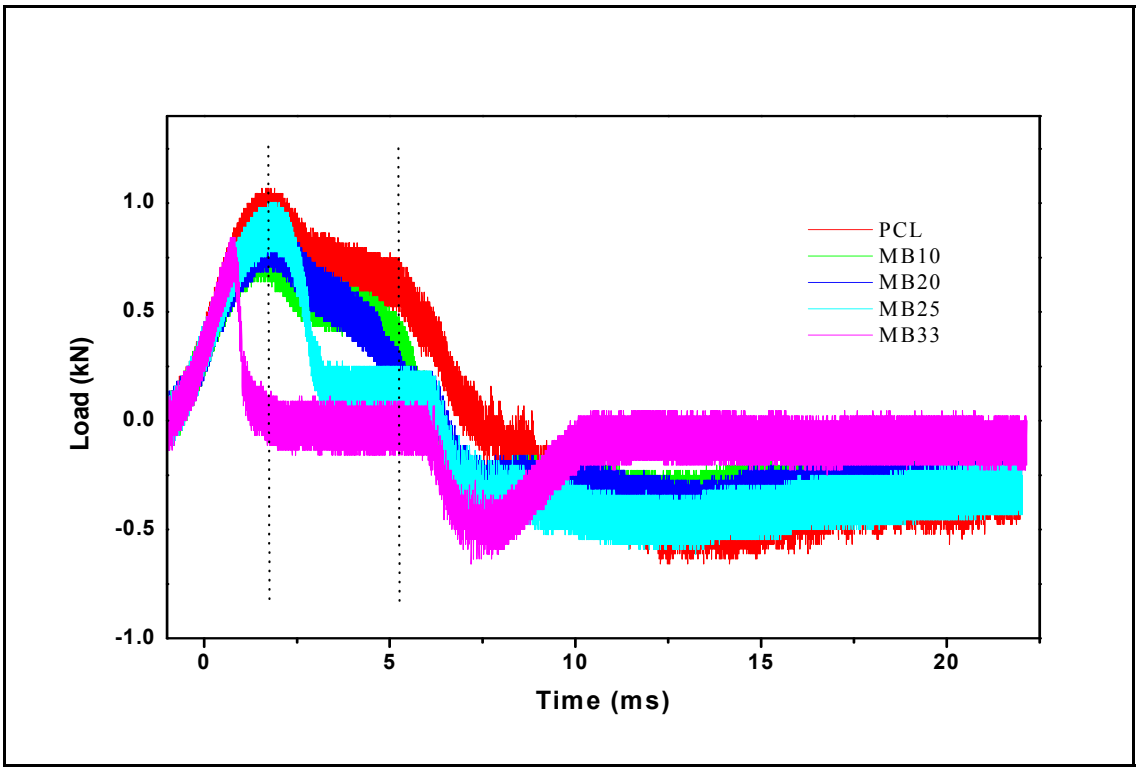

Figure 30 Plot of load applied to the unfoamed samples as a function of time.

From Figure 30, we can see that the maximum load reached for all the unfoamed samples occurred at approximately 2ms except for the 33% wt MB concentration which was at approximately 1ms. At the maximum load, there is a sudden plummet in the load. The steepness increases with an increase in MB concentration; this is related to fracture occurring in the samples. From this we can say that fracture occurs faster in the samples with an increase in MB concentration.

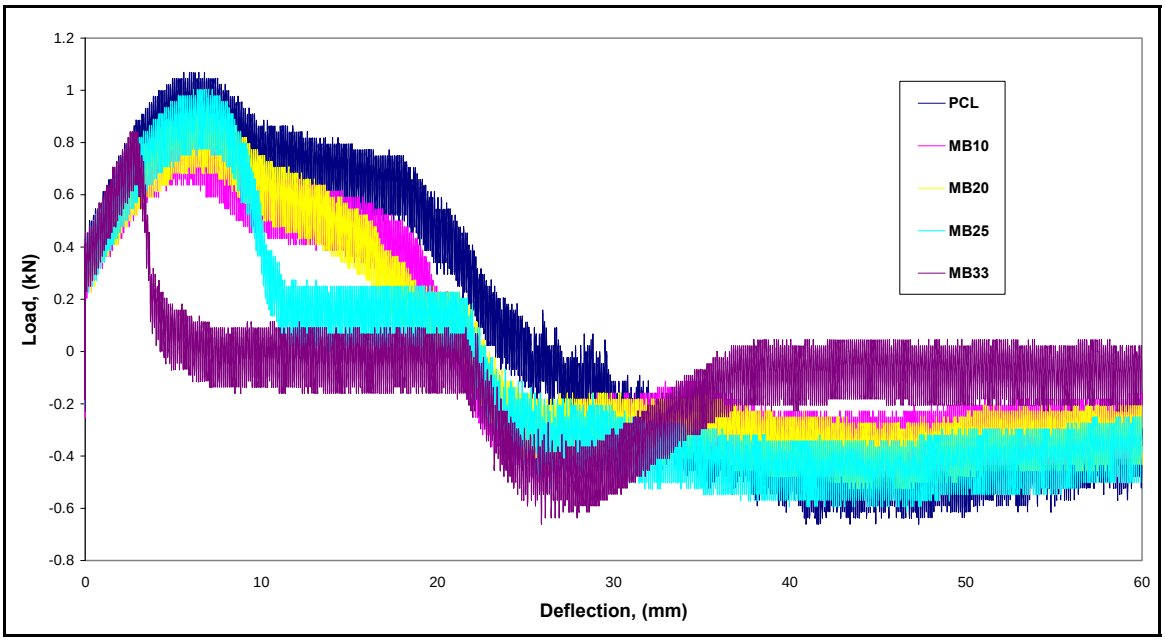

Figure 31 Plot of load applied to the unfoamed samples as a function of deflection.

In Figure 31, we can also see that the maximum load reached for all the unfoamed samples were at approximately 6mm except for the 33% wt MB concentration which was at approximately 3mm. At the maximum load, there is a sudden plummet in the load. The steepness increases with an increase in MB concentration. We can therefore conclude that the ductility and stiffness also increases with increase MB concentration. Table 15 shows the values of some parameters obtained from the impact test of the foamed samples. It can be seen that the total energy required to fracture the samples have very little difference which could be insignificant.

Table 15 Values obtained after impact test of foamed samples.

% wt MB	Maximum load-1 (kN)	Time to max load-1 (ms)	Impact velocity-1 (m/s)	Total energy-1 (J)	Total time-1 (ms)
0	0.0911±0.01	4.2603±0.009	3.6839±0.006	-4.0857±0.0003	4.2694±0.0003
10	0.1133±0.0005	4.1077±0.002	3.6861±0.0003	-3.8955±0.003	4.1199±0.008
20	0.114±0.0004	4.1718±0.0003	3.6874±0.0002	-4.1508±0.0005	4.1809±0.00007
25	0.1138±0.0005	3.6804±0.0004	3.684±0.0006	-3.9083±0.001	3.6896±0.0005
33	0.0902±0.005	5.1453±0.0005	3.6505±0.0003	-4.4462±0.003	5.1514±0.006

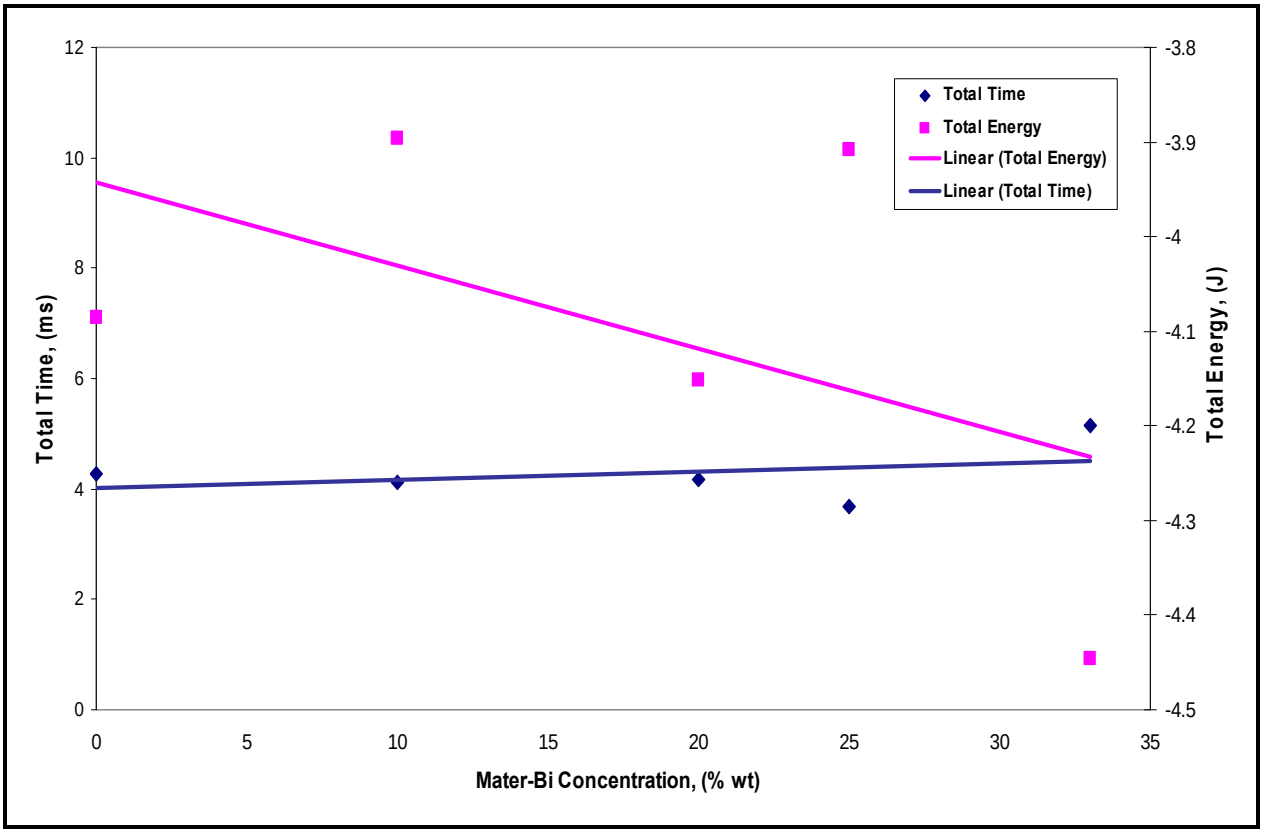

Figure 32 Plot of total time and energy required to cause fracture in the foamed samples as a function of MB concentration.

In Figure 32, the total time and total energy required to fracture the foamed samples increased slightly and decreased respectively with an increase in MB concentration. We can say that the MB concentration is inversely and directly proportional to the total energy and total time respectively.

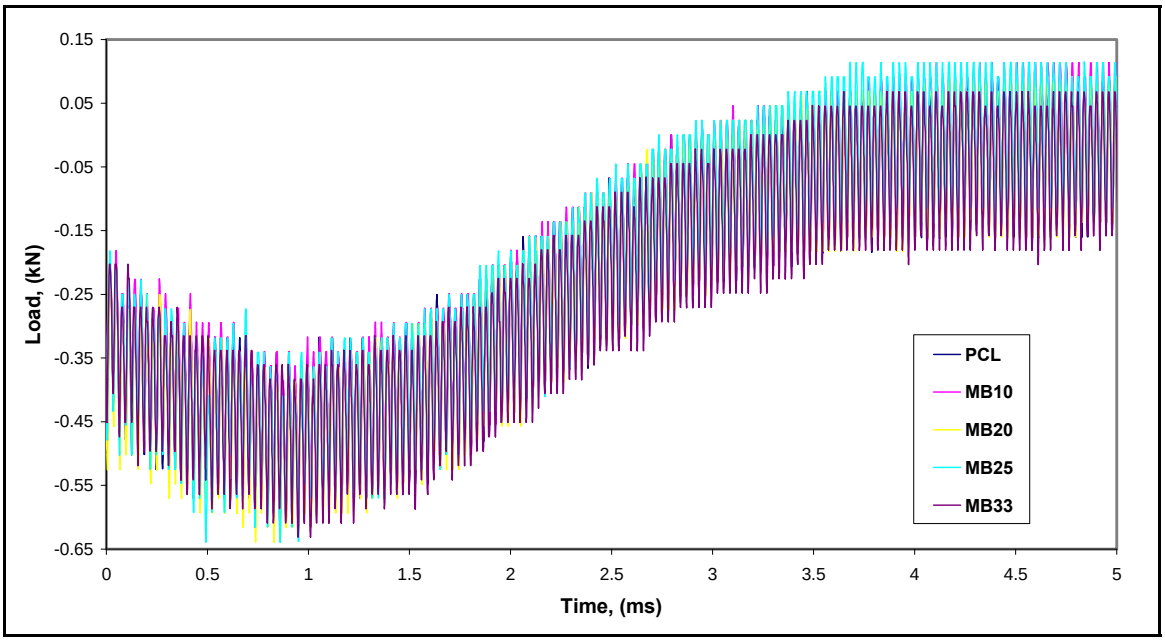

Figure 33 Plot of load applied to the foamed samples as a function of time.

In Figure 33, the load decreases up until the time approximately equals to 1ms and then starts to increase until about 3.5ms where it stabilizes. There is no significant difference in the samples with different MB concentration.

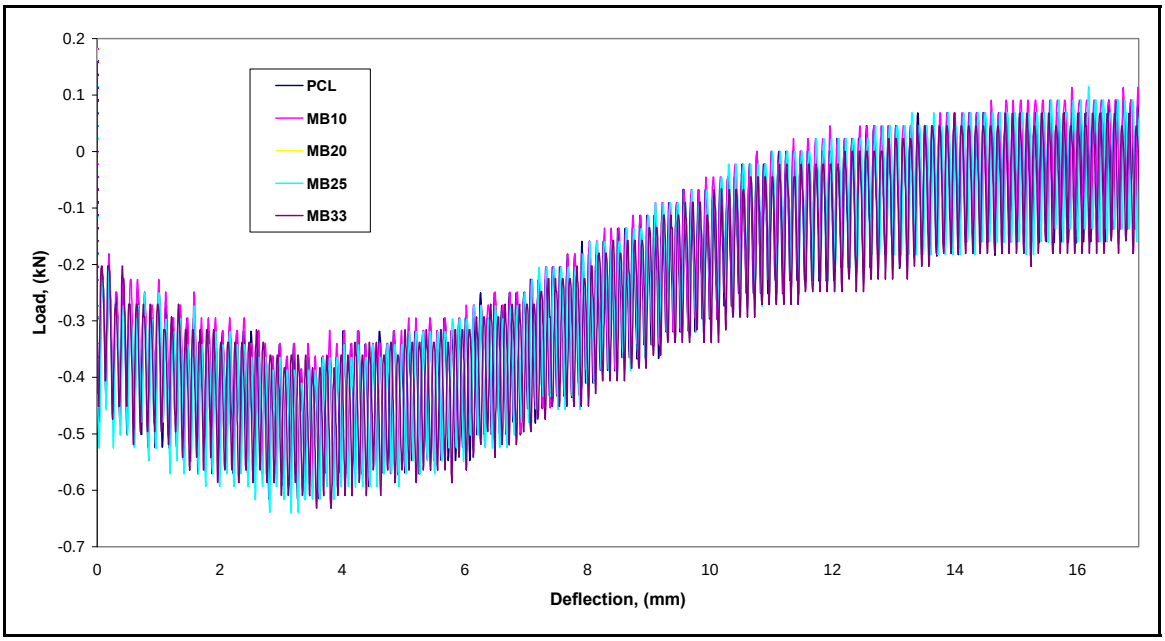

Figure 34 Plot of load applied to the foamed samples as a function of deflection.

In Figure 34, the samples with different MB concentrations exhibit the same deflection characteristics. The load decreases in the first few milliseconds and then begins to increase. We can say that the strain causes the samples to work harden.

4.3.4. Compression Test

A lot of mechanical tests like compression tests have been done on rigid cellular plastics and just a few on semi flexible and flexible cellular plastics. PCL when foamed is a flexible cellular plastic while MB which has never been foamed before is a rigid plastic. A blend of the two polymers with increasing MB concentration gives rise to a semi flexible polymer.

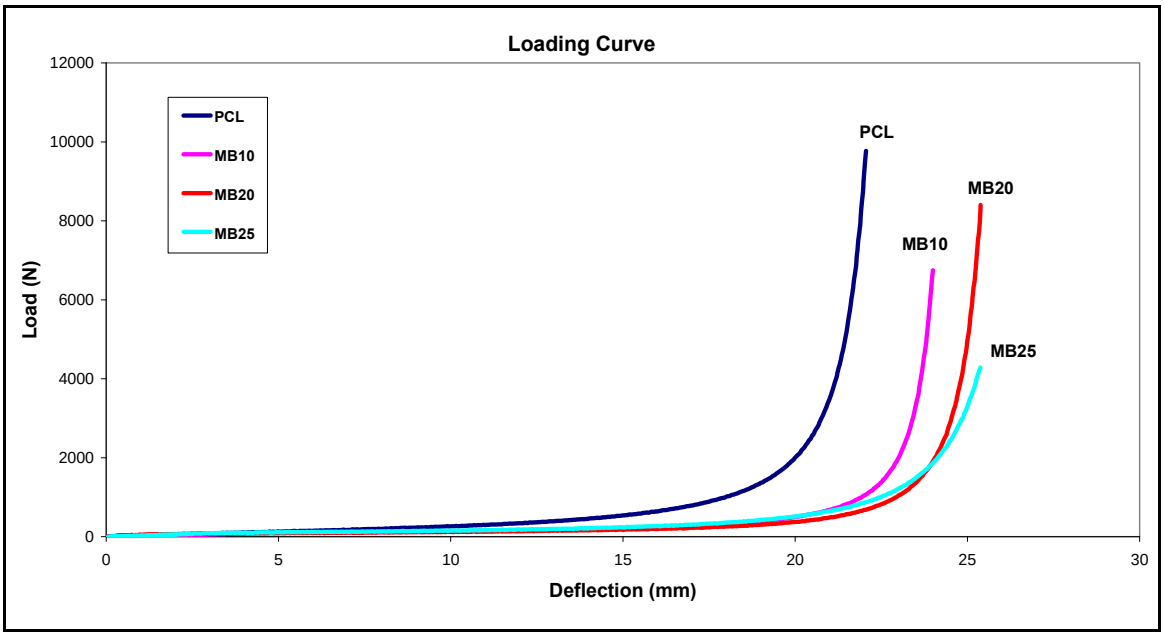

Figure 35 Plot of load-deflection curve (loading curve) of foamed polycaprolactone-MB blends.

In Figure 35, it can be seen that the maximum load and deflection decreases and increases respectively with the increase in the MB concentration. This is attributed to the reduction in elasticity and ductility of the samples as MB concentration is increased. PCL is a more elastic, flexible and ductile polymer than MB; this is due to the storage modulus differences they have.[65] A compression test was not performed for the sample PCL 100D 33% wt. MB due to low foamability which does not produce enough material for standard testing. The addition of MB to PCL is to improve the physical appearance and the mechanical properties of the foam. When looking at the compression test, it can be seen that the increase in MB concentration reduces the maximum load that can be applied on the samples. In a study made by J.M. Gomez et. al., it was found that having a ceramic-polymer composite foam material rather than just $SiO_2.ZrO_2$ ceramic foam improved the initial strength between 50 to 200 times.[71]

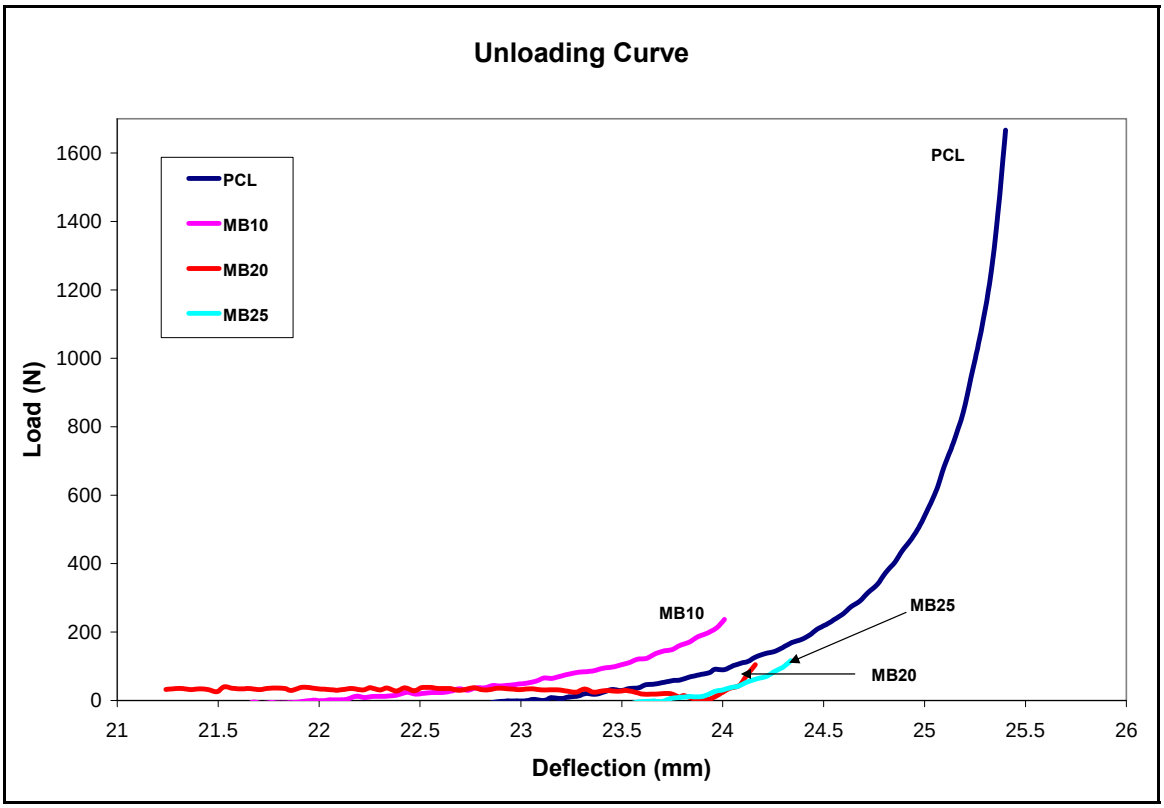

Figure 36 Plot of load-deflection curve (unloading curve) of foamed polycaprolactone-MB blends.

From Figure 36, it can be noticed that the load and deformation recovery of PCL 100D 0% wt. MB is distinct from its blends. It has a recovery load approximately 8 times that of its blends and a steep decline in the recovery deflection after the 10% MB concentration.

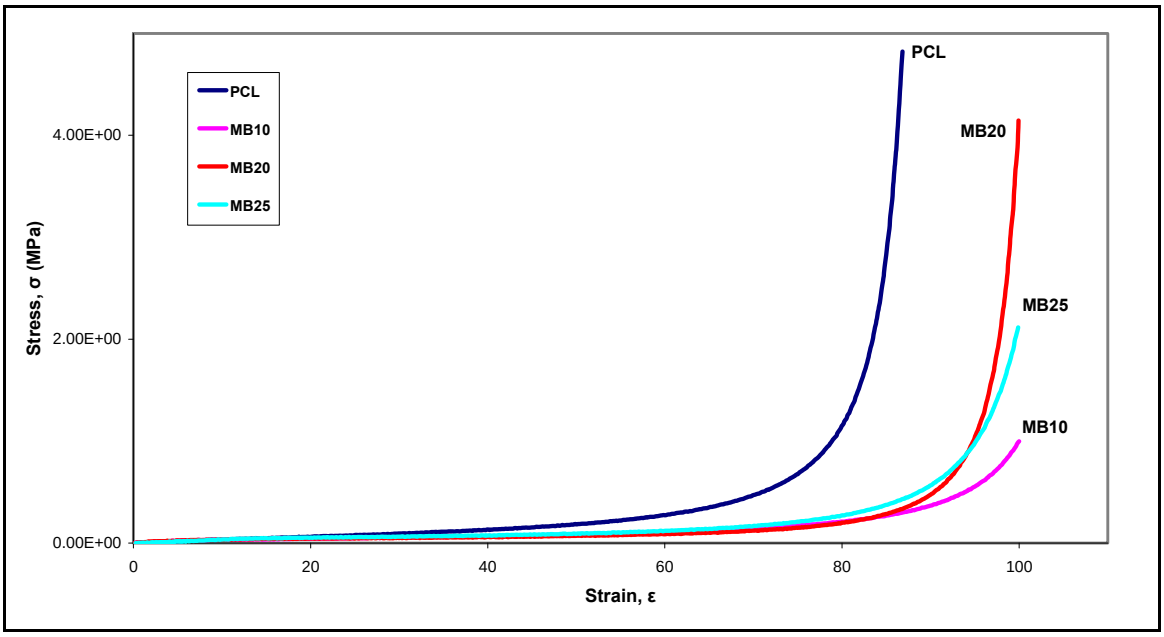

Figure 37 Plot of stress-strain curve of foamed polycaprolactone-MB blends.

From Figure 37, we can see that the PCL 100D 0% wt. MB exhibits the highest modulus. The other compositions have close modulus; in order to confirm the modulus of each composition, the portion of the stress-strain curve which shows the modulus has been enlarged.

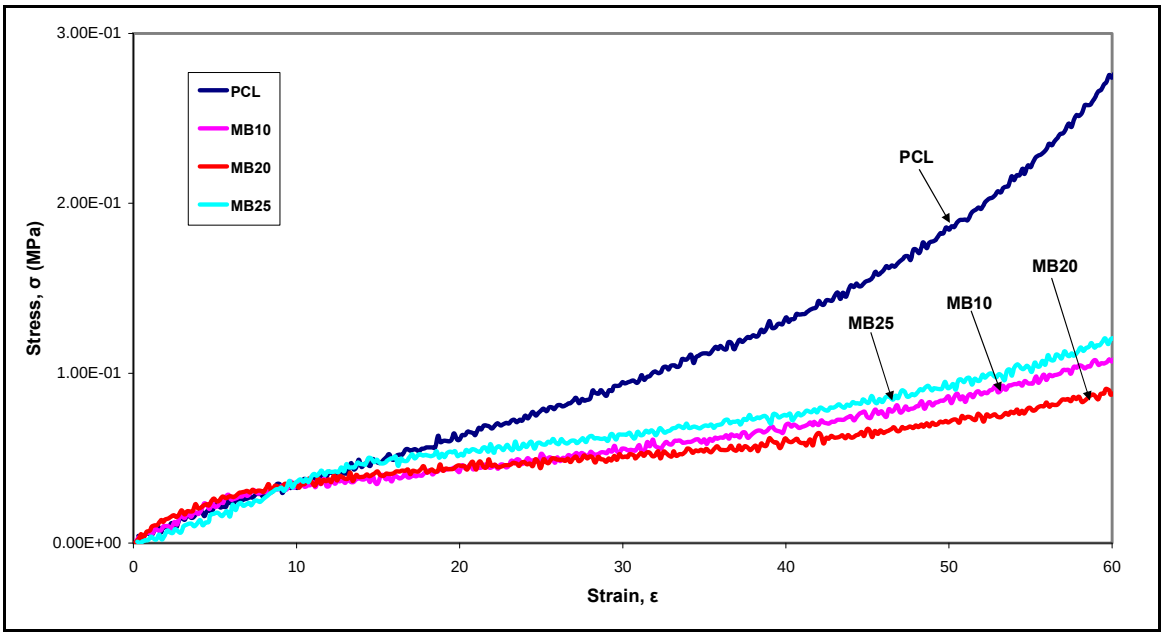

Figure 38 Enlarged portion of the stress-strain curve of foamed polycaprolactone-MB blends showing the modulus of the different compositions.

Figure 38 shows the enlarged portion of the modulus of the compositions. It can be seen that there is scattering of the data; this is due to some of the weak struts of the foam structure buckling or deforming under the compressive force.

We can clearly see that the modulus decreases with the following weight percentage: 0%, 25%, 10%, and 20%. We can see that the compressive modulus does not follow a linear function with MB concentration. We see that the 25% has the highest modulus when it comes to the compositions. This makes it the optimum composition at which the best compressive modulus is achieved.

Table 16 shows the various parameters calculated and obtained from the stress-strain curve of the compression test of the foamed samples.

Table 16 Values obtained and calculated from stress-strain curve of the compressive test of the foamed samples.

Parameters	% wt MB				
	0	10	20	25	33
Compressive Modulus E, (MPa)	0.0031±0.0003	0.0019±0.00015	0.0019±0.0002	0.0018±0.00009	N/A
Maximum Deflection, (mm)	22.06±0.07	24.00±0.1	25.38±0.04	25.38±0.2	N/A
Deformation Recovery, (mm)	2.37±0.01	1.99±0.02	0.25±0.004	0.6±0.03	N/A
Yield Stress σ_Y, (Pa)	0.15±0.005	0.078±0.003	0.075±0.0002	0.085±0.001	N/A

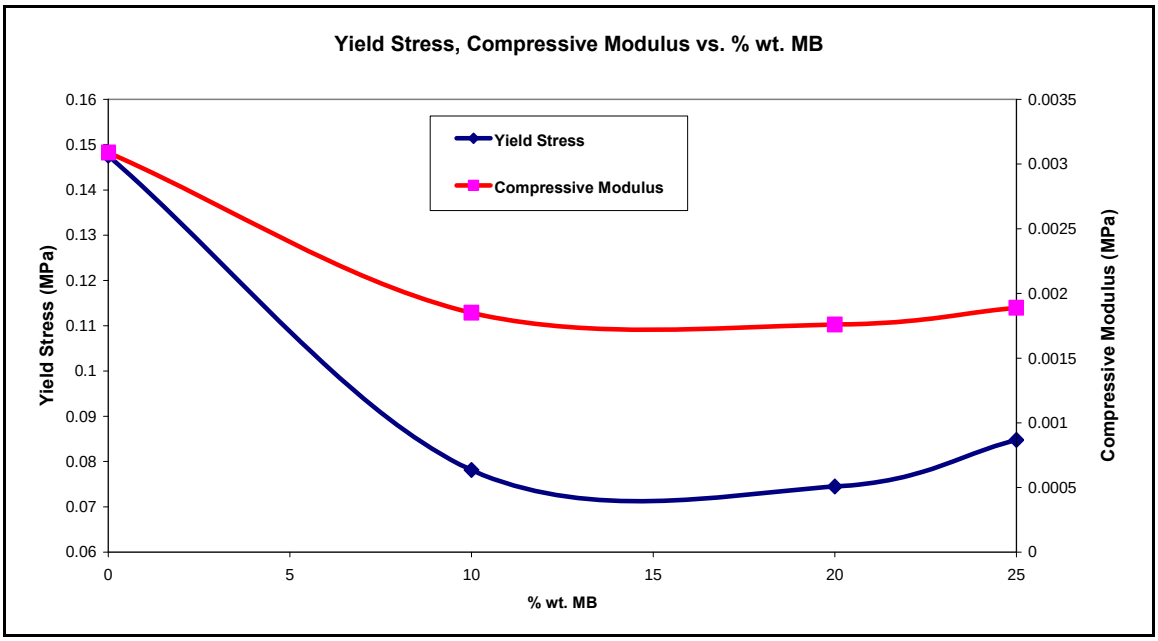

Figure 39 Plot of yield stress, compressive modulus vs. % wt. MB of foamed polycaprolactone-MB blends.

In Figure 39, we can see that the yield stress and compressive modulus decrease with an increase in the MB concentration up until approximately the 15% wt. MB where it begins to increase. To further understand why this is so, we would have to perform compression test on pure MB with an increasing PCL concentration but this is not possible at the processing conditions we are look at. Therefore we cannot fully understand why these compositions exhibit these behaviors. Very little work has been done on PCL, MB or their blends. In a study that was done on PCL-MB blends by

Dagnon et. al., it was found that the yield stress decreased with an increase in MB concentration and the storage modulus for MB was higher than that of PCL.

4.4. X-ray Diffraction

Both unfoamed and foamed samples were analyzed using x-ray diffraction. The PCL has a 110 peak at 21.29°, a 111 shoulder, A peak at 23.68° corresponds to the 200 and a peak at 45 degrees to 121. Mater-bi has only one peak at 20 degrees with a minor peak at around 12 degrees. With increasing MB, there was no change in the peak position of the PCL peaks. However as shown in Figure 8A, the intensities of the PCL (at 21.29° and 23.68°) reduced slightly with the increase of MB. All the blends with the exception of Pure PCL and MB show a new peak at 44.61°; this is attributed to the interaction of PCL and MB creating a phase with some crystallinity.

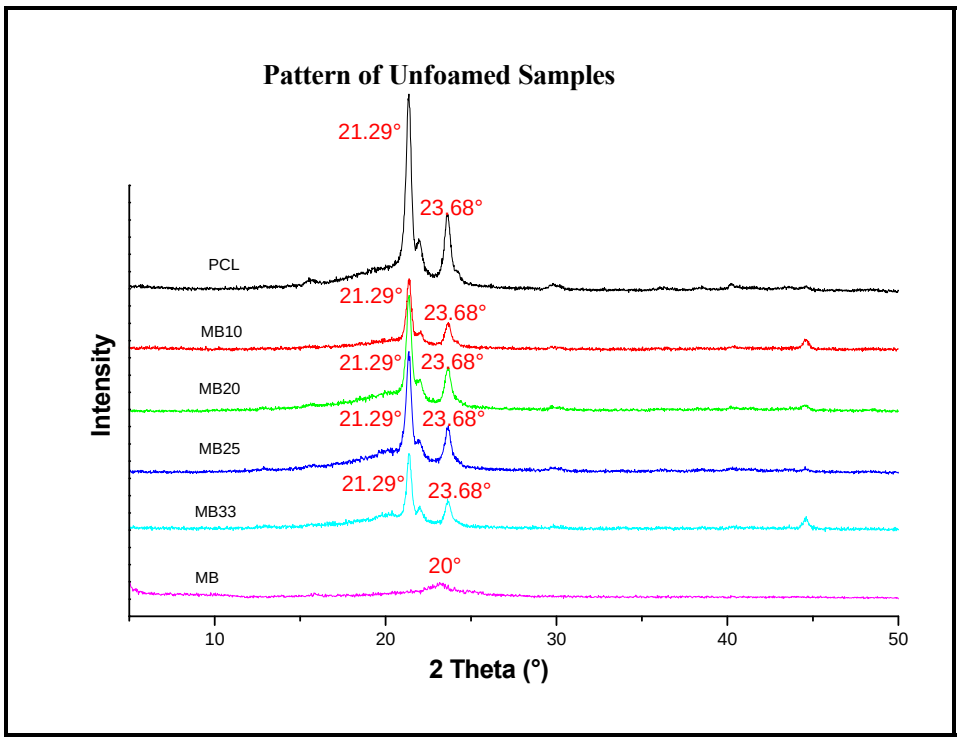

Figure 40A XRD patterns for unfoamed PCL 100D, MB and their blends (intensity is offset).

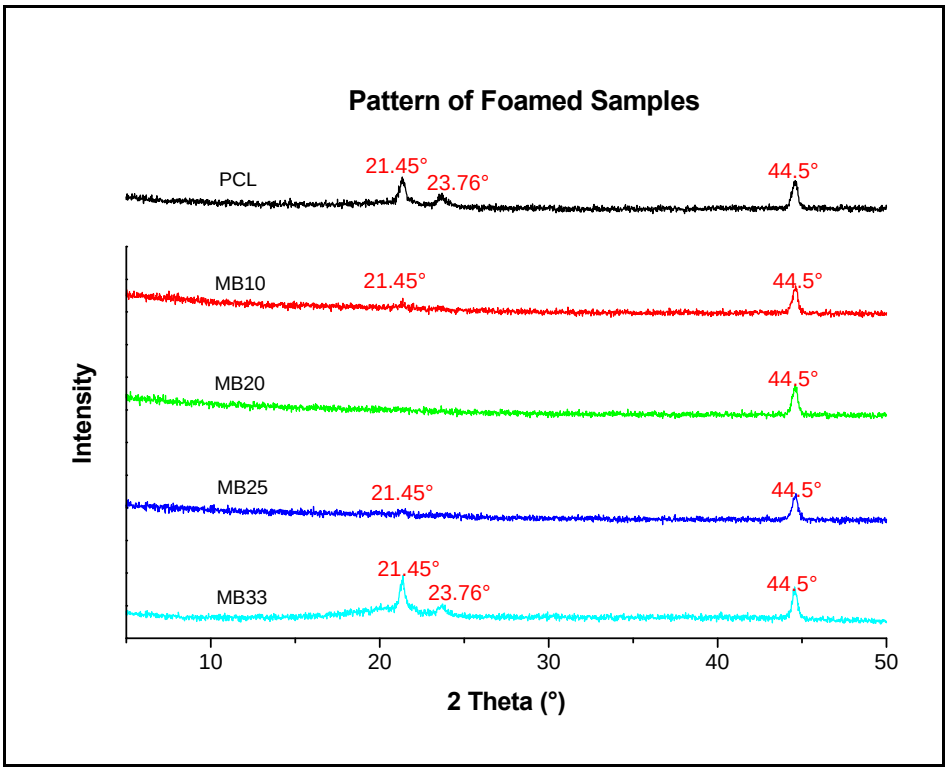

Figure 40B XRD patterns for foamed PCL 100D, MB and their blends (intensity is offset).

In Figure 40B, the foamed samples show a rapid reduction in the PCL peaks at 21.45° and 23.76°. There is a disappearance of the 21.45° at the 20% wt. MB concentration. This can be due to the carbon dioxide and foaming which prevents the chains of the individual polymers from interacting and hence prevents crystallization from taking place. The peak at 23.76° disappears at the 10% wt. MB concentration and appears again at the 33% wt. MB. The peak at 44.5° is seen to increase in the intensity compared to the unfoamed samples at that peak. The intensity is the same at this peak. It can be seen that the intensity of PCL peaks reduced after foaming was carried out on it and its blends. The table below shows the peaks found in the foamed and unfoamed samples after XRD characterization (Table 17). The crystallite size of the peak at 21.45°

did not significantly change in samples with concentrations of 0% and 33% MB concentration.

Table 17 XRD peaks for PCL 100D, MB and their blends.

% wt. MB	Unfoamed Samples				Foamed Samples		
	2θ (°)						
0	-	21.29	23.68	-	21.45	23.76	44.5
10	-	21.29	23.68	44.61	21.45	-	44.5
20	-	21.29	23.68	44.61	-	-	44.5
25	-	21.29	23.68	44.61	21.45	-	44.5
33	-	21.29	23.68	44.61	21.45	23.76	44.5
100	20	-	-	-	N/A	N/A	N/A

4.5. Differential Scanning Calorimetry

Only unfoamed samples were examined by the DSC. The thermal transition temperatures which corresponded to the values of the maximum for each endoderm peak and the values of the minimum for each peak were recorded in table 18 and 19. Figure 41A, 41B, 42A and 42B show the DSC scan of the first and second heating and cooling cycle of PCL, MB and their blends respectively.

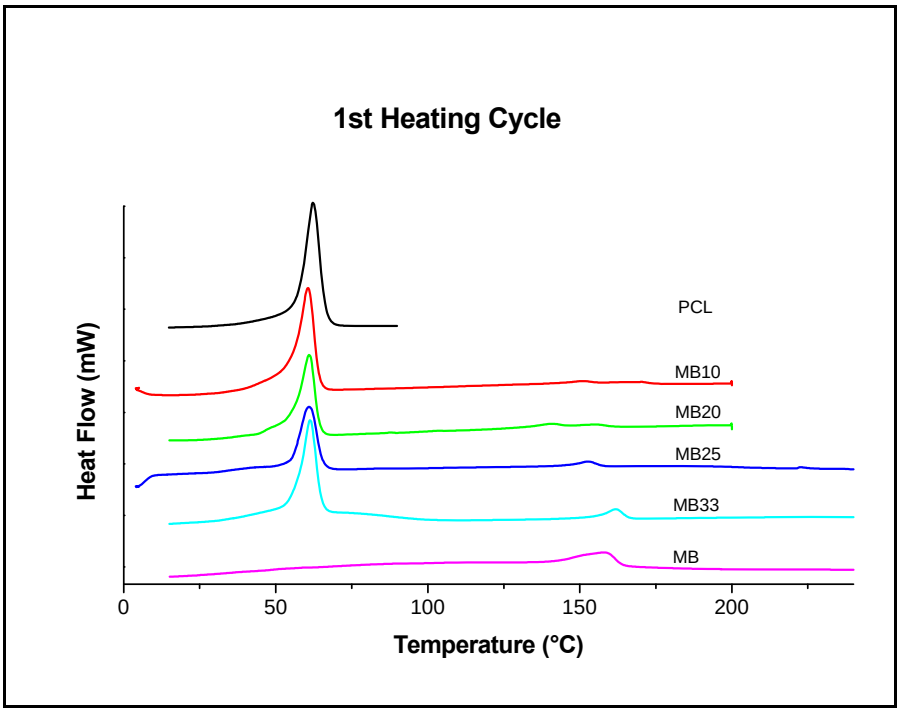

Figure 41A DSC curves of PCL, MB and their blends (first heating).

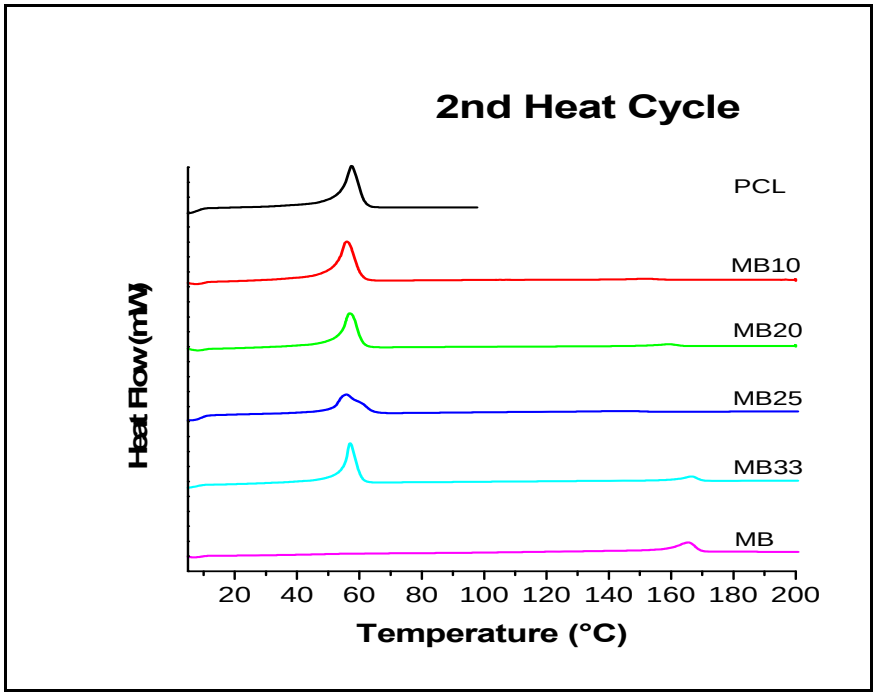

Figure 41B DSC curves of PCL, MB and their blends (second heating).

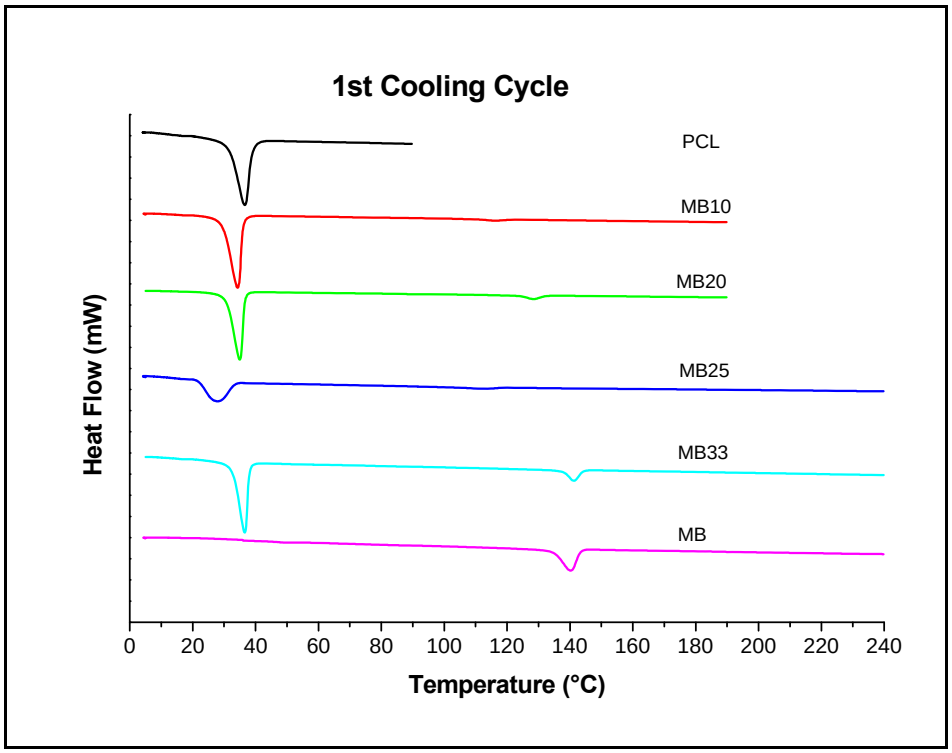

Figure 42A DSC curves of PCL, MB and their blends (first cooling).

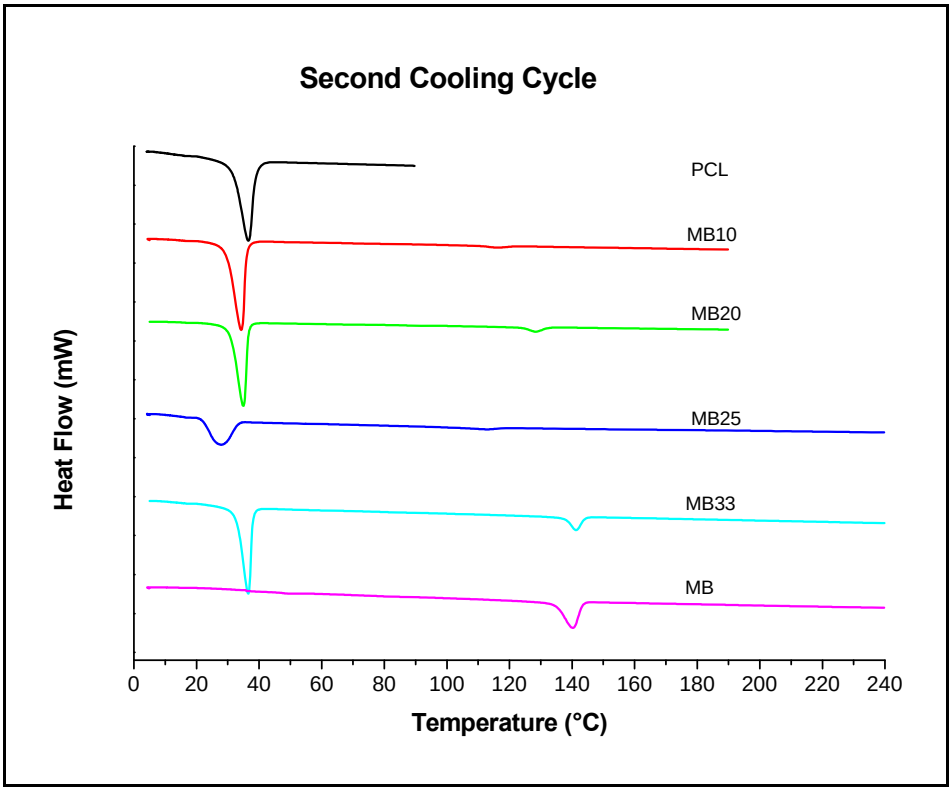

Figure 42B DSC curves of PCL, MB and their blends (second cooling).

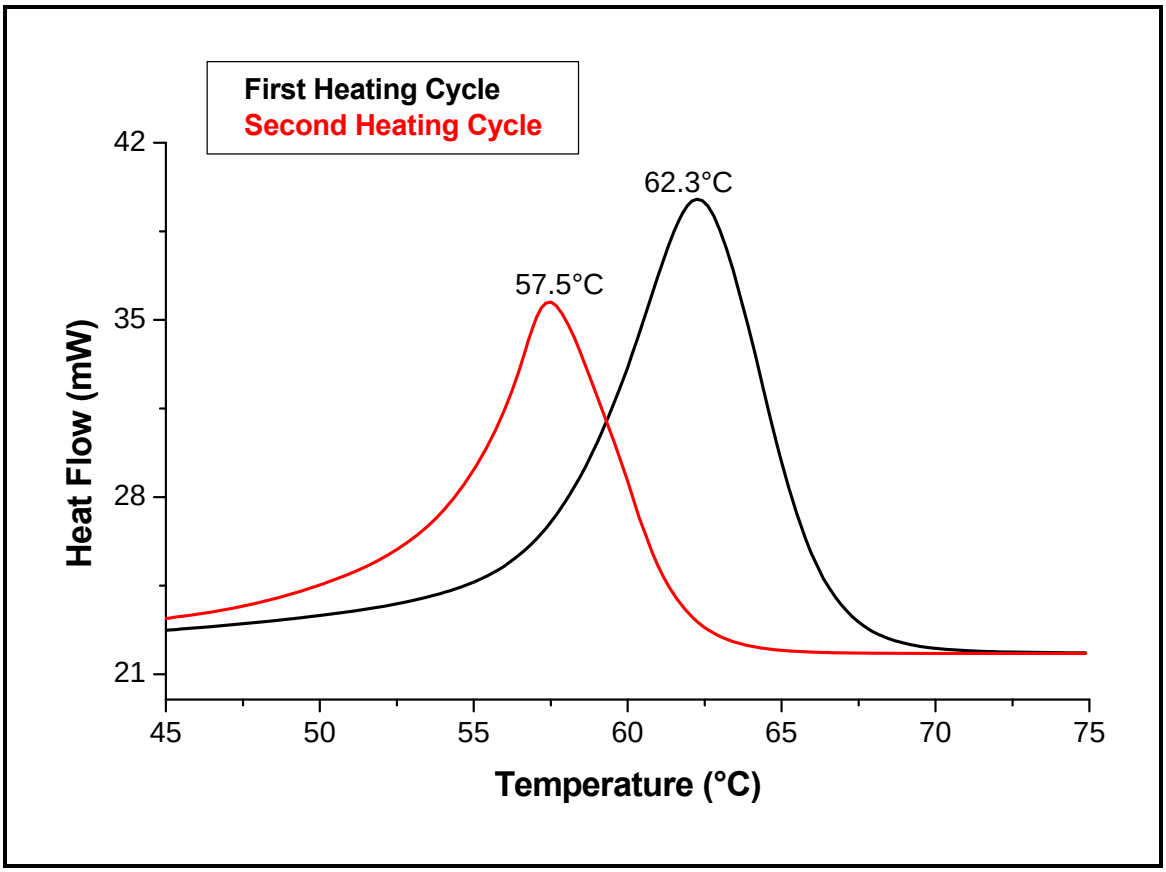

Figure 43A DSC curves of PCL (first and second heating scan).

In Figure 43A, PCL 100D shows a main endothermic peak at 62.3°C and 57.5°C for the first and second heating cycle, respectively. The endothermic peaks are attributed to the melting point of pure PCL 100D. It can be seen that there is a slight shift in the peak after the second heating cycle. The results gotten agree with those from other authors who studied the thermal analysis of PCL.[59, 60]

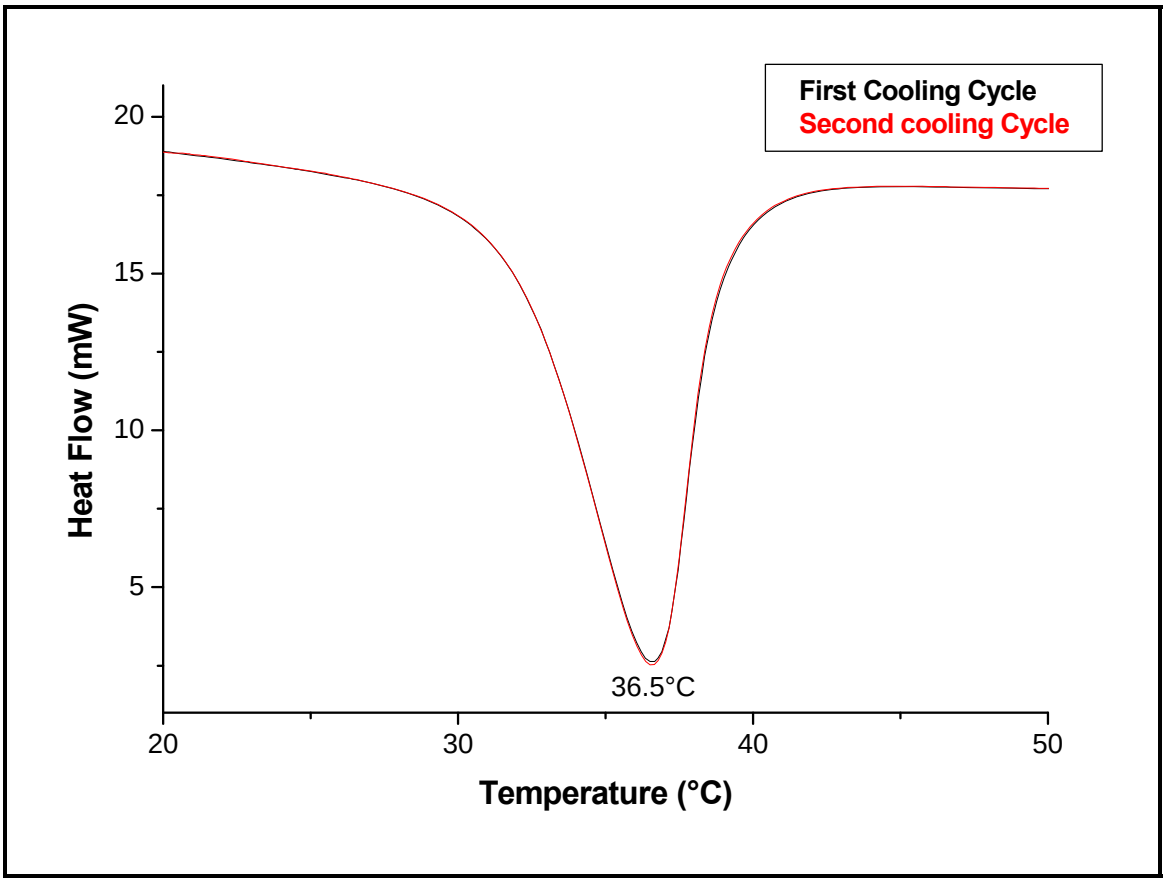

Figure 43B DSC curves of PCL (first and second cooling scan).

Figure 43B shows the crystallization temperature of PCL 100D for the first and second cooling scan. The endothermic peak seen at 36.5°C can be attributed to the crystallization temperature of PCL 100D.

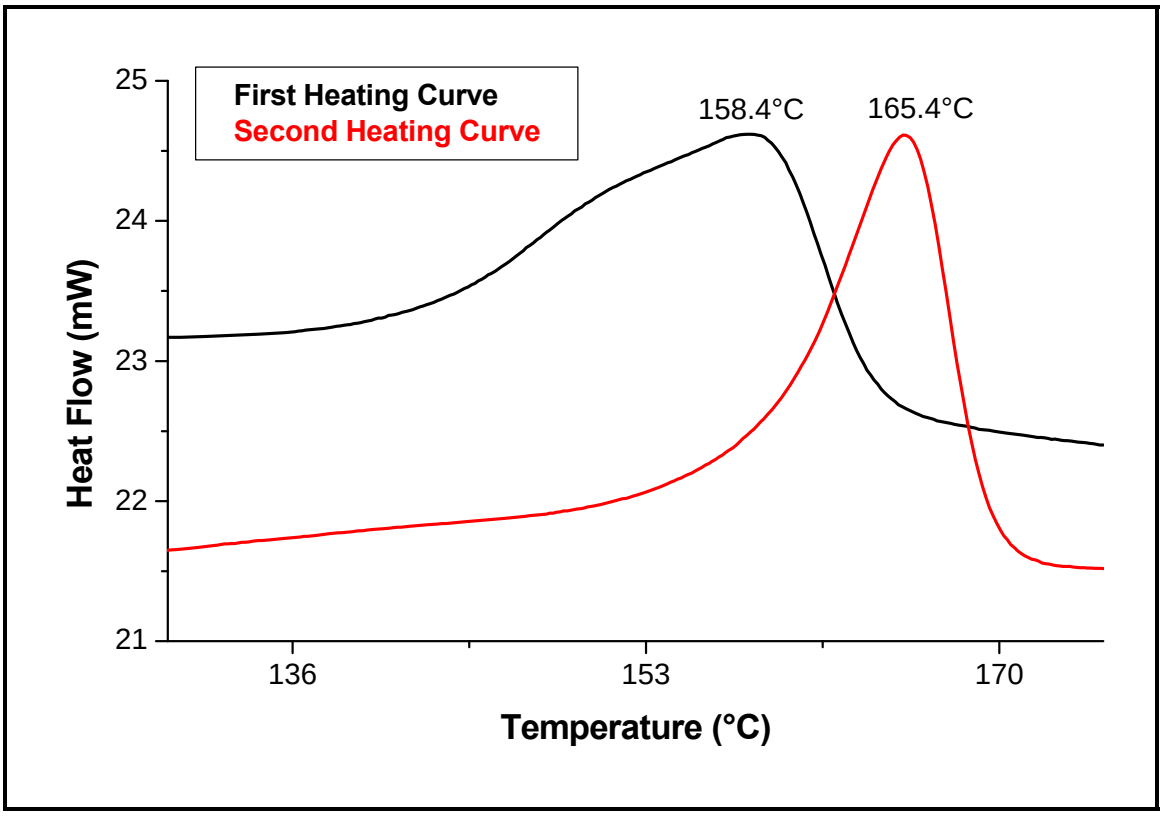

Figure 44A DSC curves of MB (first and second heating scan).

Figure 44A shows the DSC curves of MB for the first and second heating scan. The DSC scan of MB exhibits a melting endotherm with maxima at 158.4°C and 165.4°C for the first and second heating curve, respectively. It can be seen that there is a little shift in the peak from the first to the second heating cycle resulting in a change in the melting temperature of the major component of MB from 158.4 to 165.4. This temperature difference can still be accepted within the ranges of fluctuating melting temperature.

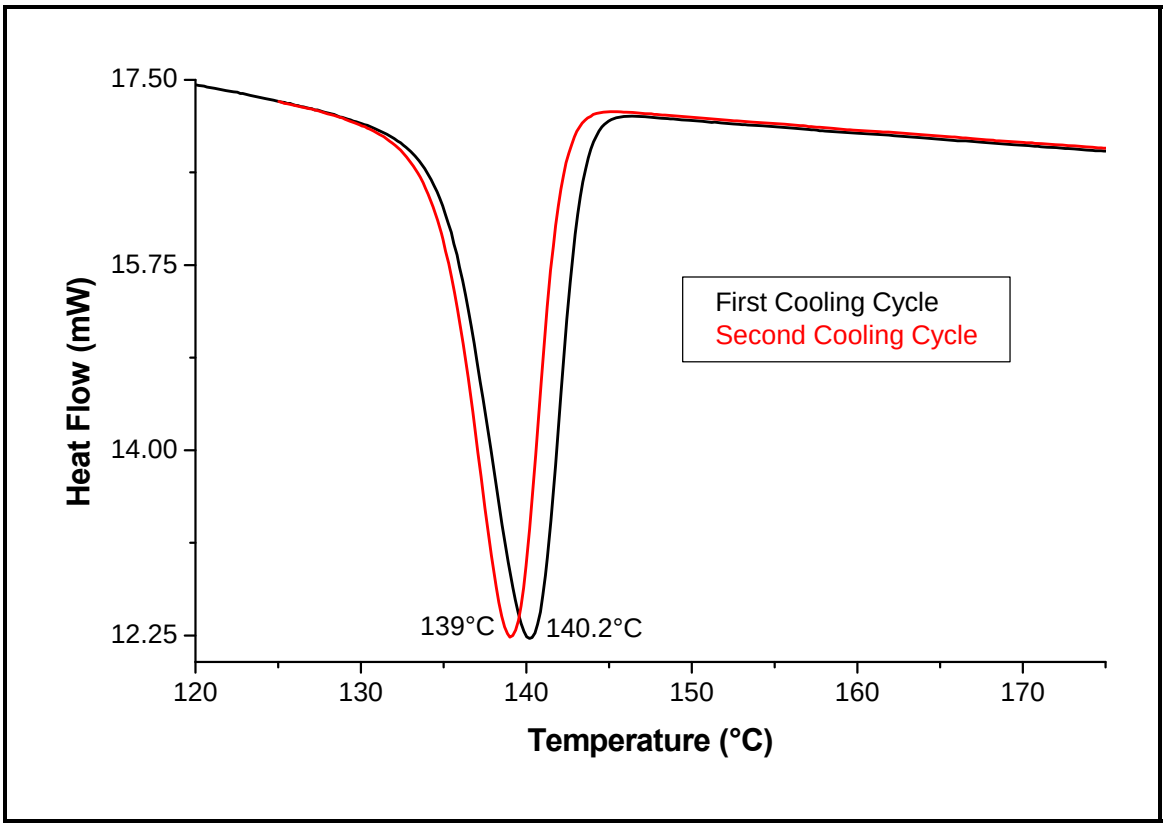

Figure 44B DSC curves of MB (first and second cooling scan).

Figure 44B shows the crystallization temperature for the first and second cooling scan. In both cases, the exothermic peaks at 139°C and 140.2°C for the first and second cooling cycle, respectively, can be attributed to the crystallization temperature of MB. The effect of weight percent MB on the melting, crystallization temperature of PCL 100D rich phase was studied when PCL 100D was blended with MB and the thermal properties are summarized in table 18 and 19.

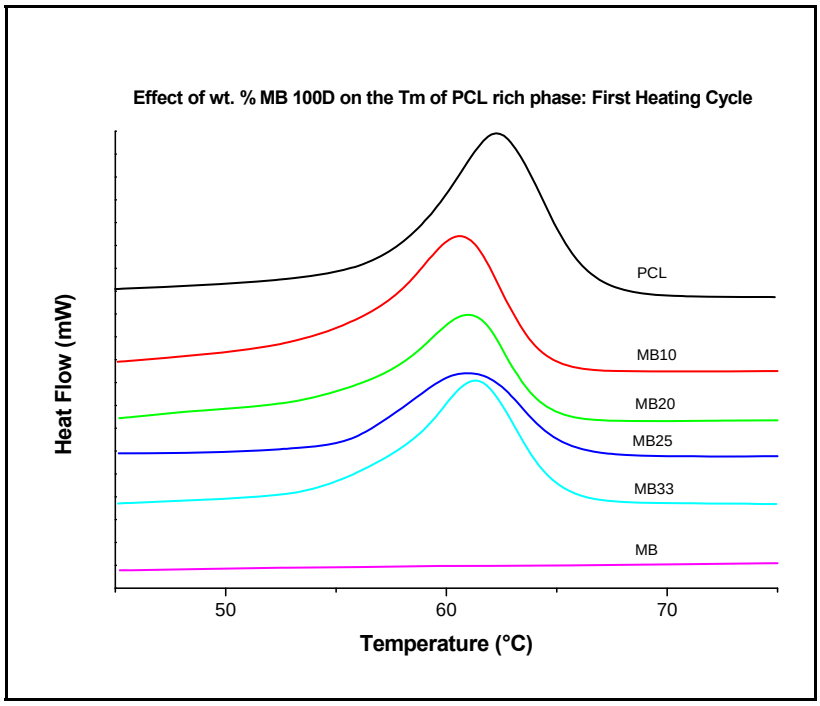

Figure 45A Effect of % wt. MB on the melting temperature T_m of PCL 100D rich phase (first heating cycle).

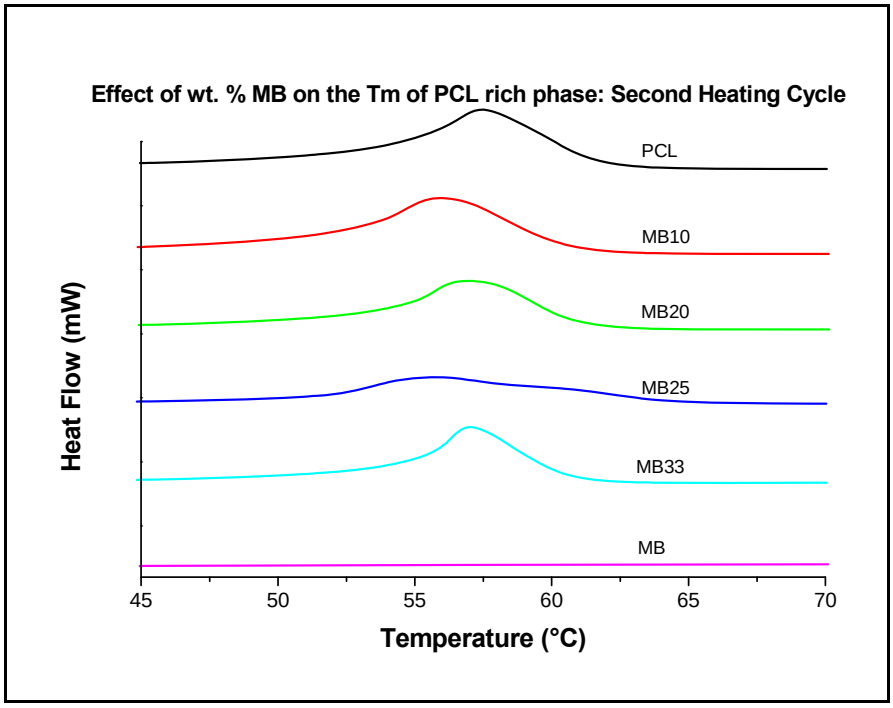

Figure 45B Effect of % wt. MB on the melting temperature T_m of PCL 100D rich phase (second heating cycle).

Figures 45A and 45B show the DSC curves of the effects of % wt. MB on PCL 100D rich phase of the first and second heating cycle, respectively. PCL 100D showed endothermic peaks for the first and second heating cycles at 62.3°C and 57.5°C respectively. The values of the endothermic peaks of their blends did not change significantly throughout except for the % wt. MB concentration in the second heating cycle that had an increase in the melting temperature to 60°C. Generally, there was a change in the values by approximately 1°C (take or give).

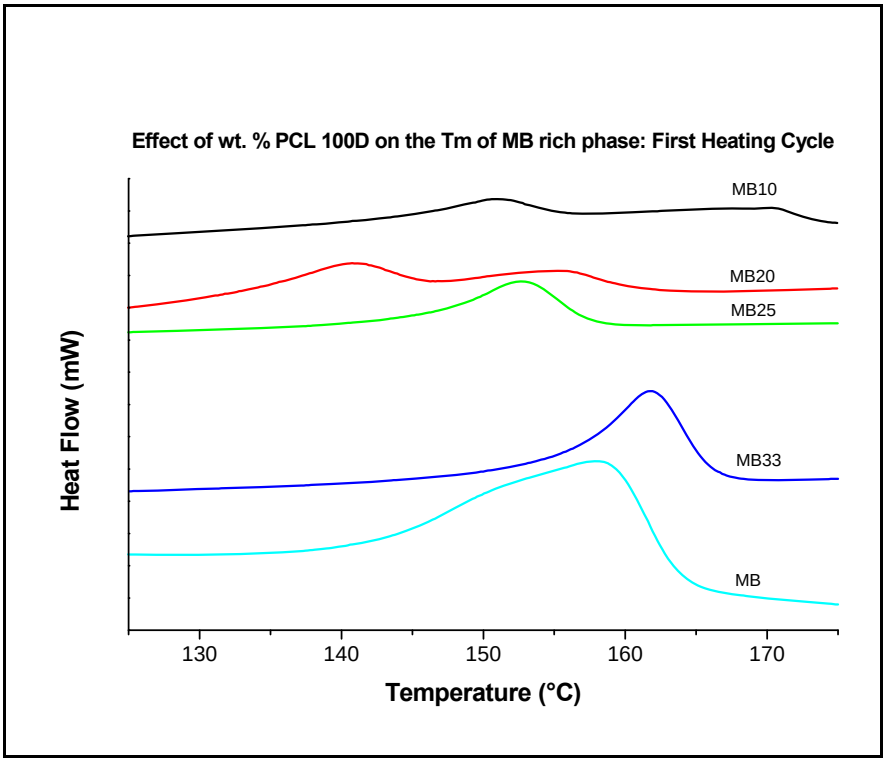

Figure 46A Effect of % wt. PCL on the melting temperature T_m of MB rich phase (first heating cycle).

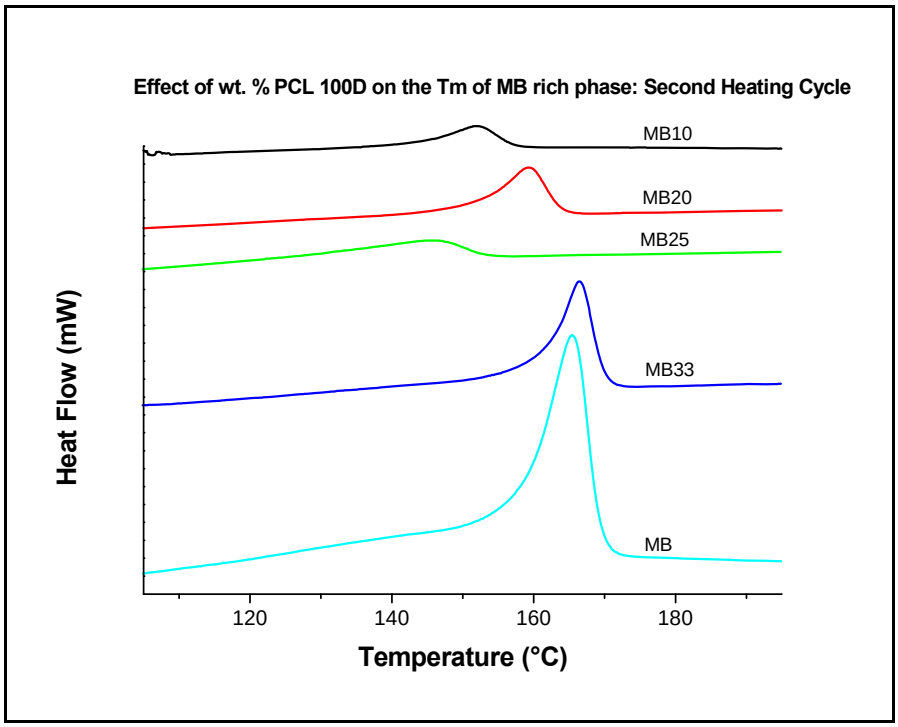

Figure 46B Effect of % wt. PCL on the melting temperature T_m of MB rich phase (second heating cycle).

Figure 46A and 46B show the DSC curves of the first and second heating cycles of the effects of % wt. PCL on melting temperature of MB rich phase. In Figure 46A, an erratic shifting of the peaks is noticed. MB shows two melt peaks at 150.6°C, 170.4°C and 140.3 °C, 155.8°C for the 10% and 20% wt. MB concentration respectively. After this % wt. MB concentration, only one peak is visible up till the pure MB. The disappearance of the second peak is evident during the second heating cycle.

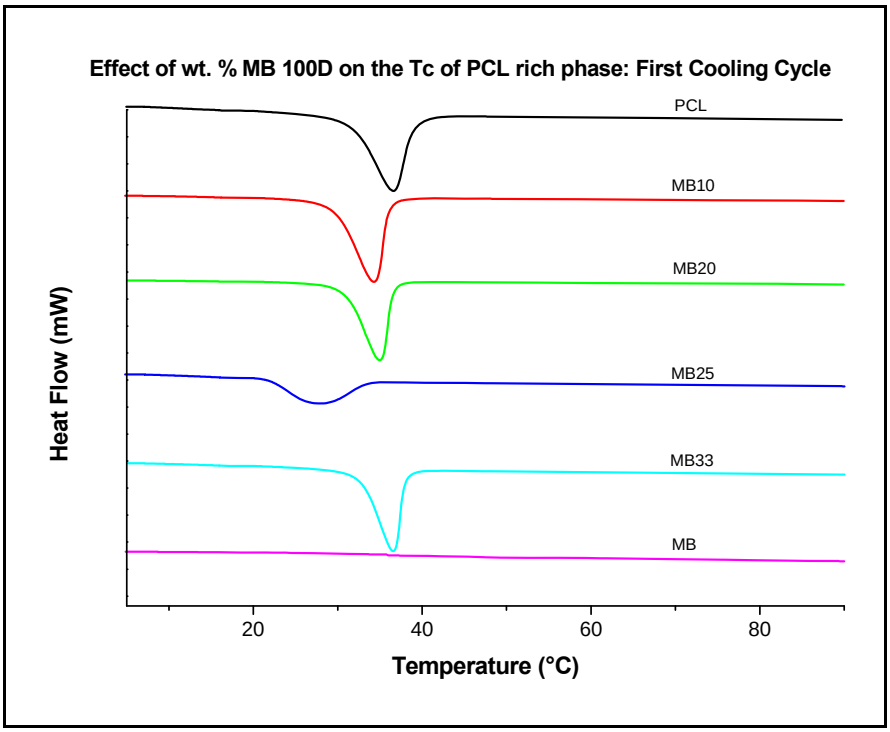

Figure 47A Effect of % wt. MB on the crystallization temperature T_c of PCL 100D rich phase (first cooling cycle).

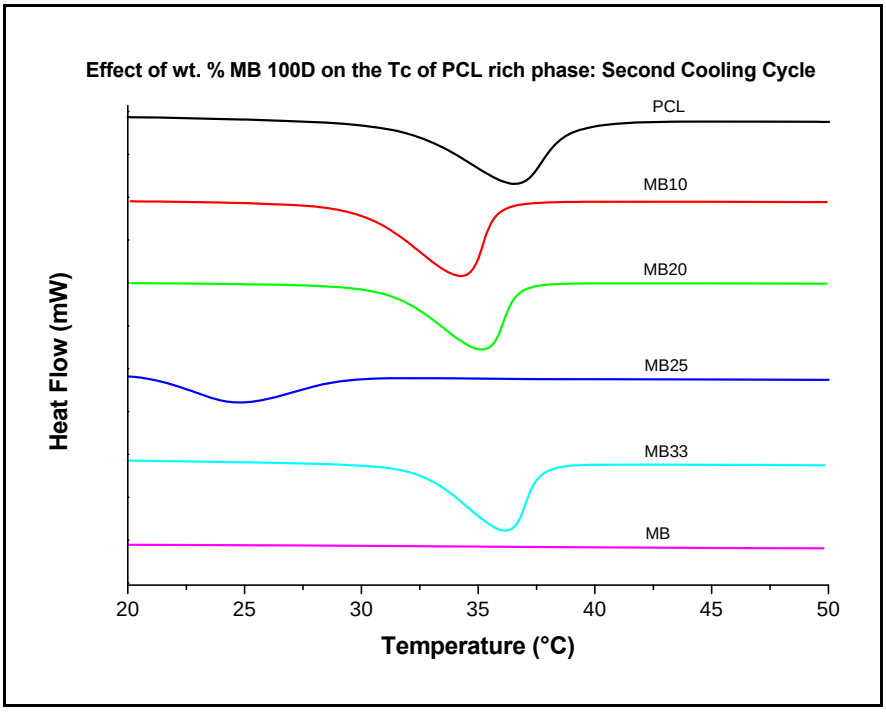

Figure 47B Effect of % wt. MB on the crystallization temperature T_c of PCL 100D rich phase (second cooling cycle).

Pure PCL 100D showed a main exotherm peak at around 36.5°C for the first and second cooling scans (Figure 47A and 47B). This value is relatively modified for the blends. It is shifted to lower temperature for the 10%, 20% and 25% wt. MB concentration. This goes to explain that there are certain interactions that are taking place due to the shifting, decreasing and increasing of the endo- and exotherms of the various blends. Thermodynamic rules of miscibility suggests that a decrease in the thermal transition enthalpies in indicative of a miscible polymer system. This decrease relative to the base polymer system (especially with the 25% wt. MB in the second cooling cycle) reflects enhanced interaction in the blend compared to the base polymer systems.

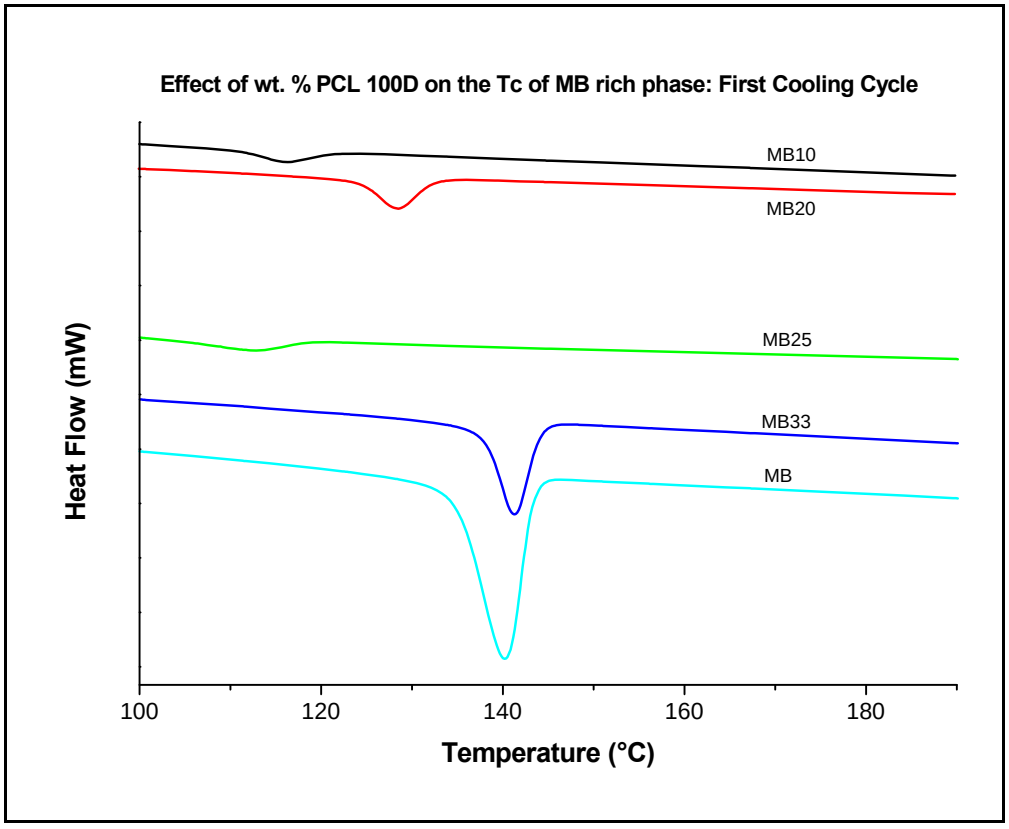

Figure 48A Effect of % wt. PCL on the crystallization temperature T_c of MB rich phase (first cooling cycle).

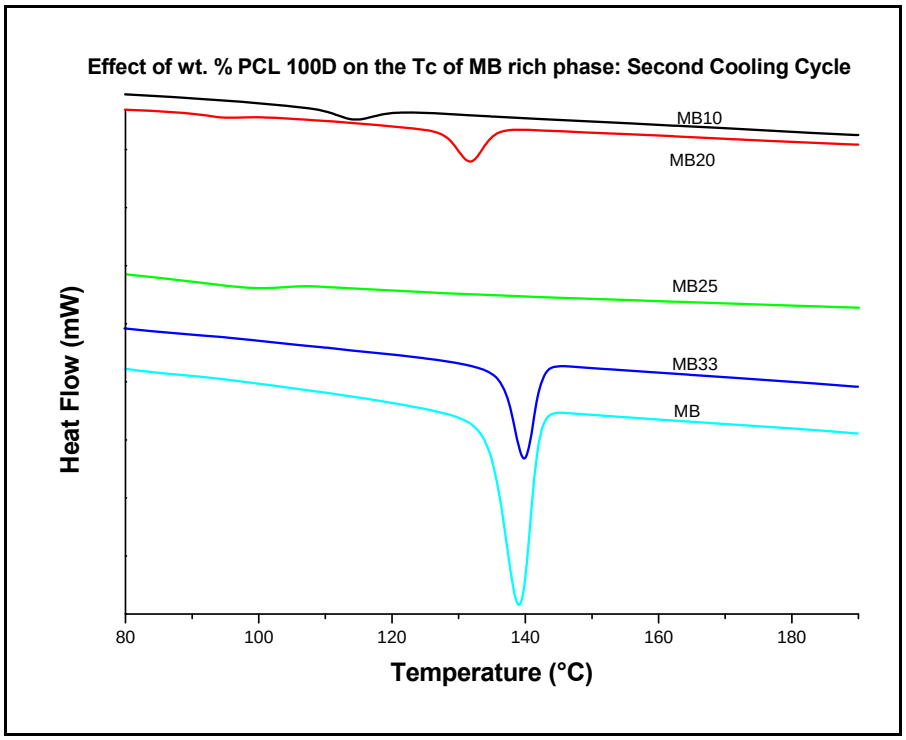

Figure 48B Effect of % wt. PCL on the crystallization temperature T_c of MB rich phase (second cooling cycle).

The study of the effect of weight percent PCL 100D on the crystallization temperature of MB rich phase during the first and second cooling scan showed peaks that shifted to higher values (Figure 48A and 48B and Table 18 and 19). The 25% weight MB shows a very small peak in the first cooling which almost disappears completely in the second peak. At MB concentrations of 33% and 100%, there is evidence of very sharp peaks (enthalpy).

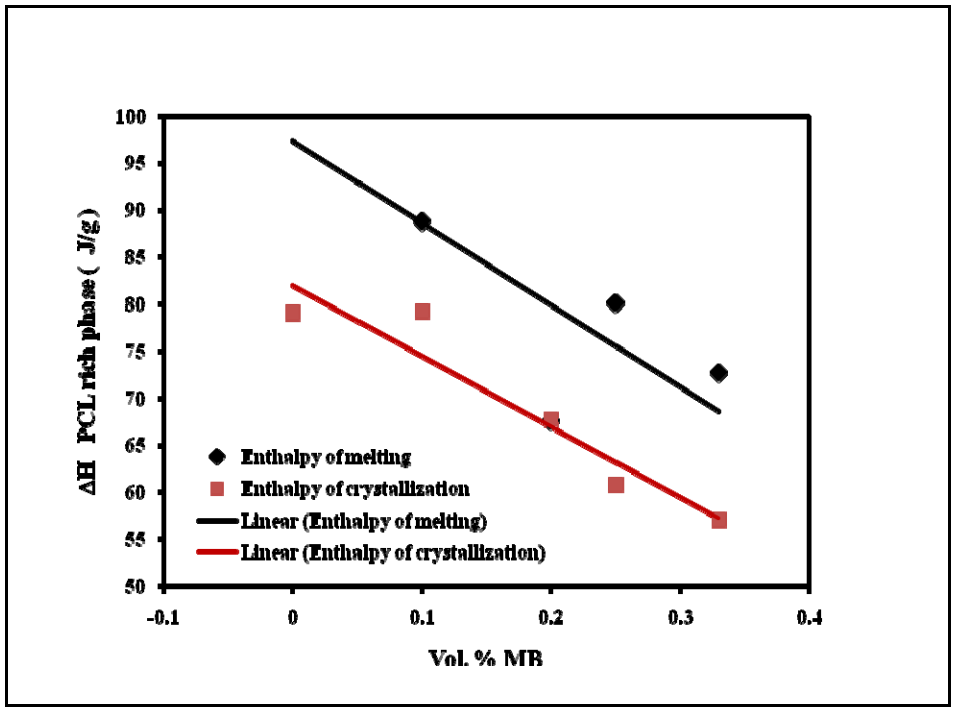

Figure 49A Variation of ΔH_m and ΔH_c of PCL 100D rich phase vs. vol % MB (first heating and cooling).

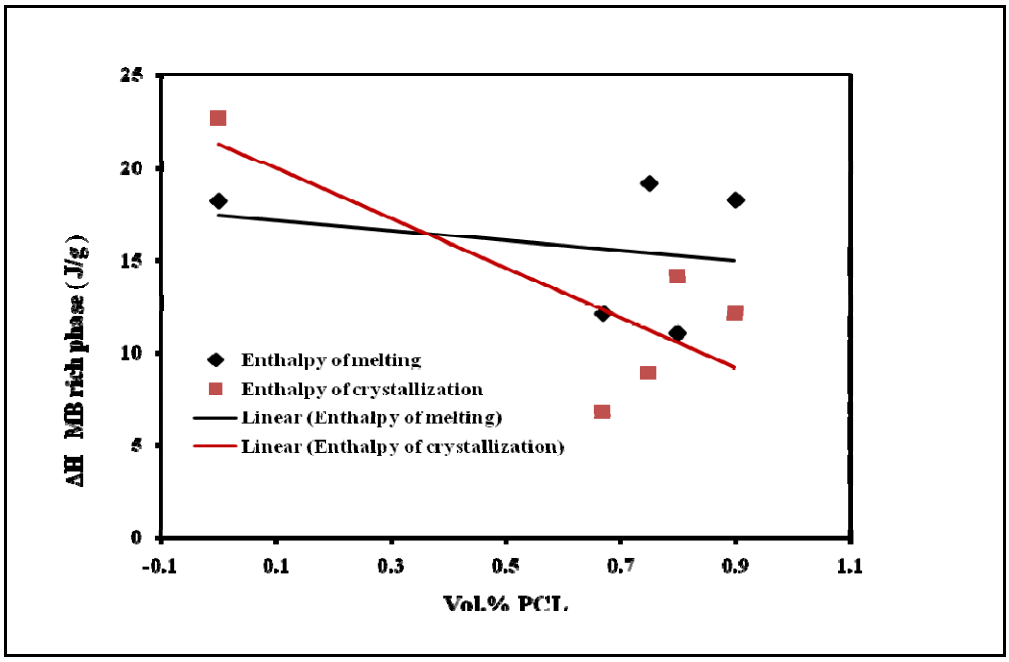

Figure 49B Variation of ΔH_m and ΔH_c of MB rich phase vs. vol % PCL (first heating and cooling).

Variations in the enthalpy of melting and crystallization of the blends as a function of the % wt. MB were studied for the first and second heating and cooling scans respectively. It is seen in Figure 49A and 49B that the enthalpy of melting and crystallization strongly depend on the blend composition; they decrease with the increase in the % wt. MB. In Figure 49A, it can be seen that the rate of decrease of the enthalpy of melting was more noticeable for MB content up to 25% after which there is a slight increase. The lowering of the enthalpy with increased MB concentration could be explained by the low interaction of the two polymers with each other.

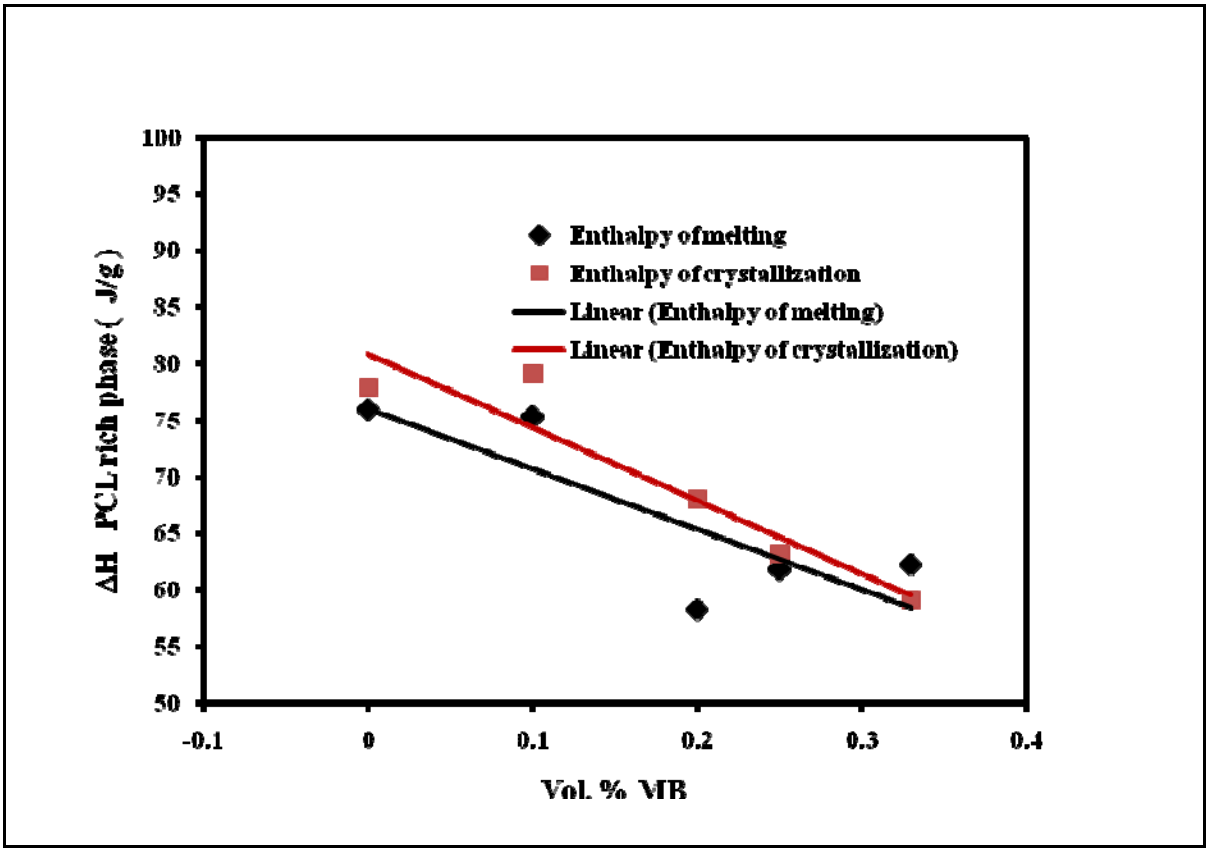

Figure 50A Variation of ΔH_m and ΔH_c of PCL 100D rich phase vs. vol % MB (second heating and cooling).

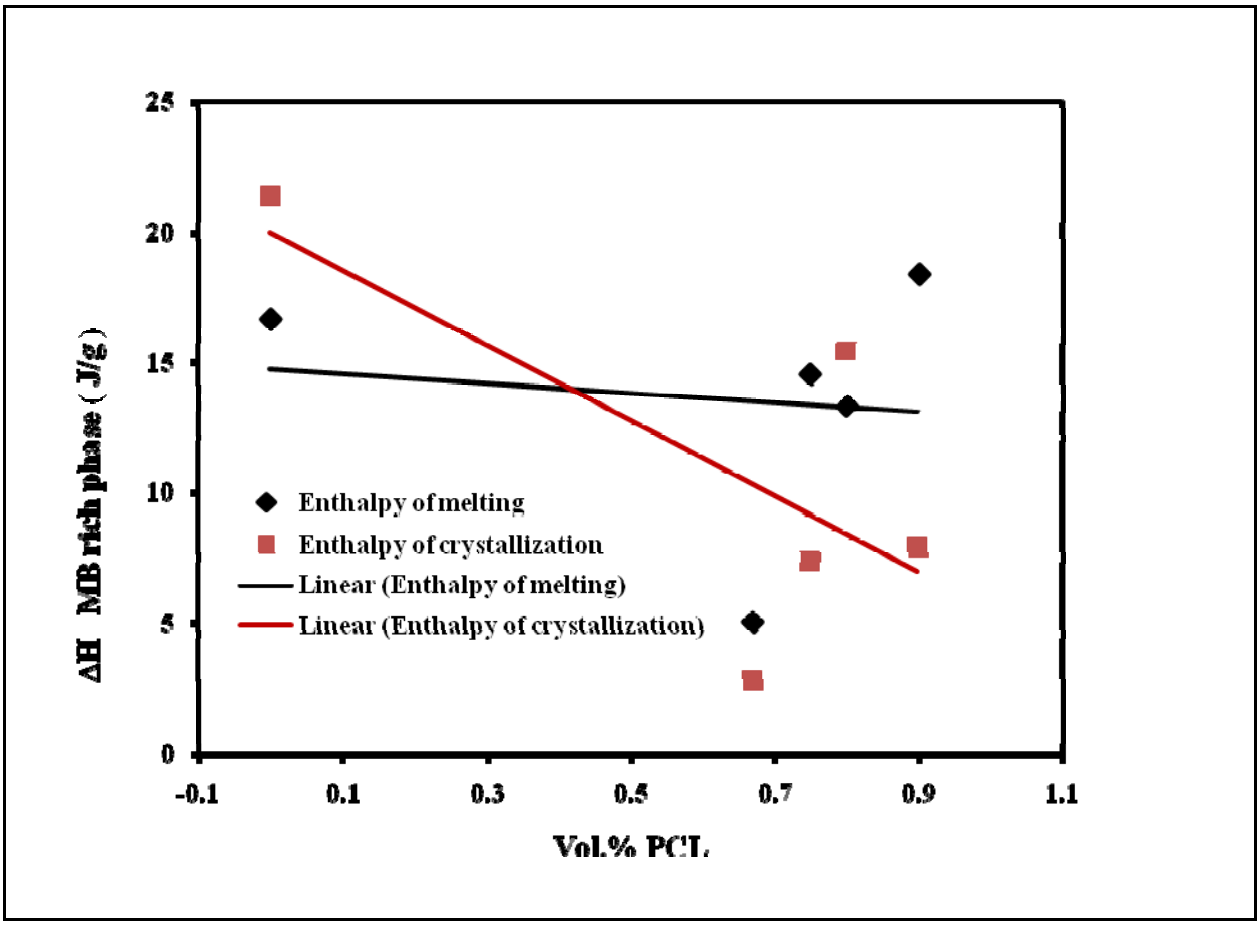

Figure 50B Variation of ΔH_m and ΔH_c of MB rich phase vs. vol % PCL (second heating and cooling).

Variations in the enthalpy of melting and crystallization of the blends as a function of weight percent PCL 100D was studied for the first and second heating and cooling, respectively. As shown in Figure 50A and 50B, the enthalpy of melting and crystallization are strongly dependent on the blend composition; they decrease with the increase of the % wt. PCL 100D in the blend. The rate at which it reduced was more evident up to concentrations of 75% PCL 100D. After this composition, a slight increase can be noticed.

Table 18 Experimental data from the first and second heating cycle.

% WT. MB	First Heating Cycle								Second Heating Cycle			
	PCL		MB						PCL		MB	
	(°C)	(J/g)	(°C)			(J/g)			(°C)	(J/g)	(°C)	(J/g)
	T_m	ΔH	T_{m1}	T_{m2}	T_{m3}	ΔH_1	ΔH_2	ΔH_3	T_m	ΔH	T_m	ΔH
0	62.3	105.95	-	-	-	-	-	-	57.5	83	-	-
10	60.57	82.96	150.6	170.4	196.1	1.597	1.134	0.001	60	80.70	151.8	2.1
20	60.96	53.71	140.3	155.8	-	2.412	1.204	-	56.9	60.7	159.3	5.537
25	60.93	47.88	152.6	222.5	237	5.480	0.551	0.202	55.8	45.8	145.5	4.423
33	61.28	55.77	161.8	-	-	8.206	-	-	57.1	51.44	166.4	6.564
100	-	-	158.4	-	-	20.23	-	-	-	-	165.4	30.07

Table 19 Experimental data from the first and second cooling cycle.

Samples	First Cooling Cycle				Second Cooling Cycle			
	PCL		MB		PCL		MB	
	(°C)	(J/g)	(°C)	(J/g)	(°C)	(J/g)	(°C)	(J/g)
	T_c	ΔH	T_c	ΔH	T_c	ΔH	T_c	ΔH
PCL	36.5	-78.9	-	-	36.5	-78.9	-	-
MB10	34.2	-71.14	116	-1.84	34.3	-70.79	114.1	-2.12
MB20	34.9	-54.06	128.5	-2.99	35.2	-54.54	131.7	-3.15
MB25	27.8	-46.26	112.4	-2.89	24.7	-46.48	97.7	-1.88
MB33	36.6	-48.76	141.2	-7.55	36.2	-49.42	139.9	-6.99
MB	-	-	140.2	-25.99	-	-	139	-23.79

Table 18 and 19 show the first and second heating cycle and first and second cooling cycle of PCL 100D, MB and their blends.

4.6. Dynamic Mechanical Analysis

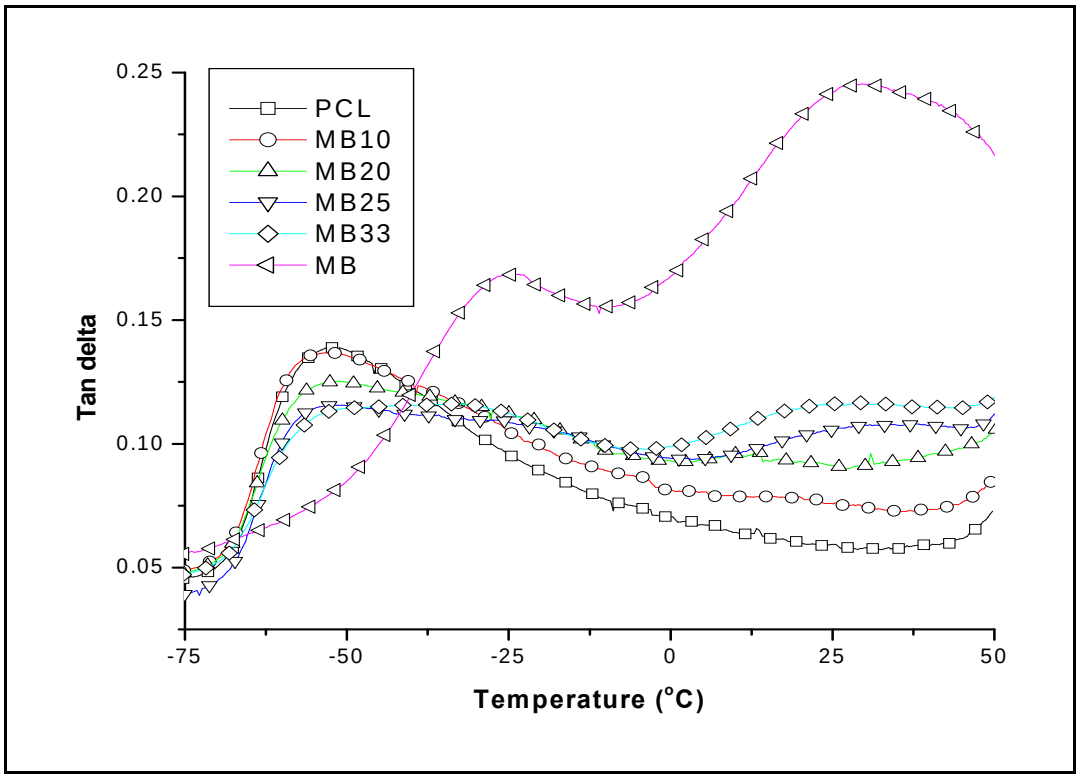

Figure 51A Mechanical spectra of PCL 100D, MB and their blends in terms of tan δ as a function of temperature.

Figure 51A shows the mechanical spectra of PCL 100D, MB and their blends in terms of tan δ as a function of temperature. It shows the α-relaxation peaks which are used to determine the glass transition temperature of the samples. Since the glass transition temperature of PCL 100D lies at sub ambient temperature and the limitations of the DSC used to go to sub ambient temperatures, DMA was used to obtain the glass transition temperature of the samples.

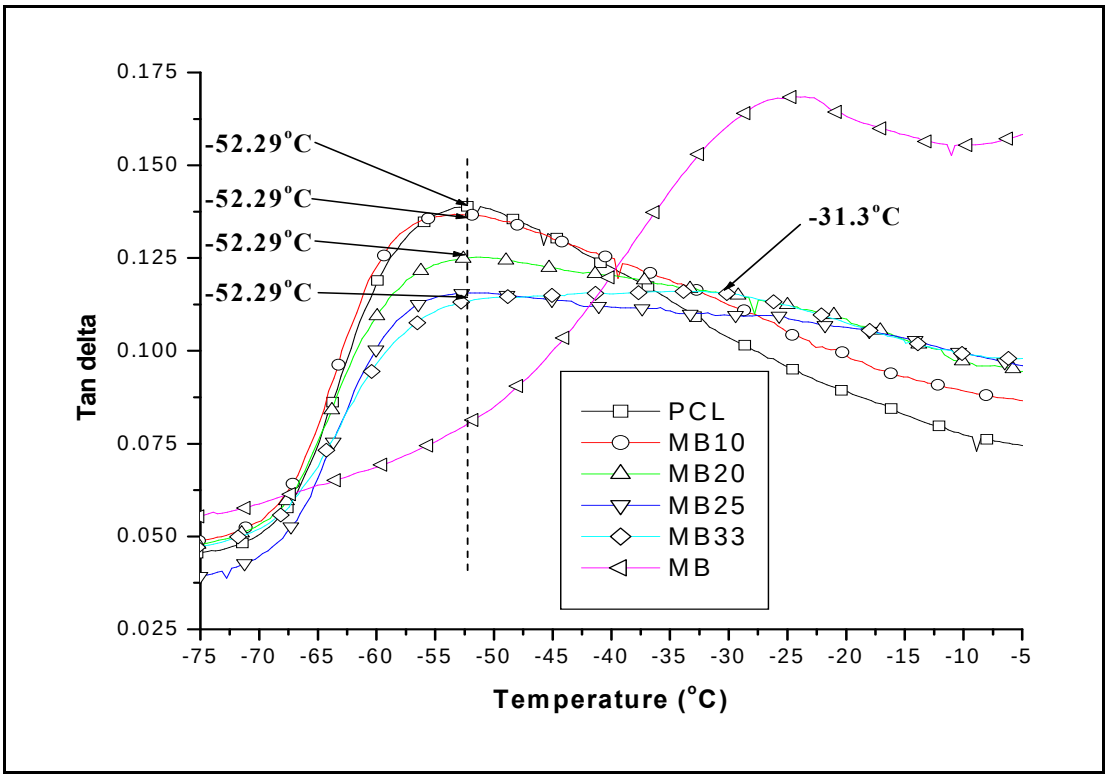

Figure 51B Mechanical spectra of PCL 100D rich phase in terms of tan δ as a function of temperature.

Figure 51B shows the glass transition temperature (T_g) of PCL 100D rich phase. It can be seen that pure PCL 100D and all its blends did not peak shift and have a glass transition of -52.23°C with the exception of the 33% wt. MB concentration which peak shifts to the right, reduces in the intensity of tan delta and has a glass transition temperature of -31.3°C. Concentrations of 20% and 25% MB also show reduction in the peak intensity.

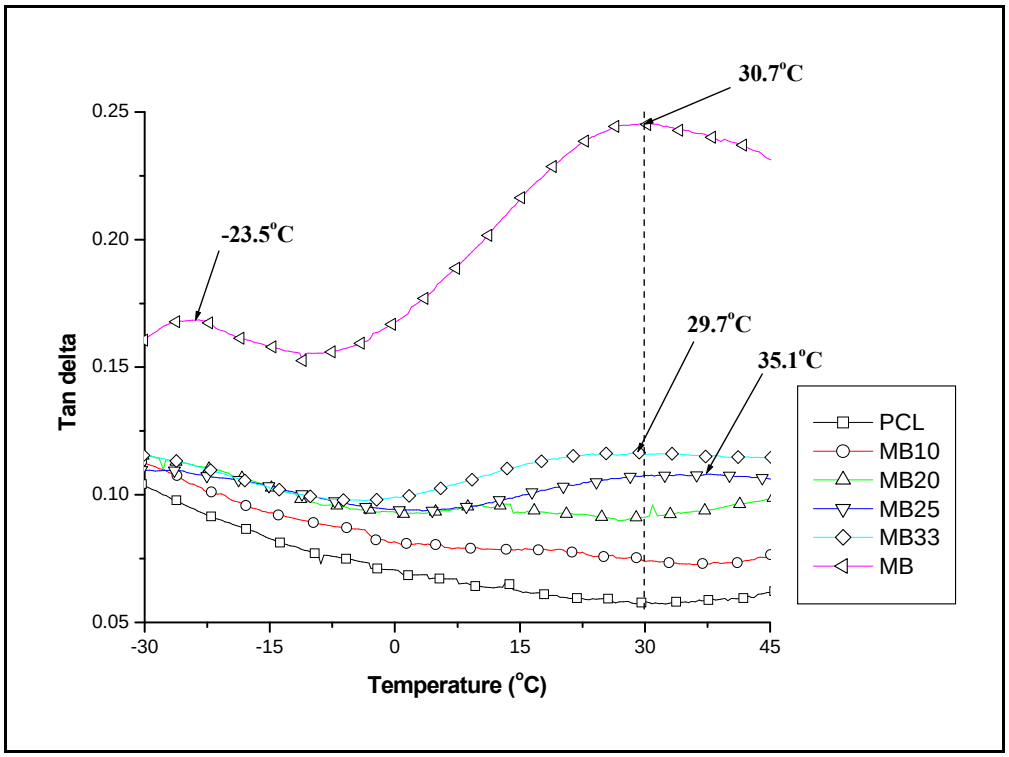

Figure 51C Mechanical spectra of MB in terms of tan δ as a function of temperature.

Figure 51C shows the mechanical spectra of MB rich phase. Two glass transition temperatures for MB can be seen at -23.5°C and 30.7°C and respectively. It can also be seen that blends with MB concentrations of 25% and 33% show a second glass transition temperature at 35.1°C and 29.7°C respectively. This suggests that the polymer blends are immiscible since miscibility can be determined by a single glass transition within a blend. Table 20 shows the glass transition temperatures of PCL 100D, MB and their blends.

Table 20 Glass transitions of PCL 100D, MB and their blends.

Sample	PCL 100D	MB	
	T_g (°C)	T_{g1} (°C)	T_{g2} (°C)
PCL	-52.2	N/A	N/A
MB10	-52.2	N/A	N/A
MB20	-52.2	N/A	N/A
MB25	-52.2	N/A	35.1
MB33	-31.3	N/A	29.7
MB	N/A	-23.5	30.7

4.7. Morphology Analysis

After performing mechanical tests on PCL, MB and their blends it can be noticed that the 25% wt. MB concentration shows distinct improvement in the mechanical properties compared to that of pure MB. This could result from special interaction between the two components at that composition or optimum composition, so to further understand why this improvement in the mechanical properties is seen, the morphology of the virgin blends were studied. The morphological analysis of binary PCL/MB mixtures was performed by using scanning electron microscopy (SEM). The interactions between the individual polymers at various compositions were studied from the morphology. In Figure 61, the cryo-fractured morphology of PCL 100D, MB and their blends in liquid nitrogen can be seen. The pure PCL 100D and MB show a finer fracture profile compared to their blends which show rough fracture profile.

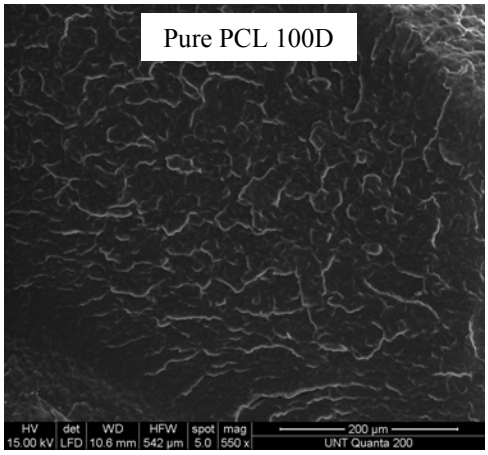

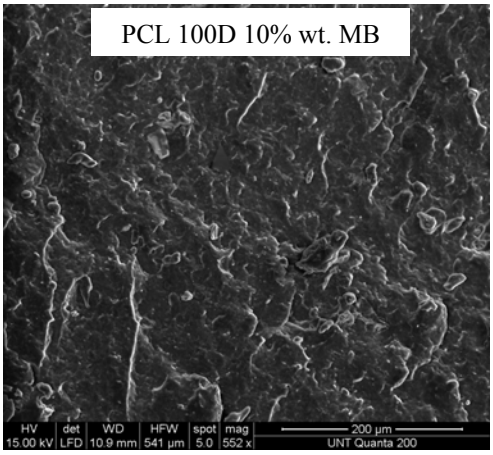

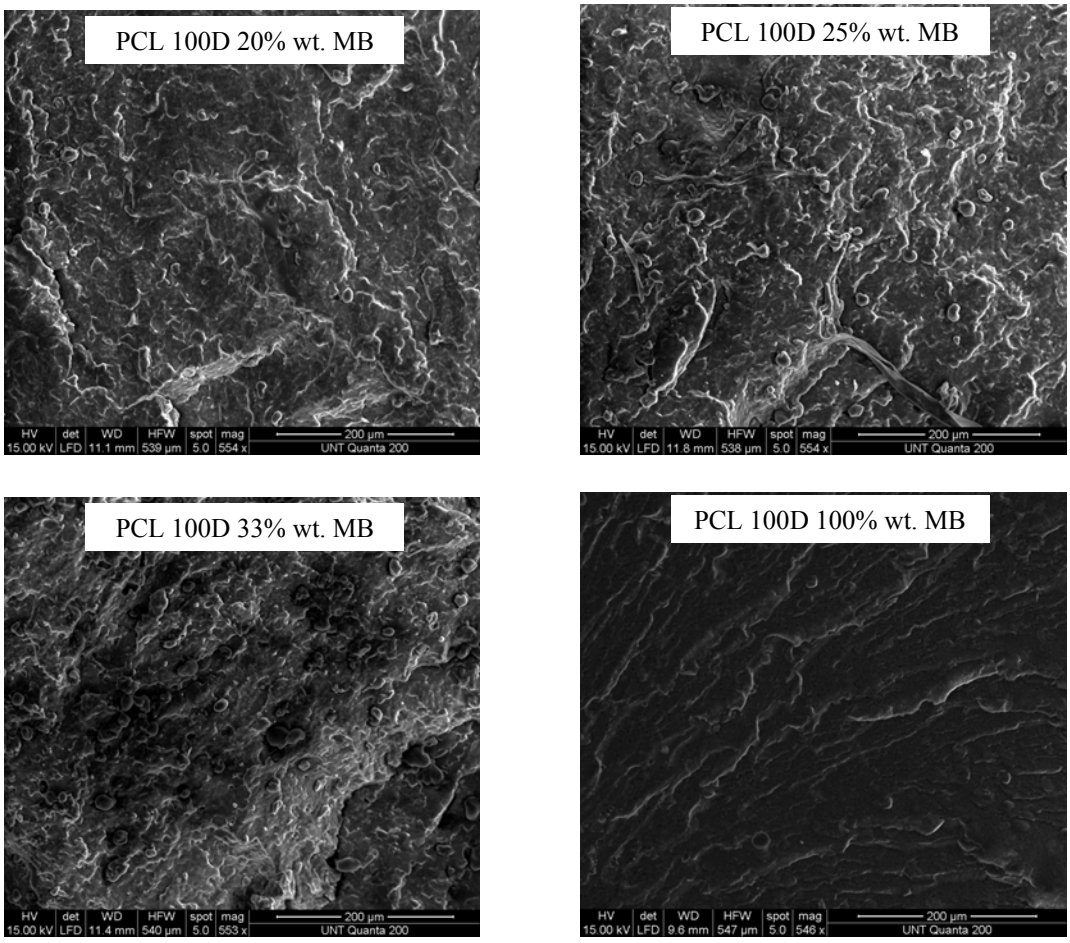

Figure 52 Micrographs of cryo-fractured PCL 100D, MB and their blends at X550.

In order to further understand the improved mechanical properties of the 25% wt. MB concentration, we look at magnified micrographs of Figure 61 (Figure 62). Figure 62 shows the micrographs of the morphology of PCL, MB and their blends at magnifications of X2525.

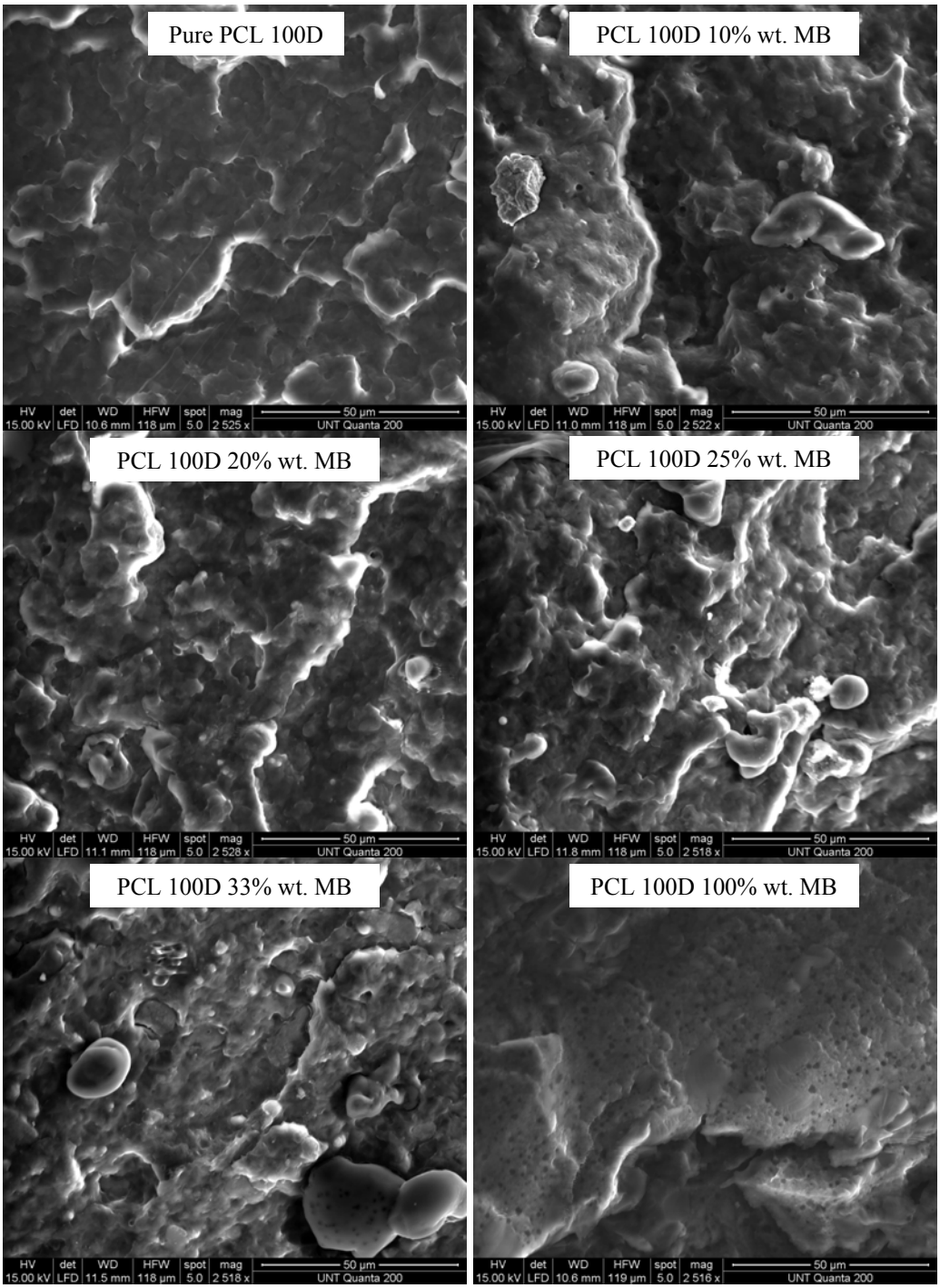

Figure 53 Micrographs of cryo-fractured PCL 100D, MB and their blends at X2525.

On careful examination of Figure 62, different features can be seen in each micrograph as the composition changes. In pure PCL 100D, crazing can be seen on the edges where fracture occurred and micro fibers can also be seen which have occurred

during fracture. Incomplete fracture of the sample even in liquid nitrogen caused drawing of the sample into fibers. This shows the extent to which pure PCL is ductile. 10% wt. MB micrograph shows little miscibility and relatively large dispersed phases of MB within the matrix of PCL 100D. It also shows micro-pores in the matrix which is from the ejected MB particles (phases) during fracturing. The micrograph shows a MB particle which is loosely bonded with the PCL 100D matrix This is caused by weak bonds between PCL 100D and MB. The 20% wt. MB micrograph shows lesser, smaller and more scattered dispersed MB phases within the PCL 100D matrix. Micro-pores can also be seen in the micrograph but they are also smaller and more scattered within the matrix. This suggests increased compatibility between PCL 100D and MB as the concentration is increased. The 25% wt. MB shows some distinct properties. It shows micro fiber drawing which is attributed to the content of PCL 100D. An almost complete homogeneity can be seen with very small and few dispersed MB particles (phases). No micro-pores can be seen in the micrograph indicating again increased miscibility between the individual polymers. In the micrograph of the 33% wt. MB, micro-pores, more and larger dispersed MB phases and loose bonding between PCL 100D and MB can be seen. In this composition, miscibility can be seen to have reduced and as a result, homogeneity is also affected. The micrograph of the pure MB shows a ternary phase. A large phase which is smooth and micro-pore free dispersed within a binary phase. A binary phase which makes up the matrix shows two partially homogeneous phase between to unknown components. In the binary phase, micro-pores can be seen every where within the phase. This is a suggested reason MB absorbs and can retain a lot of moisture. This ternary phase is a result of the three components of MB; starch, plasticizer and polyester. The

morphology reveals heterogeneity and immiscibility between the components of MB. The edges of the fracture are seen to be sharp. This can be as a result of the brittle fracture that occurs in MB.

After analyzing the micrographs, we could see that miscibility increased as MB concentration was increased and at the 25% wt. concentration, optimum miscibility can be seen, increased bond strength and exhibition of both properties of PCL 100D and MB; toughness and strength. With further increase in MB concentration, immiscibility and reduced bond strength is noticed. The improved mechanical properties of MB at the 25% concentration is as a result of the above characteristics seen in the micrograph and is the optimum composition for miscibility.

CHAPTER 5

CONCLUSION

5.1. Foam Preparation

The objective of this work was to develop and characterize a structural foam material of biodegradable thermoplastic blends using a safe and environmentally benign technology. In correlation with this goal, cellular foams of blends from MB reinforced polycaprolactone using CO_2 as a blowing agent, and were characterized by differential scanning calorimetry, X-ray diffraction, scanning electron microscopy and dynamic mechanical analysis. In order to fabricate the foams, blends of the above stated polymers were first compression molded into 3mm thick sheets. The compression molding of all the samples was done in one batch under the same condition to reduce any variations in their properties after molding, if molded at different conditions.

The foaming method used for this study was a constant temperature, variable pressure batch process in which predominately macrocellular and microcellular foams were formed by first saturating the sample sheets with supercritical CO_2 in a high pressure reactor, and then rapidly quenching the pressure to allow the CO_2 nucleate and grow cells. Saturation of the samples took place via diffusion of SCF through the blends. Solubility of CO_2 in the blends was an essential variable in the foaming process because it affected the magnitude of plasticization of the pre-foamed samples, as well as the gas available for cell growth. The processing conditions were limited due to the plasticization and service pressure of the reactor. In this study, the minimum and maximum processing temperature was at 31°C and 35°C, due to the critical temperature of the SCF used and the depression of the T_g of the samples.

The rate of depressurization was also of critical importance to the generation of foam. Low reactor evacuation times, 5 to 10 seconds were required in order to produce fine cell structures with consistent density distribution. Slower quench rates resulted in partially foamed or no foam generation.

Mechanical testing of foams indicates that the 25% weight MB concentration has the best mechanical properties. It is theorized that the improved mechanical properties of that composition is due to high interaction between the two polymers (PCL and MB) based on analysis of the polymer crystallinity

5.2. Characterization

DSC of the foamed and unfoamed blends revealed that neither the addition of low concentrations of MB nor the generation of foam cells had significant effect on the glass transition temperature of the parent polycaprolactone. It did show that the enthalpy of melting and recyrstallization was dependent on the concentration of MB in the blends. A significant decrease with MB content indicated an effect on MB crystallinity by the PCL

X-ray diffraction of the blends was performed in order to examine the crystallinity of the samples before and after the foaming process. The results showed that 2-theta peaks with high intensities were present in all the virgin samples, revealing crystallinity in the samples. 2-theta peaks were also seen the foams samples except that they were a lot lower than those found in the virgin samples. This reveals that the crystallinity in the samples reduced after the samples were foamed.

One of the polymers used (PCL) has a glass transition temperature of -60°C. DMA was performed on the virgin PCL, MB and their blends in order to investigate the effects of MB and PCL concentration on the glass transition of PCL and MB rich phase

respectively. Since it has the capability to go to temperatures as low as -180°C, DMA was used. SEM characterization revealed that MB concentration had a strong effect on the cell density and size. The micrograph showed a rapid decrease in the cell density, size and foamability as MB concentration increased.

The CO_2 sorption test showed that complete saturation of the samples were reached below the foaming temperature and pressure. From this, we know that at the foam processing conditions, we achieved complete saturation which is necessary for nucleation and growth of steady bubbles.

From the results of the mechanical tests performed, pure PCL showed better tensile, compressive and impact properties. Sample with 25% wt. MB concentration showed improved shear and tensile properties of the foamed samples. Within the samples containing % MB concentration, 25% wt. MB showed an overall improved tensile, shear and impact properties.

BIBLIOGRAPHY

1.Ghaderi, R., *A Supercritical Fluids Extraction Process for the Production of Drug Loaded Biodegradable Microparticles*, Ph.D Uppsala Biomedical Center.

2.F. Cansell, S. R., and P. Beslin, *Thermodynamic Aspects of Supercritical Fluids Processing: Applications to Polymers and Wastes Treatment*. REVUE DE L'INSTITUT FRANCAIS DU PETROLE VOL. 53, N0. 1, 1998

3.Sameer P. Nalawade, F. P., Leon P. B. M. Jassen, Vishal E. patil, Jos. T. F. Keurentjes, Reiner Staudt, *Solubilities of Sub- and Supercritical Carbon Dioxide in Polyester Resins*. Prog. Polym. Sci. 31 (2006) 19-43

4.Ryan Gosselin, D. R.,*Cell morphology analysis of high density polymer foams*. Polymer testing 24 (2005) 1027-1035

5.Strauss, W., *Saturation and Foaming of Thermoplastic Nanocomposites Using Supercritical CO2*. MS Thesis, university of North Texas (2004).

6.Blaga, A., CBD-166. *Plastic Foams* (1974).

7.Reedy, M. E., *Chemical Foaming Agents Improve Performance and Productivity* Reedy International Corporation Keyport, New Jersey, US.

8.Hongliu Sun, G. S. S., James E. Mark, *Microcellular foams from polyethersulfone and polyphenylsulfone. Preparation and mechanical properties*.

9.Xioapeng Chen, J. J. F., Christopher A. Bertelo, *Plasticization Effects on Bubble Growth during Polymer Foaming*. Polymer Engineering and Science; Jan 2006; 46,pg 97

10.Yaolin Zhang, D. R., Abdellatif Ait-Kadi, *High-density Polyethylene Foams. I. Polymer Foam Characterization*. Journal of applied polymer Science, Vol. 990, 2111-2119 (2003)

11.E. Reverchon, S. C., *Production of controlled polymeric foams by supercritical CO2*. J. of Supercritical Fliuds 40 (2007) 144-152

12.Zhu N., C. F. Z., Hu K., Zhu L., *Biomedical Modification of poly (L-lactide) by blending with lecithin*.

13.Chen C. C., C. J. Y., Tseng H., Huang H. M., Lee S. Y., *Preparation and characterization of biodegradable PLA+ PCL polymeric blends*.

14.F. Rezgui, M. S., J. M. Hiver, C. G'Sell, T. Sadoun, *Deformation and damage upon stretching of degradable polymers (PLA and PCL)*.

15.Miller, D., *Characterization of Polyetherimide Carbondioxide System and Mechanical Properties of high Relative density Polyetherimide Nanofoams*, M.S. Thesis, University of Washington.

16.W. J. Work, K. H., M. Hess, R. F. T. Stepto, *Definition of Terms Related To Polymer Blends, Composites, and Multiphase Polymeric Materials*.

17.Dilip Gersappei, Darrell Irvine, Anna C. Balazs, Yun Liu, Jon Sokolov, Miriam Rafailovich, steven Schwarz, Dennis G Peiffer, *The use of Grafted Copolymers to Bind Immiscible blends.*

18.Satoshi Kubo, John F. Kadla *The formation of strong Intermolecular Interactions in Immiscible Blends of Poly (Vinyl alcohol) (PVA) and Lignin.*

19.Goh, S. H., *Miscible blends of poly (tetrahydrofurfuryl methacrylate) with two hydroxyl-containing polymers*.

20.Shiao Wei Kuo, Chih Feng Huang, Feng Chih Chang, *Study of Hydrogen-Bonding strength in Poly (ε-Caprolactone) Blends by DSC and FTIR.*

21.Wang, W. C. V., Kramer, E., Sachse, W., J. Polym. Sci., Polym. Phys. Ed., 20, 1371 (1982).

22.Gabriel O. Shonaike, G. P. S., *Polymer Blends and Alloys*

23.B. Y. Tay, S. X. Z., M. H. Myint, F. L. Ng, M. Chandrasekaran, L. K. A Tan, *Processing of polycaprolactone porous structure for scaffold development.* Journal of Materials Processing Technology 182 (2007) 117-121

24.Mandal T. K., W. E. M., Polym J 1999; 31; 226.

25.Zhong Z., G. Q., Mi Y. , Polymer 1999; 40; 27.

26.De Juana, R., Cortazar, M. , Macromolecules 1993, 26, 1170.

27.Jieh- Ming Huang, S.-J. Y., *Studying the miscibility and thermal behavior of polybenzoxazine/poly (ε-caprolactone) blends using DSC, DMA, and Solid state 13C NMR spectroscopy*.

28.Lezcano, E. G., Coll, C. S., Prolongo, M. G., . Polymer 1996, 37, 3603.

29.Cael J.J, K. J. L., Blackwell, J., Biopolymers, 1975,14,1885.

30.Otey, F. H., Doane, W. M., *in Starch chemistry and technology,* ed. R. O. Whistler et al. Academic Press, New York, 1984, pp. 154, 667.

31.Bastioli, C., Bellotti, V. and Del Tredici, G. F., Eur. Pat. Appl. WO 90/EP1286, 1990.

32.Colonna, P. a. M., C., phytochemistry, 1985, 24 (8), 1667.

33.Silbiger, J., Sacchetto, J. P. and Lentz, D. J., Eur. Pat. Appl. O 404 728, 1990.

34.Bastioli, C., Bellotti, V. and Del Giudice, L., et al., US Pat. No. 52,62,458, 1993.

35.Lay, G., Rehm, J., Stepto, R. F. T. and Tomka, M. , Eur. Pat. Appl. No. 0327525, 1989.

36.Otery, F. H., Westhoff, R. P. and Doane, W. M. , *Ind. Eng. Chem*. Prod. Res. Dev., 1980, 19, 592. .

37.Otey, F. H., , Doane, W. M., US Pat 41,33,784, 1979.

38.Sacchetto, J. P. a. S., R. F. T., US 4,900,361, 1990.

39.Sacchetto, J. P. E., M., Stepto, R. F. T. and Zeller, J., Eur. Pat. Appl. No. 0391853.

40.Bastioli, C., *Properties and applications of MB starch-based materials. Polymer Degradation and Stabillity*, 59 (1998) 263-272

41.Hyatt, J. A., *Liquid and Supercritical carbon dioxide as organic solvents*. J Org Chem 1984; 49; 5097-101.

42.Tomasko D. L., L. H., Liu D., Han X., Wingert M. J., Lee L. J., et al. , *A review of CO2 application in the processing of polymers*. Ind Eng Chem res 2003; 42; 6431-56.

43.Sameer P. Nalawade, F. P., L. P. B. M. Jassen., *Supercritical carbon dioxide as green solvent for processing polymer melts: Processing aspects and applications*. Prog. Polym. Sci. 31 (2006) 19-43

44.Séverine A. E. Boyer, J.-P. E. G., *Simultenuous measurements of the concentration of a supercritical gas absorbed in a polymer and of the concomitant change in volume of the polymer. The coupled VW-pVT technique revisited*. Polymer 46 (2005) 3737-3747

45.Kiran, E., (1994) *Supercritical fluids-Fundamentals for application*. Nato ASI ser. E 273, Kluwer, Dordrecht, 541-588.

46.Durill P. L., G. R. G., *Diffusion and solution of gases in thermally softened or molten polymers: part I. Development of technique and determination of data* AIChE J 1966; 12; 1147-51.

47.Durill P. L., G. R. G., *Diffusion and solution of gases in thermally softened or molten polymers: part I. Relation of diffusivities and solubilities with temperature, pressure and structural characteristics*. AIChE J 1969; 15; 106-10.

48.Newitt D. M., W. K. E., *Solution and diffusion of gases in polystyrene at high pressures*. J Chem Soc 1948; 2; 1541-9.

49.V. Wiesmet, E. W., S. Behme, G. Sadowski, and W, J. Arlt, J. Sup. Fluids, 17, 1 (2000).

50.Y.Sato, M. Y., K. Fujiwara, S. Takishima, and H. Masuaka, *Fluid Phase Equil*., 125, 129 (1996).

51.Y. Kamiya, K. M., K. Terada, Y. Fujiwara, and T. –S. Wang, Macromolecules, 31, 472 (1998).

52.R. Kleinrahm and W. Wagner, J. C., Therm., 18, 739 (1986).

53.Berens, A. R., Huvard, G. S., Korsmeyer, R. W., Kunig, F. W., J. Appl. Polym. Sci., 46, 231 (1992).

54.Dey, S. K., Zhang Q., Faridi. N., Xanthos, M., *Conference Proceedings* – ANTEC 1997, 43.

55.Zhang, Q., Xamthos, M., Dey, S. K., J. Cellular Plastics, 37 (6), 517 (2001).

56.*Standard Test Method for Apparent Density of Rigid Cellular Plastics* ASTM (D1622-98).

57.V. Kumar, J. W., *Production of Microcellular Polycarbonate Using Carbon Dioxide for Bubble Nucleation*. Journal of Engineering for industry, NOVEMBER 1994, Vol. 116/413

58.Scintag, I., *Basics of X-ray Diffraction* Chpt. 7.

59.D. S. Rosa, C. G. F. G., M. A. G. Bardi, *Evaluation of thermal, mechanical and morphological properties of PCL/CA and PCL/CA/PE-g-GMA blends*. Polymer Testing 26 (2007) 209-215

60.Ernesto Di Maio, S. I., Luigi Sorrentino, Luigi Nicolais, *Isothermal crystallization in PCL/clay nanocomposites inestigated with thermal and rheometric methods*. Polymer 45 (2004) 8893-8900

61.*Standard Test Method for Density of Plastics by Density-Gradient Technique* ASTM(D1505-98).

62.Naquib, H. E., Nawaby, A. V., Day, M, *CO2 Sorption and diffusion in polymethyl methacrylate-Clay nanocomposites*.

63.*Standard Test Method for Tensile And Tensile Adhesion Properties of Rigid Cellular Plastics* ASTM(D1623-78).

64.*Standard Test Method for Tensile Properties of Plastics* ASTM(D638-00).

65.Dagnon, K., Sahu, L., and D'Souza A., *Thermomechanical Properties of PCL, MB and their Blend*s.

66.Gdoutos, E. E., Daniel I.M. and Wang, K.A, (2002). *Failure of Cellular Foams under Multiaxial Loading*, J. of Comp., Part A33, -176.

67.Krishnan Kanny, H. M., Tonnia Thomas and Shaik Jeelani, *Static and Dynamic Characterization of Polymer Foams Under Shear Loads*. Journal of COMPOSITE MATERIALS, Vol. 38, No. 8/2004

68.ASTM Standard: C 273-61 *Standard Test Methods for the shear Properties in Flatwise Plane or Flat Sandwich Construction or Sandwich Cores*.

69.ASTM Standard: D5628-96 *Standard Test Method for Impact Resistance of Flat Rigid Plastic Specimen by Means of a Falling Dart (Tup or Falling Mass)*.

70.*Standard Test Method for Compressive Properties of Rigid Cellular plastics* (D1621-00).

71.J. M. Gomez de Salazar, M. I. B., G. Morales, L. Matesanz, N. Merino, *Compression strength and wear resistance of ceramic foams-polymer composites*. Materials Letter 60 (2006) 1687-1692